Delayed Onset of Return Flow and Stabilization of Vortex Flow through Sidewall Converging and Duct Inclination in Mixed Convection of Gas over a Heated Circular Plate in a Horizontal Rectangular Duct

：

：

Delayed Onset of Return Flow and Stabilization of Vortex Flow through Sidewall Converging and Duct Inclination in Mixed Convection of Gas over a Heated Circular Plate in a Horizontal Rectangular Duct

Student　Wei-Shen Kuo

Advisor　Tsing-Fa Lin

A Thesis

Submitted to Institute of Mechanical Engineering

Collage of Engineering

National Chiao Tung University

in Partial Fulfillment of the Requirements

for the degree of

Doctor of Philosophy

in

Mechanical Engineering

December 2005

Hsinchu, Taiwan, Republic of China

國 立 交 通 大 學

論 文 口 試 委 員 會 審 定 書

本校＿＿機 械 工 程＿＿學系博士班＿＿郭 威 伸＿＿君

所提論文（中文）<u>水平漸縮管道之圓型底板加熱面漸縮管道對於浮</u>
<u>力所驅動空氣混合對流渦旋流結構之穩定與迴流</u>
<u>消除之影響研究</u>

（英文）<u>Delayed Onset of Return Flow and Stabilization of</u>
<u>Vortex Flow through Sidewall Converging and Duct</u>
<u>Inclination in Mixed Convection Of Gas over a</u>
<u>Heated Circular Plate in a Horizontal Flat</u>

合於博士資格水準、業經本委員會評審認可。

口試委員：＿＿＿＿＿＿＿＿＿＿＿＿＿＿　＿＿＿＿＿＿＿＿＿＿＿＿＿＿

＿＿＿＿＿＿＿＿＿＿＿＿＿＿　＿＿＿＿＿＿＿＿＿＿＿＿＿＿

＿＿＿＿＿＿＿＿＿＿＿＿＿＿　＿＿＿＿＿＿＿＿＿＿＿＿＿＿

＿＿＿＿＿＿＿＿＿＿＿＿＿＿　＿＿＿＿＿＿＿＿＿＿＿＿＿＿

指導教授：＿＿＿＿＿＿＿＿＿＿＿＿＿＿　＿＿＿＿＿＿＿＿＿＿＿＿＿＿

系 主 任：＿＿＿＿＿＿＿＿＿＿＿　教授

中 華 民 國　九十四　年　十二　月　二十六　日

5

50   7,200   21,000

5.7°   11°

(longitudinal roll)   (transverse

roll)   (Return Flow)

(buoyancy-to-inertia ratio)

i

1°   2°

(aiding mixed convection)

Delayed Onset of Return Flow and Stabilization of Vortex Flow through Sidewall Converging and Duct Inclination in Mixed Convection of Gas over a Heated Circular Plate in a Horizontal Rectangular Duct

Student: Wei-Shen Kuo   **Advisor: Prof. Tsing-Fa Lin**
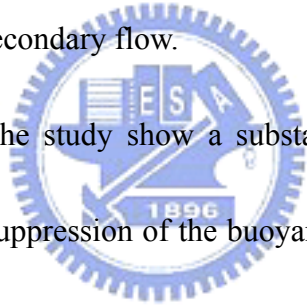
Institude of Mechanical Engineering

National Chiao Tung University

ABSTRACT

In this study an experimental flow visualization combined with temperature measurement are conducted to investigate how the sidewall converging and duct inclination affect the buoyancy induced return flow structure and stabilization of vortex flow in mixed convection of gas in a horizontal rectangular duct. The buoyancy driven secondary flow including the return flow and vortex flow is driven by a heated circular disk embedded in the bottom plate of the duct, simulating that in a horizontal longitudinal MOCVD reactor. Specifically, in the first part of the present study the sidewalls of the duct are inclined toward the duct core so that the gas flow in the duct is accelerated, causing the buoyancy-to-inertia ratio to decrease in the main flow

direction. While in the second part of the study the duct is inclined upwards with its exit end above the entry end and the component of the buoyancy force normal to the heated plate is reduced. In the experiment the Reynolds and Rayleigh numbers of the flow at the duct inlet are respectively varied from 5 to 50 and from 7,200 to 21,000. In the first part of the study the duct aspect ratio is reduced from 20 at the inlet to 16 or 12 at the exit. The duct is slightly inclined from the horizontal in the second part. Particular attention is paid to delineating the spatial changes of the return flow structure with the sidewall converging and to explore how the duct inclination possibly suppresses and stabilizes the secondary flow.

The results obtained in the study show a substantial delay in the onset of the return flow and the effective suppression of the buoyancy driven unstable longitudinal and transverse vortex flows by the sidewall converging and the duct inclination. Besides, the sidewall converging and the duct inclination can weaken the return flow more effectively at slightly higher Reynolds numbers. An empirical equation is provided to correlate the present data for the onset condition of the return flow in the duct. Some preliminary results from the second part of the study indicate that the slight inclination of the duct at 2 ° can significantly weaken the return flow. The reduction in the size of the return flow zone and the intensity of the return flow is prominent. Besides, the onsets of longitudinal and transverse vortex rolls are delayed substantially.

…

CONTENTS

LIST OF TABLES

LIST OF FIGURES

°, 1 °and 2 °.

NOMENCLATURE

A	Aspect ratio of duct, b/d
b	Channel width
d	Channel height at the duct inlet
g	Gravitational acceleration
Gr	Grashof number, $g\beta d^3(T_{in}-T_{cp})/\nu^2$
Pr	Prandtl number, ν/α
Ra	Rayleigh number, $\beta g d^3 \Delta T /\alpha\nu$
Re	Reynolds number, $W_m d/\nu$
Gr/Re^2	Buoyancy-to-inertia ratio
T	Temperature
T_{in}, T_{cp}	Gas temperature at inlet of test section and temperature of copper plate
ΔT	$T_{cp} - T_{in}$
t	Time, s
W_m	Mean velocity of gas in axial direction
X,Y,Z	Dimensional Cartesian coordinates
x,y,z	Dimensionless Cartesian coordinates scaled with b, d, l
α	Thermal diffusivity
β	Thermal expansion coefficient
γ_{crit}	Critical buoyancy-to-inertia ratio
ν	Kinematic viscosity
	Inclined angle of the side walls
	Inclined angle of the duct

CHAPTER 1

INTRODUCTION

The buoyancy driven vortex flow and associated thermal characteristics in low speed mixed convective gas flow through a horizontal rectangular duct uniformly heated from below and cooled from above have been extensively investigated in the past. Combined experimental measurement and numerical simulation were carried out to explore various vortex flow patterns and their temporal-spatial structures. These investigations are mainly motivated by the important role the vortex flow plays in growing high quality thin semiconductor crystal films from the horizontal metal-organic chemical vapor deposition (MOCVD) processes. In this particular flow configuration a number of buoyancy induced secondary flow patterns have been reported in the literature, including the return flow, longitudinal, transverse and mixed vortex rolls and others [1,2]. Some of the roll patterns are illustrated in Figs. 1.1 and 1.2. All of these secondary flows can cause a non-uniform vapor deposition on the silicon wafer and is harmful to the thin film properties. Especially, the existence of the return flow zone will block the forced flow to move smoothly over the substrate and blur the interfaces in the multi-layer thin film structure. Hence the return flow is most unwanted and unwelcome in the MOCVD processes [3,4]. Thus how to eliminate the

return flow in the MOCVD processes is very important. The previous studies on the buoyancy driven secondary flows in rectangular ducts mainly focused on a simpler thermal boundary condition with the ducts heated uniformly from below and cooled uniformly from above. It is well known that the buoyancy driven secondary flow is very sensitive to the geometry of heating surface, Reynolds and Rayleigh numbers of the flow and the buoyancy-to-inertia ratio [5-9]. The characteristics of the return flow predicted from the previous studies are expected to be somewhat different from those in the real MOCVD processes where the heated wafers are circular in shape. In particular, the return flow will be complex and highly three-dimensional. In a recent model study Tuh and Lin [10] examined the return flow characteristics driven by a circular heated substrate embedded in the bottom of a rectangular duct with a low speed gas flow in it. In this continuing study we intend to investigate the delay of the buoyancy driven return flow by inclining the sidewalls of the horizontal flat duct toward the duct axis so that the main flow is accelerated in the axial direction. In addition, how the return flow is affected by the inclination of the duct will be explored. Note that in the sidewall converging duct the buoyancy-to-inertia ratio reduces in the streamwise direction because of the flow acceleration in that direction. Similarly, in the inclined duct the component of the buoyancy force normal to the heated substrate is smaller than that in the horizontal duct, leading to a lower buoyancy-to-inertia ratio.
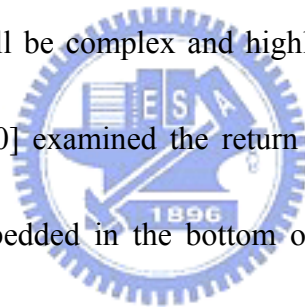
Thus, both the sidewall converging and duct inclination are expected to delay the appearance of the return flow. The flow acceleration was found to be very effective in suppressing the buoyancy induced temporal flow oscillation in MOCVD processes and hence was able to improve the properties of epitaxial layers [11]. A model experiment is conducted in the first part of the present study to investigate the buoyancy driven vortex flow affected by inclining the sidewalls of a flat duct so that the duct cross section reduces in the axial direction for mixed convection of gas in a horizontal rectangular duct. Then, in the second part of the present study the effects of the duct inclination on the return flow will be explored. In the study, both the return flow and the vortex flow induced in the duct will be examined. In the following the literature relevant to the present study of mixed convective vortex flow of gas in a horizontal rectangular duct heated from below is briefly reviewed.
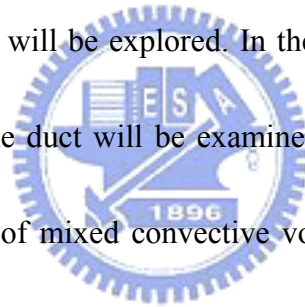
1.1 Characteristics of Longitudinal and Transverse Rolls

For the fully developed laminar forced convection between two infinite horizontal plates respectively heated uniformly from below and cooled uniformly from above, many different vortex flow patterns were predicted from theoretical linear stability and weak nonlinear analyses at the onset of Rayleigh-Benard convection. The critical Rayleigh number for the thermal instability has been found to be 1,708 by

experimental measurement [12] and linear stability theory [6], that is independent of the Reynolds number of the flow. In a finite transversal horizontal channel, Nicolas et al. [13] showed that the critical Rayleigh number for the thermal instability was larger than 1708. This means that the mixed convection flow in a laterally bounded channel is more stable than that in a laterally unbounded one. They further explained the existence of a critical Reynolds number Re^* at which the critical Rayleigh numbers Ra_L^* and Ra_T^* for the onset of longitudinal and transverse vortex rolls with their rotation axes respectively parallel and perpendicular to the forced flow direction started to bifurcate. For $Re > Re^*$ longitudinal rolls are induced first in the channel at Ra_L^*. While for $Re < Re^*$ transverse rolls prevail at Ra_T^* which is slightly lower than Ra_L^*. It is well known that Ra_L^* is independent of the Reynolds number Re, but the critical Rayleigh number Ra_T^* for the appearance of the transverse rolls increases with the Reynolds number. At a low buoyancy-to-inertia ratio for $Ra > Ra_L^*$ and $Re > Re^*$ steady longitudinal vortex flow prevails and the spanwise temperature distribution is in very regular sinusoidal shape, and the number of the vortex rolls is equal to the duct aspect ratio [14-16]. Kamotani and his colleagues [15] observed in a flow visualization experiment that at supercritical Rayleigh number the smoke which traveled certain distance over a heated surface and absorbed enough thermal energy started to rise at some downstream location and deformed into a mushroom-shape due to the shearing

4

action of the forced flow. When the mushroom-shape flow structure rose up to hit the

top wall of channel, it bifurcated and developed into a longitudinal vortex flow in the

downstream region. It is also well known that at a low buoyancy-to-inertia ratio, the

longitudinal vortex flow is characterized by the steady and regular longitudinal vortex

rolls with spanwise symmetry and all the rolls have the same size with their diameter

nearly equal to the duct height. Besides, the transverse velocities of the longitudinal

vortex flow were measured and found to be independent of the Reynolds number by

Chiu et al. [17]. They also noted that when the boundary-to-inertia ratio is much

smaller than one ($Gr/Re^2<1$), only longitudinal rolls appeared in the duct. Moreover the

critical wavelength of the thermal instability was determined by the duct height, not by

thermal boundary layer thickness. The experiment from Chang et al. [16] indicate that

the longitudinal rolls are always initiated first near the side walls of the channel and the

roll number is equal to or less than the aspect ratio of the duct. At a high

buoyancy-to-inertia ratio, the longitudinal vortex flow becomes unsteady and some

rolls split in certain period of time and later merge. Chang, Lin and their colleagues

[1,2] observed unsteady snaking longitudinal vortex flow with the presence of the

splitting and merging of the rolls nonperiodically in time. The buoyancy effects on

both heat transfer and skin friction were shown to be a strong function of the Prandtl

number by Sparrow and Minkowycz [18] with the buoyancy growing more important
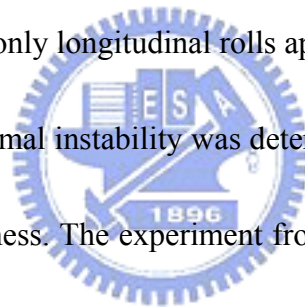
at decreasing Prandtl number.

The buoyancy driven transverse rolls only exist at relatively low Reynolds numbers and hence the buoyancy-to-inertia ratio is very high. A numerical analysis of the transverse vortex flow in a rectangular channel heated from below was conducted by Nicolas et al. [19]. It was observed that at such high buoyancy-to-inertia ratio, the buoyancy driven thermals possessed enough energy to merge with their spanwise neighbors in the upstream section of the duct, forming the transverse rolls [3,20]. Moreover, the critical Rayleigh number for the onset of the transverse rolls Ra_T^* increases with the Reynolds number and varies with the aspect ratio of the duct and the Prandtl number. Lin and his colleagues [16,21] combined flow visualization and temperature measurement to explore the transverse vortex rolls in the horizontal rectangular duct. Their studies show that the transverse rolls all have the same size with their diameters all nearly equal to the duct height and the influences of the Reynolds and Rayleigh numbers on roll size are slight. Besides, the transverse vortex rolls move downstream at the same convection speed.

1.2 Characteristics of Return Flows

Buoyancy driven vortex flow and the associated thermal characteristics in mixed convective gas flow through a horizontal plane channel heated from below recently

receive increasing attention because the important role they play in the horizontal

MOCVD processes for thin crystal film growth, as already mentioned above. It is well

known that the buoyancy driven vortex flow can result in a non-uniform vapor

deposition on silicon wafers and is harmful to the thin film properties [22]. At

sufficiently high buoyancy-to-inertia ratios [23] the buoyancy driven vortex flow can

even become unstable. Moreover, at high buoyancy the forced flow can be reversed

resulting in a return flow zone in the channel. The return flow will result in a memory

effect in the MOCVD processes. This memory effect is detrimental to the epitaxial layer

and should be avoided. In order to eliminate or weaken the vortex and return flows, the

conventional method which is widely used in the industry is to reduce the cross sectional

area of the channel in the streamwise direction. Reduction of the channel cross section

by the sidewall converging toward the channel axis can accelerate the forced flow so

that the buoyancy-to-inertia ratio in the flow decreases in the streamwise direction. This

was found to be very effective in suppressing the buoyancy induced temporal flow

oscillation in MOCVD processes. But the details on how the vortex and return flows are

affected by the sidewall converging remain largely unexplored. In a recent model

experiment [10] we examined the buoyancy driven three-dimensional return flow

pattern in a gas flow over a heated circular disk embedded in the bottom plate of a

horizontal rectangular duct, simulating that in a horizontal longitudinal MOCVD reactor.
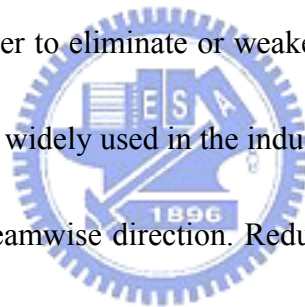
Here in the present study we move further to investigate how the buoyancy driven return flow is affected by the main flow acceleration due to the sidewall converging.

In the mixed convective flow through a bottom heated flat duct the return flow is known to result from the strong upward thermal buoyancy as the cold entering gas is suddenly heated in the entry heated section of the duct. The cold flow from the upstream is forced to lift up first and moves obliquely upwards. Then, the flow is blocked to move upstream by the strong retarding force of the upward buoyancy, forming a reverse flow zone. At high buoyancy the return flow can penetrate significantly into the upstream unheated section of the duct and becomes highly elongated. When the main flow is at a high Reynolds number, the return flow can extend substantially into the heated section of the duct and is also highly elongated.
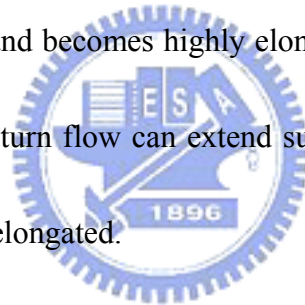
The return flow encountered in the horizontal MOCVD reactors was first investigated by Eversteyn et al. [24] by visualizing the flow. They identified a particle-free zone above the susceptor and erroneously interpreted this zone as a stagnant layer of fluid. Instead, it is well known today as the return flow zone. Kamotani et al. [15] experimentally examined the thermal instability of a laminar flow in a horizontal flat duct heated from below and found that at a high buoyancy-to-inertia ratio with $Gr/Re^2 \gg 1$ a reverse flow zone was induced near the upper plate. Flow visualization conducted by Giling [25] to investigate flow pattern and temperature

profile in horizontal MOCVD reactors proved that there was no stagnant layer above the susceptor. According to the experimental and numerical study of nitrogen and hydrogen gas flows in a bottom heated quartz reactor with a rectangular cross section, Visser et al. [3] indicated that the returning flow was mainly dominated by two dimensionless parameters, the Grashof and Reynolds numbers, Gr and Re. They proposed a critical level γ_{crit} for the mixed convection parameter Gr/Re and showed that no return flow occurred when Gr/Re γ_{crit}. The exponent is equal to 1 at low Reynolds numbers (Re 4) and goes to 2 at higher Reynolds numbers (Re 8). A similar study from Fotiadis et al. [26] also indicated that either the heated susceptor was placed in the bottom or top wall a flow recirculation could be induced. Moreover, the recirculation was noted in the upper portion of the reactor.
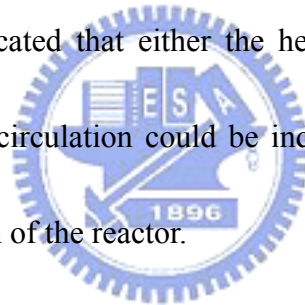
A two-dimensional numerical simulation carried out by Ouazzani et al. [27] to predict the buoyancy driven flow recirculations in the entrance region of a horizontal MOCVD reactor manifested that the presence of the return flow could result in an increase of film growth rate at the leading edge of the substrate and a decrease in the downstream. Later, they [28] extended the analysis to include the three-dimensional effects and found that at a high Ra/Re ratio, a buoyancy-induced reverse flow existed in the transition region between the isothermal entrance and the reaction section. Einset et al. [29] moved further to quantify the onset of recirculation flows in the entrance region

of horizontal CVD reactors based on the relative magnitudes of the vertical and horizontal pressure gradients in the flow. The pressure effects are independent of whether the heated substrate faces up or down, which explains their experimental observation that the flow recirculations appear at the same position in either configuration. Besides, they noted that the recirculation rolls located near the top wall of the reactor and rotated counter-clockwisely for both top- and bottom-heated reactors. Ingle and Mountziaris [30] again used a 2-D numerical simulation to investigate the onset of transverse buoyancy-driven circulations in a horizontal flat duct consisting of a cool upstream section, a middle section with a heated bottom wall, and a cool downstream section. Their results showed a transverse recirculation formed in the middle section near the top wall above the leading edge of the hot bottom wall, which rotated in a counter-clockwise direction. The other one formed near the bottom wall above the exit end of the hot bottom plate and rotated in a clockwise direction. At increasing inlet velocity, the downstream transverse recirculation was eliminated first and the upstream one shrank significantly. In addition, they proposed two criteria for the absence of the transverse recirculaton as (Gr/Re^2) 100 for 10^{-3} Re 4, and (Gr/Re^2) 25 for 4 Re 100. A similar 2-D numerical simulation from Ingham et al. [31,32] predicted that the transverse flow recirculation could extend to the upstream of the wall temperature discontinuity. The onset of the return flow for the heated lower wall was
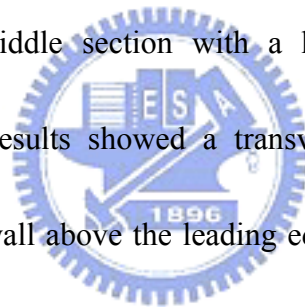
shown to occur at $Gr/Re^2 \cong 17$ for Re=10. This critical value of Gr/Re^2 slowly decreases at increasing Re. Besides, the recirculation zone is larger for a lower Re. Makhviladze and Martjushenko [33] conducted 2-D and 3-D numerical simulations to study the return flow in bottom wall heated horizontal CVD reactors. They showed the formation mechanism of the return flow and the return flow could be suppressed by cooling the side walls and/or by reducing the width of the reactors. The characteristics of three-dimensional flow, heat and mass transfer in a horizontal CVD reactor were numerically investigated by Park and Pak [34]. They concluded that for a large Gr/Re^2 the return flow appeared at the leading edge of the susceptor, and it caused an increase in the growth rate of the film in this region and a decrease in the downstream of the susceptor. Recently, the three-dimensional return flow structure driven by a heated circular disk embedded in the bottom wall of a rectangular duct was examined by Tuh and Lin [10] through experimental flow visualization.
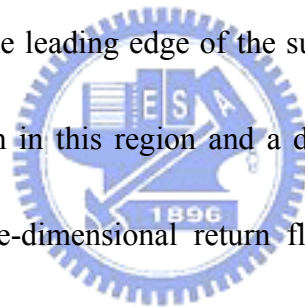
A simple mean often used to suppress and stabilize the buoyancy driven vortex flow is to accelerate the forced flow, as demonstrated by Chen et al. [35]. Gau et al. [36] revealed that in a convergent channel with the top plate inclination, the acceleration of the forced flow could delay the onset of thermal instability and effectively suppress the temperature fluctuation. Tseng et al. [37] experimentally showed that inclining the top plate of a rectangular duct uniformly heated from below could effectively and

completely wipe out the irregular temporal flow oscillation. But the induced vortex flow can only be weakened to some degree. Besides, more vortex rolls would be induced due to the increase in the aspect ratio of the duct in the mean flow direction.

The above literature review clearly indicates that how the buoyancy induced return flow is affected by the sidewall converging and duct inclination remains largely unexplored in horizontal MOCVD rectors. An experimental flow visualization is conducted here to explore the effects of the sidewall converging and duct inclination on the return flow in a horizontal rectangular duct with a heated circular disk embedded in the duct bottom, simulating that in a horizontal longitudinal reactor.

1.3 Vortex Flow Stabilization

In the chemical vapor deposition processes used to grow thin crystal films on semiconductor substrates, the unsteady vortex flow prevailed at high buoyancy will provoke a time–dependent deposition rate and should be avoided. In the past, means often used to suppress and stabilize the vortex flow are to accelerate the forced flow [35]. As mentioned above, Tseng et al. [37] experimentally showed that inclining the top plate of a rectangular duct uniformly heated from below could effectively and completely eliminate the irregular temporal flow oscillation. But the induced vortex flow can only be weakened to some degree. Besides, more vortex rolls would be

induced due to the increase in the aspect ratio of the duct in the mean flow direction.

Then, Gau et al. [36] revealed that in a convergent channel with an inclined top plate, the acceleration of the forced flow could delay the onset of thermal instability and effectively suppress the temperature fluctuation. Recently, Sun [38] investigated the stabilization of mixed convective gas flow in a sidewall inclined duct also heated from below. He found that the sidewall inclination only caused slight delay in the onset of the longitudinal and transverse rolls, and at high buoyancy-to-inertia ratio the flow stabilization was insignificant. Wang [39] examined the stabilization of mixed convective air flow over a heated circular plate embedded in the bottom of horizontal rectangular duct by inclining the bottom plate of the duct. The flow acceleration associated with the duct bottom inclination results in more regular and stable longitudinal and transverse rolls and causes some delay in the onset of the return flow.

Bai [40] delayed the onset of the return flow by inserting curved blocks in the upstream region of the channel. The insertion of curved blocks reduces the cross sectional area in the entrance region of the duct, causing a reduction in the buoyancy-to-inertia ratio. This local flow acceleration was found to be very effective in suppressing the buoyancy induced temporal flow oscillation in CVD processes and substantially delayed the onset of the return flow.
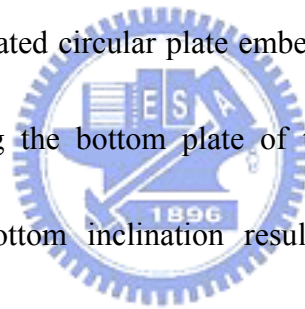
1.4 Objective of the Present Study

The above literature review clearly indicates that the mixed convective vortex flows of gas in a horizontal rectangular duct uniformly heated from below has been extensively investigated. However, it is also well known that the vortex flow is very sensitive to the geometry of the heated surface. Recently, Tuh [4] experimentally investigated the characteristics of mixed convective vortex flow driven by a circular heated plate in detail. The results indicate that the induced vortex flow driven by the circular heated surface is somewhat different from that driven by the rectangular heated bottom. Moreover, Tuh and Lin [10] moved further to reveal the unique return flow structure driven by a circular heated plate, which was characterized by an incomplete circular roll around the upstream edge of the circular plate. In the present study, we continue the study of Tuh and Lin [10] by examining some simple methods for the suppression of the return flow. More specifically, in the first part of the study an experiment combining flow visualization and temperature measurement is conducted here to investigate the possible suppression of the buoyancy driven return flow by inclining the sidewalls of the test section torward the duct cone. Attention is focused on how the return flow is affected by the sidewall inclination which causes the acceleration of the forced flow in the test section. Meanwhile, the effects of the inclined sidewalls on the characteristics of the longitudinal and transverse vortex flows

will also be explored. The effects of the Reynolds and Rayleigh numbers and the duct

aspect ratio on the vortex flow and the associated thermal characteristics will be

examined in detail. Moreover, in the second part of the study the return and vortex

flow characteristics affected by the duct inclination will be explored.
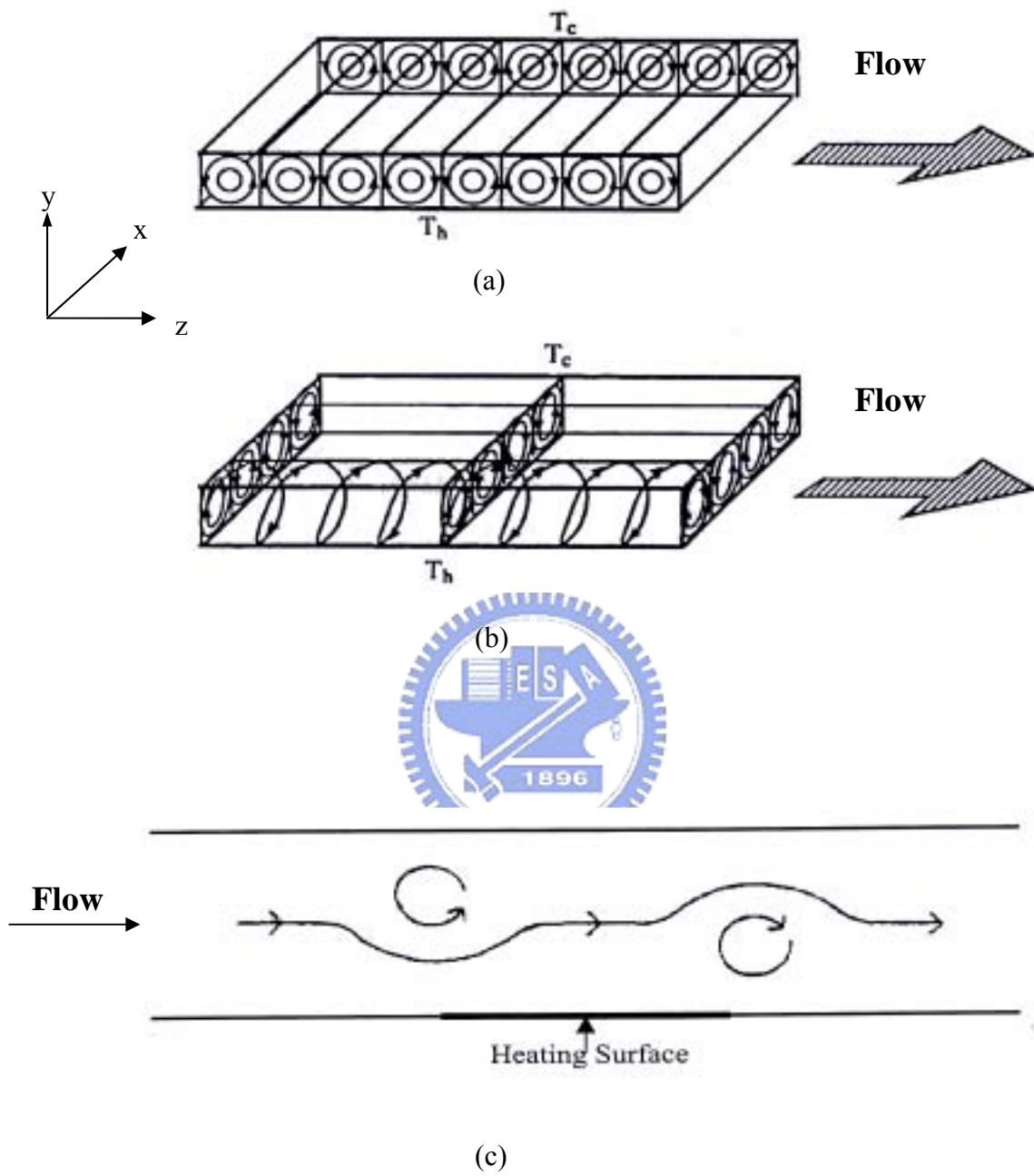
Fig.1.1 (a) Schematic of transverse rolls, (b) representation of longitudinal rolls in a
rectangular channel and (c) formation of return flow

Top view **End view**

Flow

(a)

Top view

Flow

Side view

Return flow

(b)
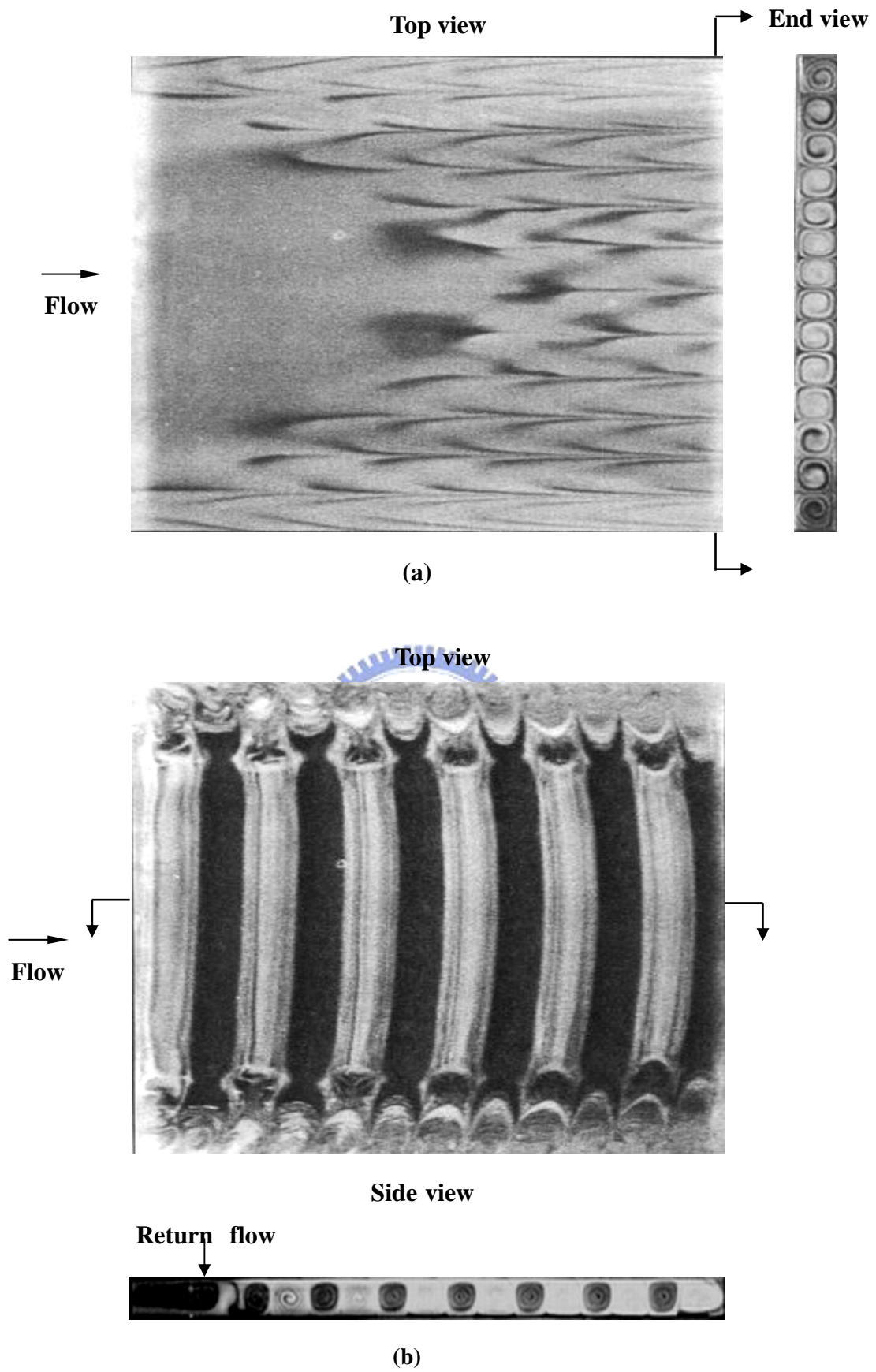
Fig.1.2 Photos from the characteristic flow visualization in a horizontal flat duct uniformly heated from below [1,2].

17

CHAPTER 2

EXPERIMENTAL APPARATUS AND

PROCEDURES

An open-loop mixed convection apparatus with air flowing in a horizontal rectangular duct with a circular heated disk embedded in its bottom plate is established in the present study to explore the suppression of the buoyancy driven return flow and vortex flow by the sidewall converging and inclination of the duct. The major constituents and the associated experimental procedures are briefly described in the following.

2.1 Experimental Apparatus

A sketch of the experimental apparatus for the mixed convective air flow over a heated circular plate in a horizontal plane channel and the adopted coordinate system are schematically shown in Fig. 2.1. The apparatus begins with the air regulated from a 300-liter and 100-psi high-pressure tank. Then, the air passes through a settling chamber, a contraction nozzle and a developing channel before entering the test section. After leaving the test section, the air is sent through an exhaust section and discharged into the ambient.

The test section of the experimental loop is a horizontal rectangular duct and has a

cross section of 22.5 mm in height and 450 mm in width, providing an aspect ratio of

A=20, and has a total length of 450 mm. In the first part of this study the sidewalls of

the test section are tilted symmetrically toward the duct core at the same convergent

angle , which is defined as the angle between the sidewalls and the vertical central

plane at x = 0. Both the bottom and top walls of the test section are horizontal. Thus

the test section, in fact, is a sidewall convergent flat duct and is schematically shown in

Fig. 2.2. Therefore the duct aspect ratio is 20 at the inlet of the test section, which is

reduced to 16 and 12 at the outlet of the test section in the present experiment

corresponding to = 5.7°& 11°. The side and top walls of the duct are constructed of

10-mm thick transparent acrylic plates to allow for the visualization of secondary flow

patterns. The bottom of the test section is a thick flat bakelite plate embedded with a

15-mm thick, high purity circular copper plate of 300 mm in diameter to model a

12-inch semiconductor substrate. The upper surfaces of the bakelite and copper plates

are kept at the same horizontal level so that the air flow does not experience any step

when moving over the copper plate. To obtain the uniform copper plate temperature,

the heating elements attached onto the lower surface of the copper plate are divided

concentrically into seven semi-circular zones and the heater for each zone is

independently controlled by a GW GPC 3030D laboratory power supply. Besides, a

mica sheet is placed between the copper plate and heating elements to prevent the
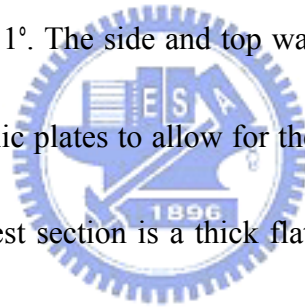
electric current leaking to the copper plate (Fig. 2.3). While in the second part of the

present study the rectangular duct is slight inclined from horizontal so that its exit end

is above its inlet at a small angle   , as schematically shown in Fig. 2.4.

A good control of the flow condition upstream of the test section is essential in the

experiment. More specifically, at the inlet of the loop the working fluid (air) is driven

by a 7.5-hp air compressor and sent through a dryer installed with water vapor and oil

filters. This dry air then moves into the high-pressure tank. To proceed with the

experiment, the air flow is further controlled by a pressure regulator and its volume

flow rate is measured by Brooks 5850E and/or 5851E flow controllers both having an

accuracy of ±1%. These two flow controllers individually operate in the ranges of 0 to

10 and 0 to 50 liter/min. Through a flexible tube, the air enters the settling chamber, in

which four fine-mesh screens, a divergent buffer section, a honeycomb and another

four fine-mesh screens are installed in sequence to reduce the turbulence in the air flow.

The air turbulence was further suppressed by passing the air through a contraction

nozzle with a contraction ratio of 44:1, which provides a nearly uniform velocity at the

inlet of the developing section.

The developing section is 1400 mm in length, approximately 62 times of the duct

height. This insures the flow to be fully developed before it arrives at the test section

inlet for Re≤100. An insulated outlet section of 450 mm long is added to the test

20

section to reduce the effects of the disturbances from discharging the air flow to the ambient. The developing section and outlet sections are both made of 10-mm thick acrylic plate, whereas the settling chamber and contraction nozzle are made of stainless steel SS-304 plates. The settling chamber, developing section, test section and outlet section are all thermally insulated with a 20-mm thick Superlon insulator and the entire loop is fixed on a rigid supporting frame.

Visualization of the buoyancy driven secondary flow in the test section is realized by injecting smoke at some distance ahead of the settling chamber. The smoke is produced by a smoke generator, which is a cubic space with incense burned in it. By keeping the smoke concentration at a suitable level, the incense particles can be illuminated by a plane light sheet from a 550 Watt overhead projector. With an adjustable knife edge a sharp contrast could be achieved between the duct walls and smoke. The flow photos from the top, side and end views of the test section can then be taken. The exposure time is about 1/125 second in taking the photos.

The temperature of the heated copper plate is measured by 17 calibrated and electrically insulated T-type thermocouples embedded at selected locations in the plate (Fig. 2.5). The thermocouple beads are fixed at about 1 mm from the upper surface of the copper plate through the small holes drilled from the back side of the plate. A T-type thermocouple is also used to measure the inlet air temperature at locations just

upstream of the test section. The signals from the thermocouples are recorded by the

Hewlett-Packard 3852A data acquisition system with a resolution of ±0.05 .

To measure the temperature distribution of the air flow in the horizontal duct, a

thermocouple probe is inserted from the downstream end of the test section. The probe

is supported by a three-way traversing device. More specifically, the thermocouple

probe is an OMEGA (model HYP-O) mini hypodermic extremely small T-type

thermocouple (33 gauge) implanted in a 1-inch long stainless steel hypodermic needle.

This movable thermocouple probe can measure the time-average and instantaneous

temperature of the flow. The temperature data are recorded when the flow reaches

steady or statistically stable state, usually 5-6 hours after starting the test. It was noted

that in all tests the maximum temperature differences between any two locations in the

copper plate were below 0.1 . The error in the temperature difference between the

copper plate surface and the air at the duct inlet is estimated to be within ±0.1 .
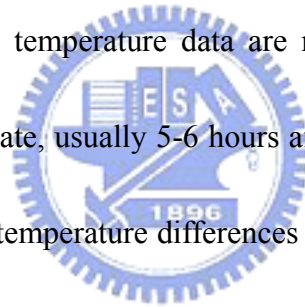
2.2 Analysis of Time-average and Instantaneous Air Temperature

The time-average temperature distributions in the air flow are obtained by

averaging 1000-3000 sampled data at each detection point. The period of the sampling

time may be different for different cases. Most importantly, the period has to be long

enough to capture all the slowest temperature oscillations in the air flow. The response

time of the thermocouple is about 0.12 second and the sampling rate is chosen to be

about 5 Hz in the transient temperature measurement. This sampling rate is high

enough for the present low Reynolds number mixed convection experiment.

2.3 Investigation of Flow Field

In order to confirm the fully developed condition at the entrance of the test

section, measurements using a hot-wire anemometer (DANTEC probe Type 55P01

with 56C17 CTA bridge) in connection with a HP data acquisition system (the

Hewlett-Packard VXI series-E1411B multimeter and E-1347A multiplexers) for the

inlet velocity profiles are conducted. For calibrating the hot wire, the pipe-flow method

that the probe is placed in the center of a fully developed laminar pipe flow is used.

The total volume flow rate is measured and the pipe center velocity is calculated from

the parabolic distribution. Figures 2.6 and 2.7 respectively show the measured inlet

velocity profiles in the rectangular duct along the vertical centerline at x=0.5 and

horizontal centerline at y=0.5 for two cases with Re=100 and 10 with no heat input to

the circular copper plate. The measured data are in good agreement with the analytical

results given by Shah and London [41]. The turbulence level of the inlet stream is also

given in the figures and is all within 1%. This implies that the effects of the free stream
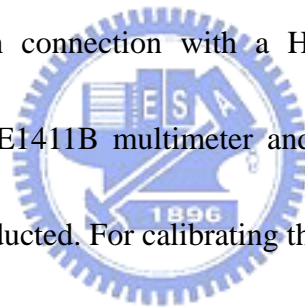
turbulence on the mixed convective flow characteristics are moderate.

2.4 Experimental Procedures

For convenience, experiments are designated according to the Reynolds and Rayleigh numbers based on the inlet conditions. In each test the flow controller is first set at the predetermined level to impose a steady flow through the entire test section. The power supplies are then turned on to raise the copper disk temperature. Usually, it takes about 3 hours for the Rayleigh number to be raised to the test point and another 2 hours are needed to maintain the secondary flow at steady or statistically stable state. The steady state is ascertained by insuring that the variation in the instantaneous temperature measured in the flow from each thermocouple be less than ±0.1 for a period of at least 25 minutes. The above choice of the steady state criterion is in accordance with the fact that the measured background temperature disturbances in the flow are found to be slightly less than ±0.1 . On the other hand, the statistically stable state is considered to be reached when the variation of the time-average temperature in the flow is within ±0.1 for more than 25 minutes. After the steady or statistically stable state is reached, we start the temperature measurement and flow visualization.

2.5 Uncertainty Analysis

Uncertainties in the Rayleigh number Ra, Reynolds number Re and other independent parameters are estimated in the light of the standard procedures proposed by Kline and McClintock [42]. The uncertainties of the thermophysical properties of air are included in the analysis. The fundamental thermophysical properties of the working fluid (air) are α=0.22 (cm^2/s), β=0.0034 (1/K), ν=0.162 (cm^2/s) and Pr=0.74 at 30 and 0.997 bar. The fluid properties are further corrected based on the temperature and pressure detected at the inlet of the test section. In addition, the deviation of temperature among the detecting points in the circular copper plate and the control unsteadiness are also accounted for in the evaluation of the data uncertainties. The analysis shows that the uncertainties of temperature, volume flow rate, dimensions, Reynolds number and Rayleigh number measurements are estimated to be less than 0.15 , 1%, 0.05mm, 3%, and 5% respectively. The uncertainties of various parameters are summarized in Table 2.1.
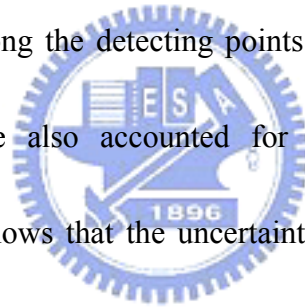
Table 2.1 Summary of the uncertainty analysis

Parameter and Estimated Uncertainty	
Parameter	Uncertainty
b, d, l (m)	±0.00005m
T_{in}, T_{cp}, T ( )	±0.15
Q (L/min)	±1 %
μ (N·m/s^2)	±0.05 %
ρ (kg/m^3)	±0.05 %
ν (m^2/s)	±0.07 %
Ra	±5 %
Re	±3 %

TOP VIEW

Settling Chamber & Nozzle
1932 mm

Developing Channel
1400 mm

Test Section
450 mm

Outlet Section
500 mm

700 mm

900 mm

450 mm

x

z

Screen

Honeycomb

Camera

SIDE VIEW

Overhead Projector

Camera

Test section

y

Copper

Mica Sheet

Air

z

Bakelite

Insulation

Heater

Screen

Honeycomb

295 mm

495 mm

22.5 mm

Camera

Overhead Projector

Air Flow

1932 mm

Settling Chamber & Nozzle

1400 mm

Developing Channel

450 mm

Test Section

500 mm

Outlet Section

Circular Pipe Diameter 70 mm

Three-way Traversing Device

Smoke Generator

0 ~ 50 slpm Flowmeter

Pressure Regulator

Oil Filter

Water Filter

Air Compressor

90 Liter

0 ~ 10 slpm

Air Flow

Air Tank 300 Liter

Dryer

Air Tank 300 Liter

Valve

Fig. 2.1   Schematic of experimental apparatus and the chosen coordinate system for the test section

Fig. 2.2   Schematic drawing of test section

150 mm

450 mm

Z

X

Flow

(a)

Copper Plate

Mica Sheet

Heater Layer

Bakelite Frame

22.5 mm

15 mm

15 mm

450 mm

(b)
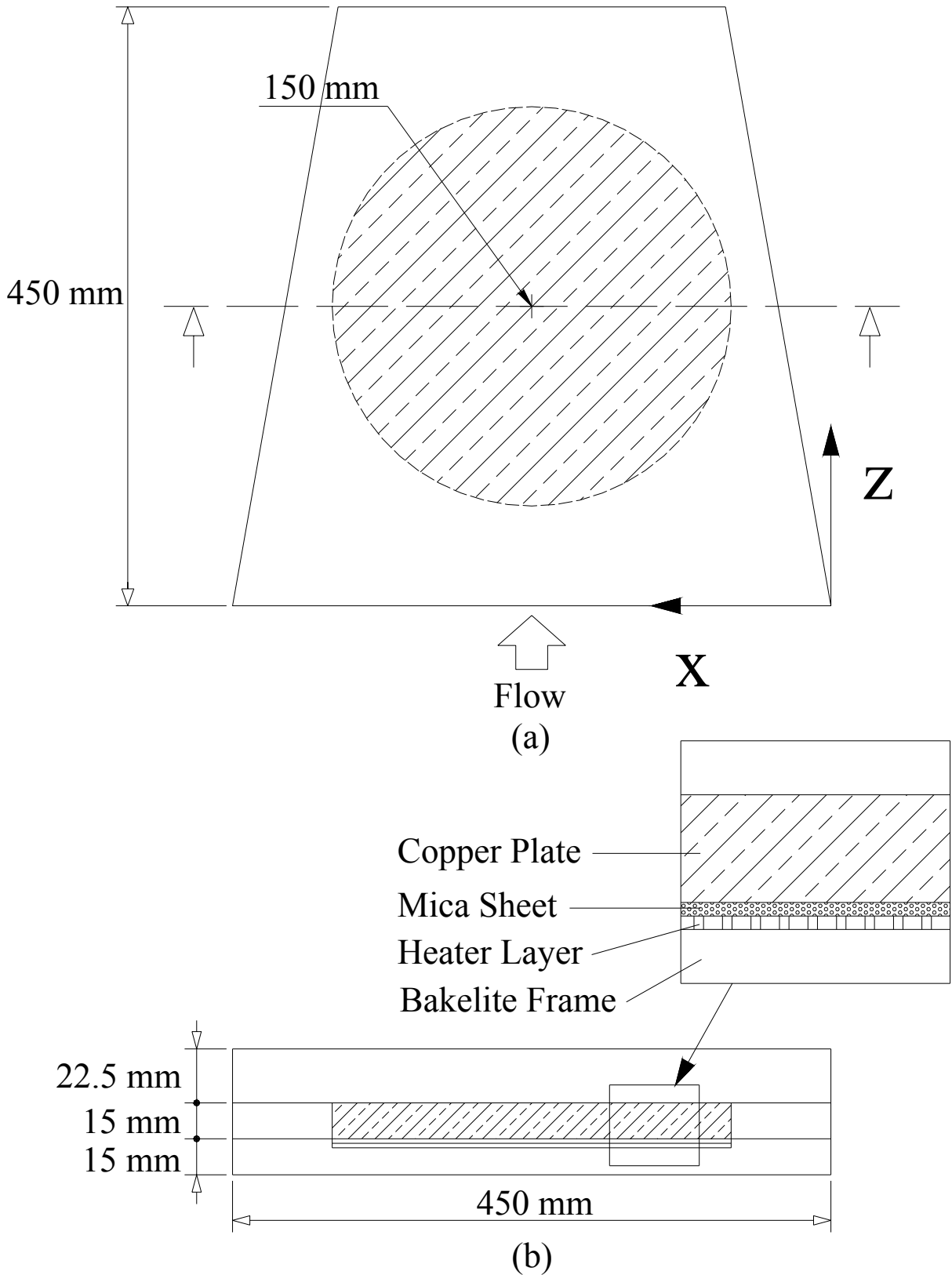
Fig. 2.3 Schematic of the test section from (a) top view and (b) cross-sectional view showing the detail of the bottom plate.

29

TOP VIEW

Settling Chamber & Nozzle
1932 mm

Developing Channel
1400 mm

Test Section
450 mm

Outlet Section
500 mm

700 mm

900 mm

450 mm

Screen

Honeycomb

x

z

Camera

SIDE VIEW

Overhead Projector

Camera

Test section

Copper

Mica Sheet

y

Air

z

Bakelite

Insulation

Heater

Screen

Honeycomb

295 mm

495 mm

22.5 mm

Camera

Overhead Projector

Circular Pipe
Diameter 70 mm

Three-way
Traversing Device

1932 mm

1400 mm

450 mm

500 mm

Air Flow

Settling Chamber
& Nozzle

Developing Channel

Test Section

Outlet Section

Smoke Generator

0 ~ 50 slpm
Flowmeter

Pressure
Regulator

Oil Filter

Water Filter

Air Compressor

90 Liter

0 ~ 10 slpm

Air Flow

Air Tank
300 Liter

Dryer

Air Tank
300 Liter

Valve

Fig. 2.4   Schematic of experimental inclined apparatus for duct inclination tests and the chosen

coordinate system for the test section   30
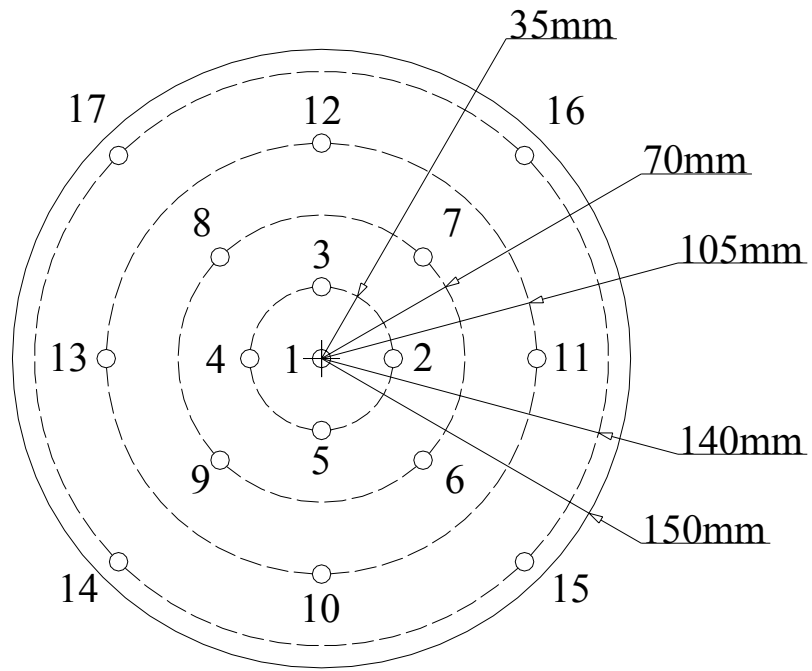
" ○ " means thermocouple
is embeded here

(a)
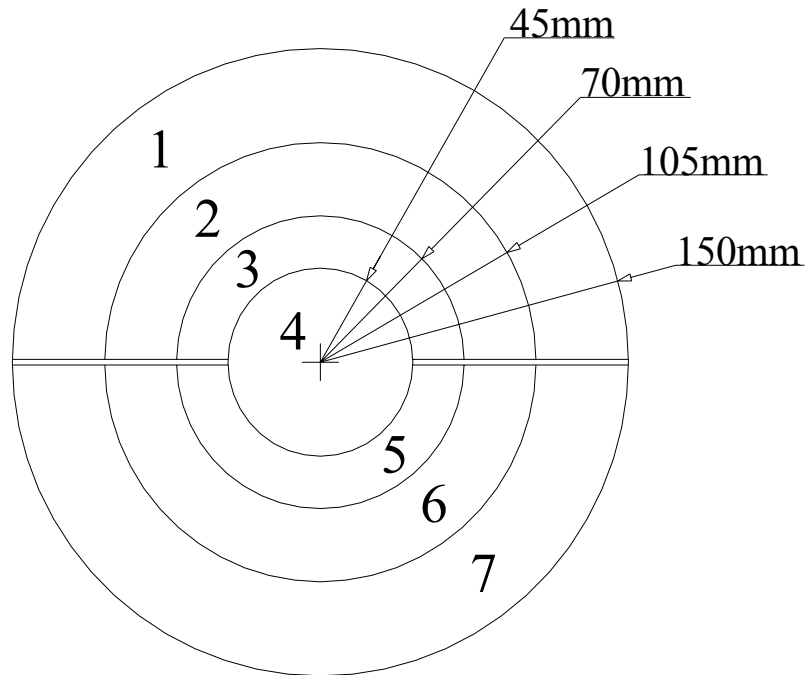
(b)

Fig. 2.5 Locations of the thermocouples (a) and the seven concentric heater sections (b).
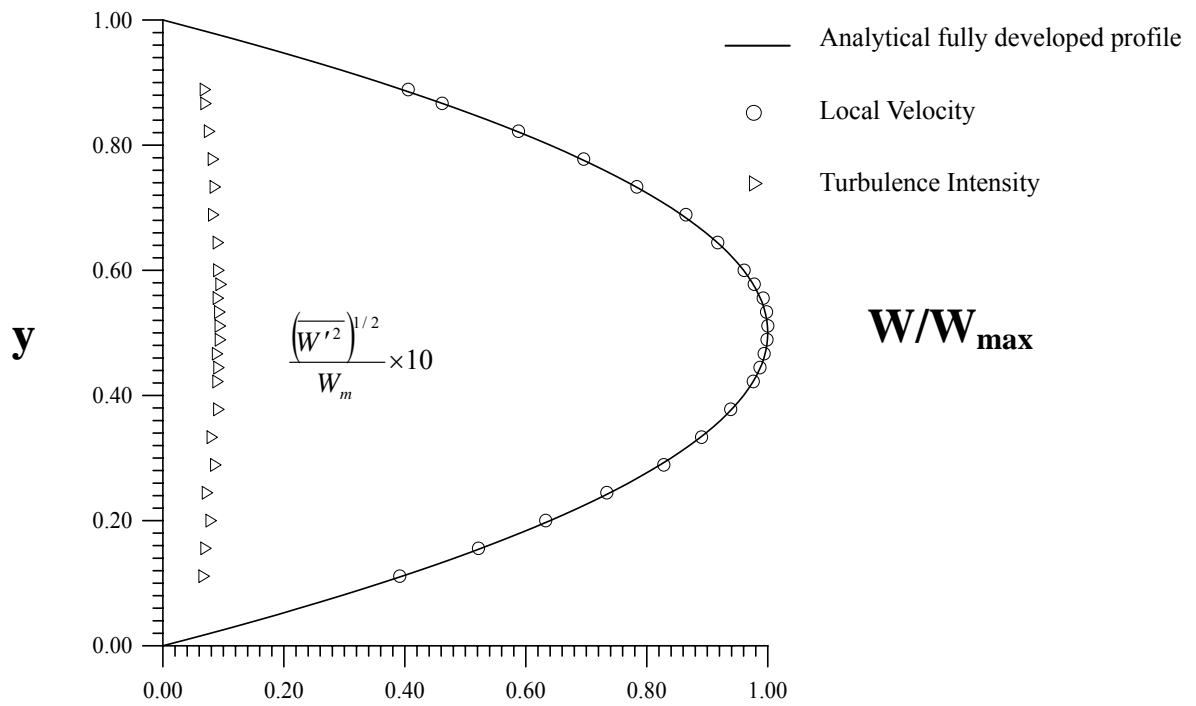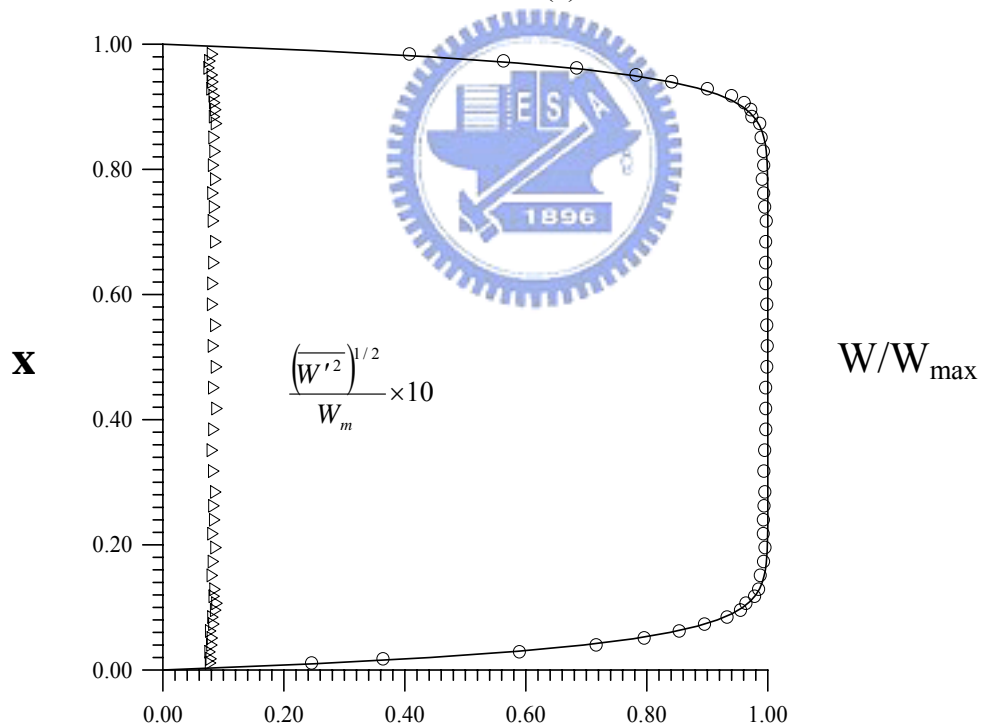
Fig. 2.6 Comparison of the measured axial velocity profiles W/Wmax at the inlet of test section with the analytical solution from Shah and London(1978) for Re=100 at (a)x=0.5 and (b)y=0.5.
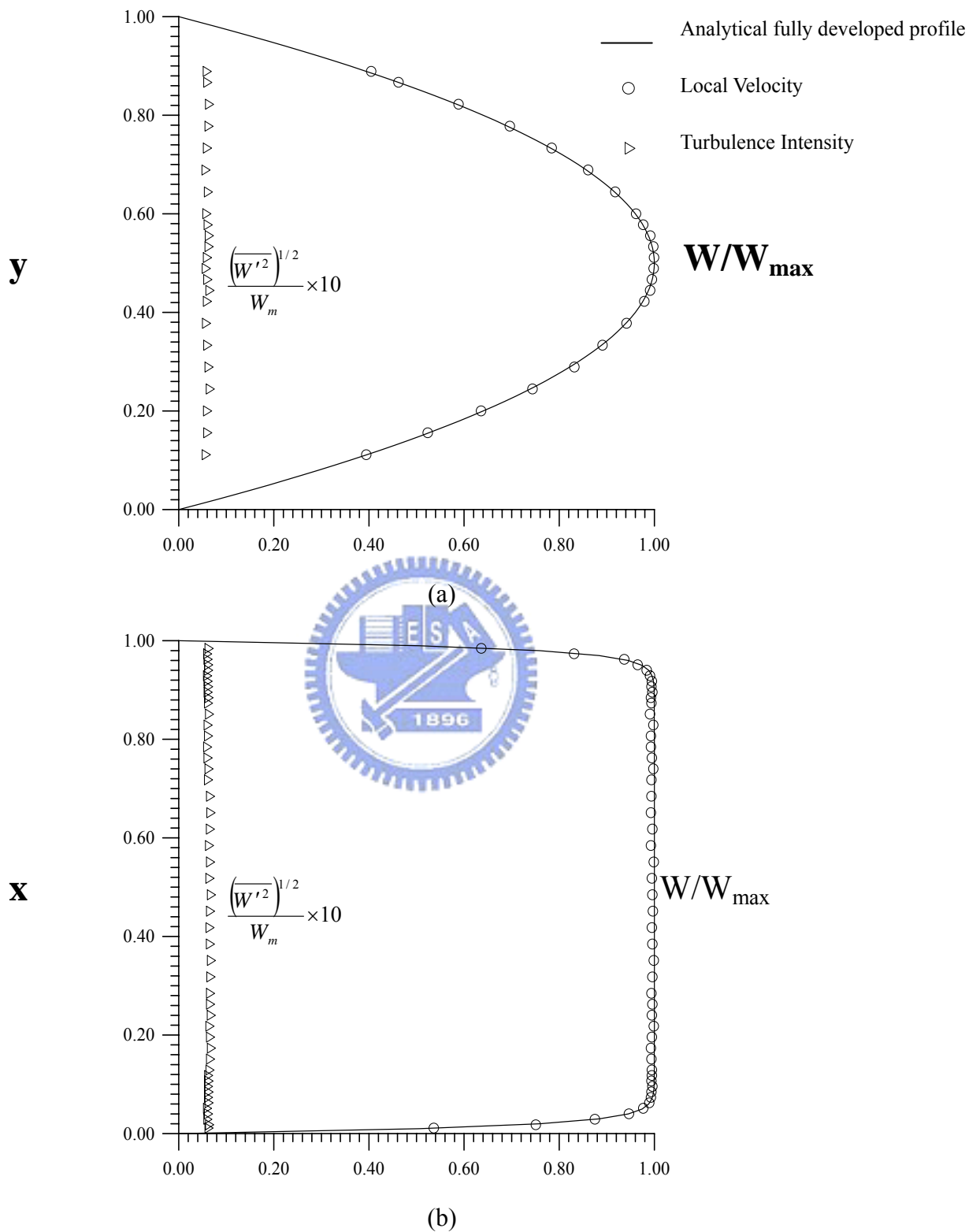
Fig. 2.7 Comparison of the measured axial velocity profiles W/W_max at the inlet of test

section with the analytical solution from Shah and London(1978) for Re=10

at (a)x=0.5 and (b)y=0.5.

CHAPTER 3

EFFECTS OF SIDEWALL CONVERGING ON RETURN FLOW

It should be mentioned that at the buoyancy high enough to induce return flow certain types of vortex flows such as the longitudinal (L-), transverse (T-), and irregular rolls can also appear in the duct above the heated disk [10,44]. Thus the effects of the sidewall converging on the vortex flows will be also examined here, in addition to the return flow. Selected results obtained in the first part of the present study are presented in this chapter to illustrate how the buoyancy induced return and vortex flows in the duct are affected by the main flow acceleration resulting from the converging of the duct sidewalls. In particular, we compare the side and top view flow photos taken from the duct with and without the sidewall converging for various Re, Ra and . In this investigation the Reynolds number of the flow is varied from 5 to 50 and Rayleigh number from 7,200 to 21,000 for = 5.7°and 11°. The ranges of the Re and Ra chosen above are in accordance with those encountered in real CVD processes [43]. In what follows the vortex flow characteristics affected by the sidewall inclination will be presented first. Then the effects of the sidewall inclination on the return flow will be examined.

3.1 Vortex Flow Characteristics

To illustrate the effects of the sidewall converging on the vortex flow, a series of top view flow photos taken from the duct with its sidewalls at different inclined angles at steady or statistically stable state are compared in Fig. 3.1 for Ra = 9,500 with the Reynolds number reduced from 30 to 20. The result in Fig. 3.1 (a) indicates that in the duct without the sidewall inclination (= 0°) we have steady and regular L-rolls at Re = 30. But as the Reynolds number is reduced to 25 and 20, the buoyancy-to-inertia ratios are high enough to cause the L-rolls to become somewhat deformed and irregular (Figs. 3.1 (b) and (c)). Now comparing the results in Figs. 3.1 (a), (d) and (g) for the same Re of 30 but for different converging angles of the sidewalls reveals that when the sidewalls are slightly inclined at =5.7° we have a significant delayed onset of the L-rolls when contrasted with that for = 0°. For a larger inclined angle of the sidewalls at =11° only a number of thermals appear above the heated disk (Fig. 3.1 (g)). At the lower Re of 25 the unstable deformed vortex flow in the rectangular duct (Fig. 3.1 (b)) can be significantly suppressed to become thermals at the large converging angle of the sidewall =11° (Fig. 3.1 (h)). But at the smaller of 5.7° we still have unstable L-rolls in the duct (Fig. 3.1 (e)), although they are nearly regular. Similar tread is noted for the lower Re of 20, as evident from the results shown in Figs. 3.1 (c), (f) and (i).

To manifest the spatial characteristics of the longitudinal vortex rolls (L-rolls)

affected by the sidewall inclination, a typical steady regular longitudinal vortex flows in the rectangular duct (=0°) and sidewall converging duct for =11° are respectively shown in Fig. 3.2 and Fig. 3.3 by presenting the steady top and end view flow photos for the two typical longitudinal flow cases (Re = 28.6 & Ra = 17,500 and Re = 27.8 & Ra = 17,600). The end view photos are taken at selected cross sections of the ducts. The top view photos are taken at the middle horizontal plane at y = 1/2 for the ducts. The results in Figs. 3.2 (d) and 3.3 (e) reveal that prior to the formation of L-rolls several thermals rise from the heated plate in both ducts. Through the simultaneous action of the forced flow and buoyancy, these thermals grow slowly in the downstream direction and become elongated in that direction with a mushroom-like cross section (Figs. 3.2 (e) and 3.3 (f)). Continuing growth of the thermals causes them to hit the duct top and the thermals evolve into L-rolls (Figs. 3.2 (f) and 3.3 (g)). Note that because of the circular geometry of the heated plate, closer to the duct core the thermals are induced at the more upstream locations. This is very different from the onset of L-rolls over a uniformly heated rectangular bottom plate in a flat duct in which the rolls first appear in the sidewall region and the rolls in the duct core are initiated at somewhat downstream locations (Fig. 1.2 (a)). More specifically, in the rectangular duct all the L-rolls driven by the circular heated plate have different size and are not spanwisely symmetric with respect to the central vertical plane x = 0.5, as evident from the end view flow photo in Fig. 3.2 (h).

36
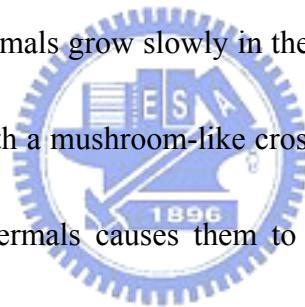
Comparing the results in Figs. 3.2 and 3.3 indicates that in the sidewall converging duct a slightly longer axial distance is needed for the L-rolls to be initiated. Thus, the sidewall inclination causes a slight delay in the onset of L-rolls.

The effects of the sidewall inclination on the vortex flow are further illustrated in Fig. 3.4 for a higher buoyancy-to-inertia ratio. The regularization of the unstable deformed longitudinal vortex flow by the main flow acceleration associated with the sidewall inclination is also clearly seen in Fig. 3.4 for Re = 30 & 25. It is noted that at the lower Reynolds number for Re = 20 deformed L-rolls prevail in the rectangular duct. But when the sidewalls are inclined, slightly asymmetric L-rolls dominate in the duct (Figs. 3.4 (c), (f) & (i)). The stabilization of the transient oscillation of the longitudinal vortex flow by the inclination of the sidewalls is also clearly seen from the measured time records of the air temperature at selected locations for various cases.

The detailed characteristics of the transverse vortex flow in the rectangular and sidewall converging ducts (= 0° and 11°) are examined next. The spatial structure of the regular T-rolls in the two ducts are presented in Figs. 3.5 & 3.6 by showing the top and side view flow photos at a certain time instants in the statistical state for the two cases with Ra = 11,600 and Re = 10.1 & 5.1. Note that the buoyancy-to-inertia ratio Gr/Re^2 for the case shown in Fig. 3.6 for the sidewall converging duct is about four times of that for the rectangular duct shown in Fig. 3.5. The top view flow photo in Fig. 3.5 (a)

indicates that in the rectangular duct the T-rolls in the upstream are somewhat bent toward the downstream and they gradually become shorter as moving downstream. The T-rolls are enclosed by an incomplete circular roll. It is in fact a return flow zone which is highly three-dimensional [10]. It should be pointed out that the bending of the T-rolls is attributed to the restriction of the incomplete circular roll induced around the upstream edge of the circular heated plate. Comparing the results in Figs. 3.5 and 3.6 clearly reveals that in the rectangular duct the return flow zone characterized by an incomplete circular roll around the upstream edge of the heated plate is rather large (Fig. 3.5 (a)) and the recirculating flow in it is very strong (Figs. 3.5 (b)-(e)). However, in Figs. 3.6 ((a)–(e)) the recirculating flow becomes much smaller and weaker. The recirculating flow is significantly suppressed by the main flow acceleration due to the sidewall converging. This weaking of the return flow clearly results from the acceleration of the main flow by the sidewall converging.
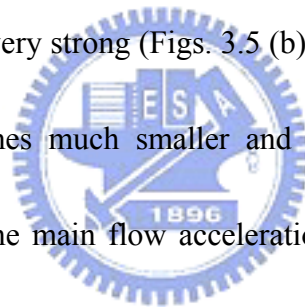
3.2 Return Flow Characteristics

To illustrate the return flow affected by the sidewall inclination, the side view flow photos taken at the central vertical plane x = 0.5 at the steady or statistically stable state for Ra ≈ 11,600 at decreasing Re are presented in Figs. 3.7 and 3.8 respectively for   = 0° and 11°. The results in Fig. 3.7 for the rectangular duct (= 0°) show that at the high

Reynolds number with Re≥30 the buoyancy-to-inertia ratio Gr/Re^2 is low and no return

flow appears in the duct (Figs. 3.7 (a)-(c)). Note that above the downstream half of the

heated plate stable L-rolls exist for this case [10]. As Re is lowered to 25 we begin to

observe a very small recirculating flow zone in the region near the upper plate in the

entrance section of the duct, indicating the onset of the return flow (Fig. 3.7 (d)). A

further reduction of the Reynolds number causes the return flow to become stronger and

occupies a larger region (Figs. 3.7 (e)-(k)). For the low Re of 7.5 and 5 the return flow

zone is relatively large and elongated in the axial direction, which extends deeply into the

upstream unheated section (Figs. 3.7 (j) and (k)). Downstream of the return flow zone the

duct is dominated by the unstable L-rolls for 17.5≤Re≤25 (Figs. 3.7 (d)-(f)) and by

T-rolls for 5≤Re≤12.5 (Figs. 3.7 (h)-(k)). While for Re = 15 unstable and somewhat

irregular L-rolls and T-rolls appear in the downstream half of the duct at the same time

(Figs. 3.7 (g)). Now for the sidewall inclined duct at   = 11°, the results in Fig. 3.8

clearly show that the return flow starts to appear at a lower Re of 18.4 (Fig. 3.8 (e)),

compared with Re = 25 for   = 0°. Thus the sidewall inclination results in a substantial

delay in the onset of the return. Moreover, even for the lower Re (≤17.5) in the

convergent duct the buoyancy induced return flow is weaker in intensity and smaller in

size (Figs. 3.8 (f)-(k)). The weakening of the return flow by the sidewall inclination can

be more clearly demonstrated by presenting the selected side view flow photos for   =
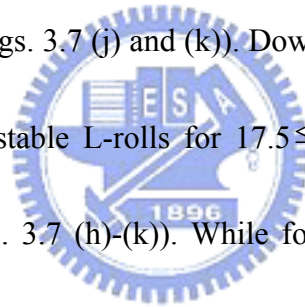
0°and 11° together in Fig. 3.9 at the same Re and Ra. A close inspection of the results in Fig. 3.9 reveals that the reduction in the size of the return flow zone by the sidewall inclination is more effective at a higher Re.

3.3 Critical Conditions for Onset of Return Flow

According to the data from the present experiment, the critical conditions for the onset of the return flow in the rectangular duct (= 0°) and in the convergent duct (= 11°) are plotted in Fig. 3.10. The results clearly show the significant increase in the critical buoyancy-to-inertia ratio for the onset of return flow by the sidewall inclination. According to the present experimental data, the onset of the return flow driven by the circular heated disk embedded in the convergent duct can be correlated as

$$Gr/Re^2 = (a+b/Re^2)/\cos(0.02 \quad) \tag{3.1}$$

where

$$a=27.5(0.04 \quad +1)^{2.5} \qquad b=2000(0.016 \quad +1)$$

The standard deviation of the above correlation is less than 12 .

The above equation is applicable for the Reynolds and Rayleigh numbers at the duct inlet ranging respectively from 5.0 to 50.0 and from 7,200 to 21,000. The above correlation is compared with the data for the convergent duct (=5.7° and 11°) in Fig.

40

3.10. Meanwhile, the critical condition for the onset of the return flow in the rectangular

duct (= 0°) compared in Fig. 3.10. The results clearly indicate that the convergent

duct causes a noticeable delay in the onset of the return flow. Besides, the return flow is

weakened by the convergent duct.

3.4 Vortex Flow Stabilization

Finally, the stabilization of the transient flow oscillation at a high

buoyancy-to-inertia ratio stabilized by the sidewall inclination is illustrated by presenting

the measured temperature variations with time at selected detection points at the

mid-height of the duct in Figs. 3.11 and 3.12 respectively for the cases with the

rectangular and convergent ducts for Re=10.1 and Ra=11,600. The results in Fig. 3.11

indicate that in the rectangular duct the flow oscillates periodically with time in the

downstream half of the duct where the moving transverse rolls dominate. Besides, the

flow essentially oscillates at the same frequency but the oscillation amplitude varies with

the locations. Now in the convergent duct with = 11°, the amplitude of the flow

oscillation is rather small at all detection points, as evident from the data given in Fig.

3.12. In fact, the flow can be regarded as steady. Thus, the flow is completely stabilized

by the sidewall inclination.

	= 0°	= 5.7°	= 11°
Flow ↓	**Flow** ↓	**Flow** ↓

(a) Re=30 (d) Re=30 (g) Re=30

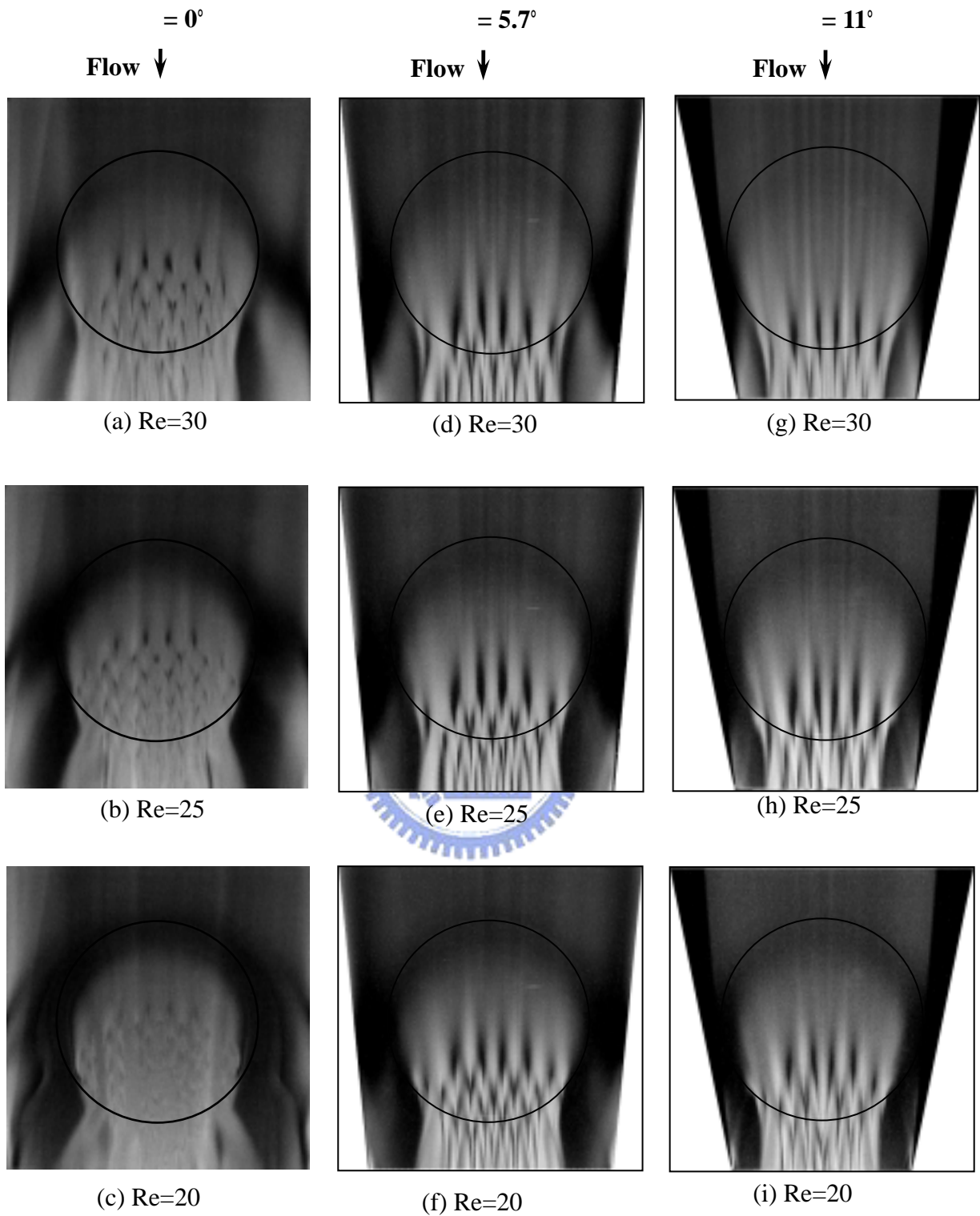(b) Re=25 (e) Re=25 (h) Re=25

(c) Re=20 (f) Re=20 (i) Re=20

Fig. 3.1 Top view flow photos of longitudinal vortex flow taken at the middle horizontal plane y = 1/2 at steady or statistical state in the duct with the sidewalls inclined at different angles for Ra = 9,500 for various Reynolds numbers.
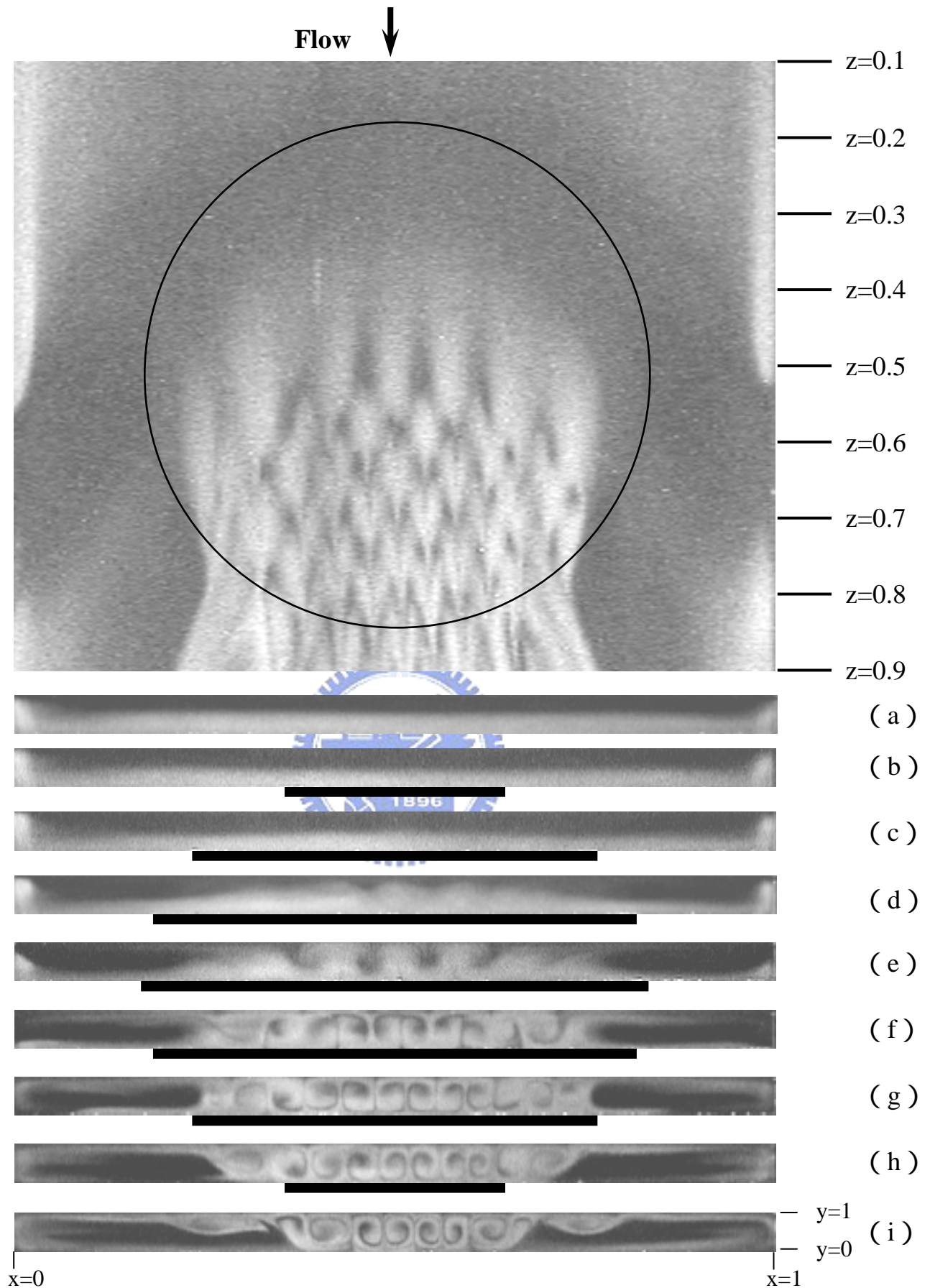
Fig. 3.2   Top and end view flow photos at steady state in rectangular duct (= 0°) for Re = 28.6 and Ra = 17,500 taken at the plane y = 1/2 and at the cross sections z = (a) 0.1, (b) 0.2, (c) 0.3, (d) 0.4, (e) 0.5, (f) 0.6, (g) 0.7, (h) 0.8 and (i) 0.9. (The dark bars right below the side view photos signify the location of the heated circular disk)

Flow ↓

z=0.1
z=0.2
z=0.3
z=0.4
z=0.5
z=0.6
z=0.7
z=0.8
z=0.9

(a)

(b)

(c)

(d)

(e)

(f)

(g)

(h)

(i)

Fig.3.3   Top and end view flow photos at steady state in convergent duct (= 11°) for Re = 27.8 and Ra = 17,600 taken at the plane y = 1/2 and at cross sections z = (a) 0.1, (b) 0.2, (c) 0.3, (d) 0.4, (e) 0.5, (f) 0.6, (g) 0.7, (h) 0.8 and (i) 0.9. (The dark bars right below the side view photos signify the location of the heated circular disk)
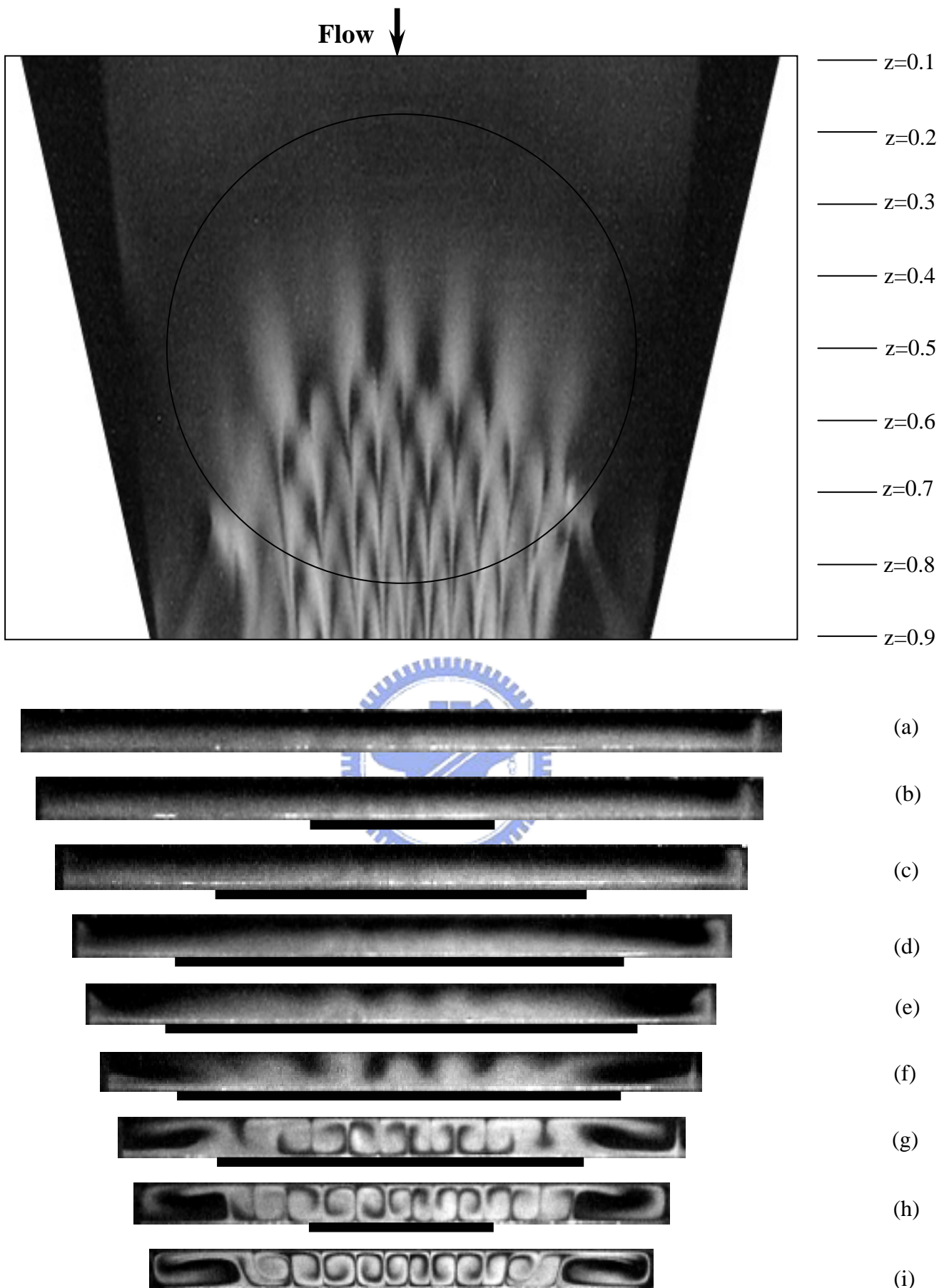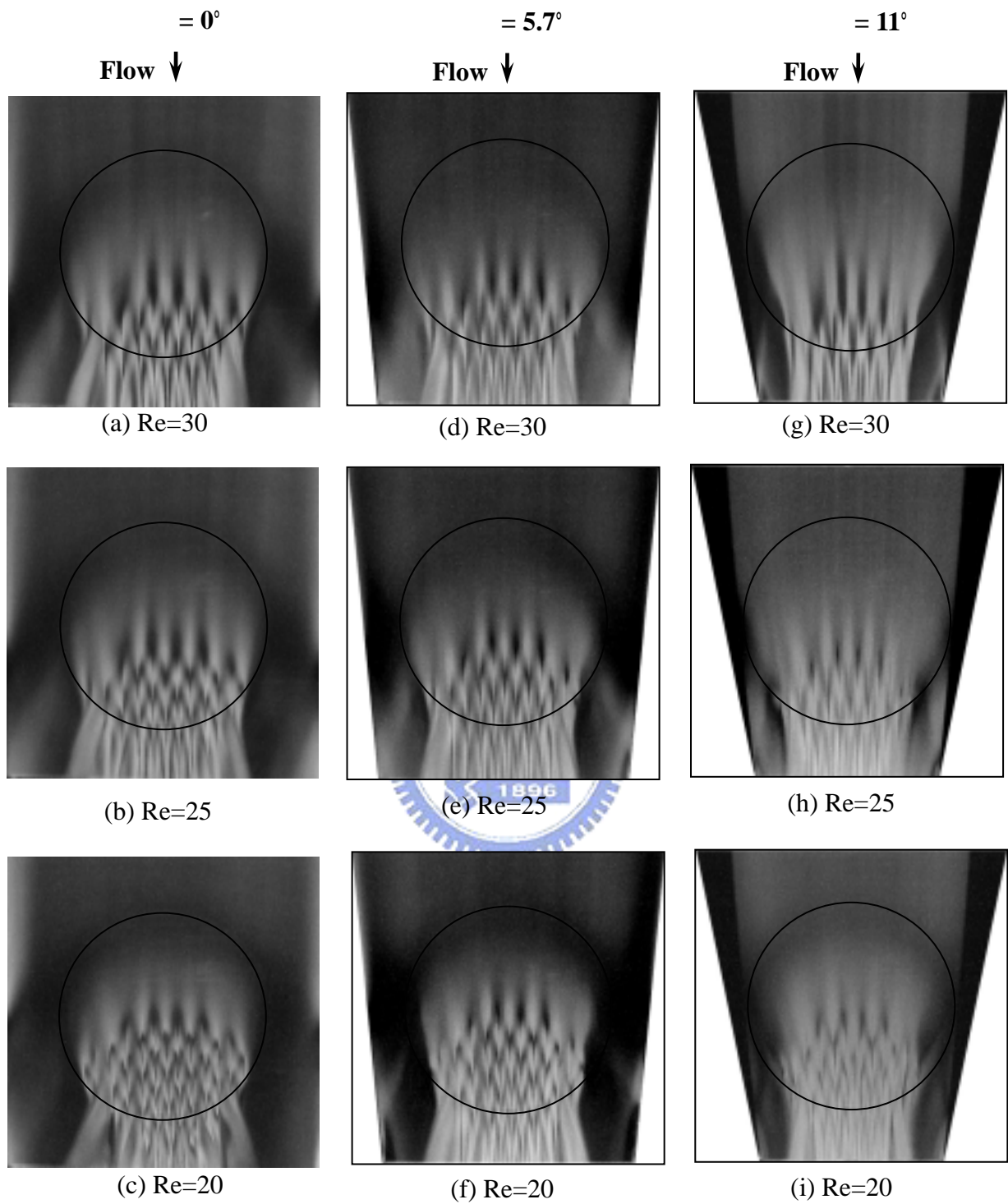
Fig. 3.4   Top view flow photos of longitudinal vortex flow taken at the plane y = 1/2 at steady state or at certain time instant in statistical state in the duct with the sidewalls inclined at different angles for Ra = 13,800 for various Reynolds numbers.

Fig.3.5   Top view flow photo taken at the plane y = 1/2 (a) and side view flow photos taken at the planes: x = 0.5 (b), 0.4 (c), 0.3 (d), 0.2 (e) at statistical state for Re = 10.1 and Ra = 11,600 in rectangular duct (=0°). (The dark bars right below the side view photos signify the location of the heated circular disk)
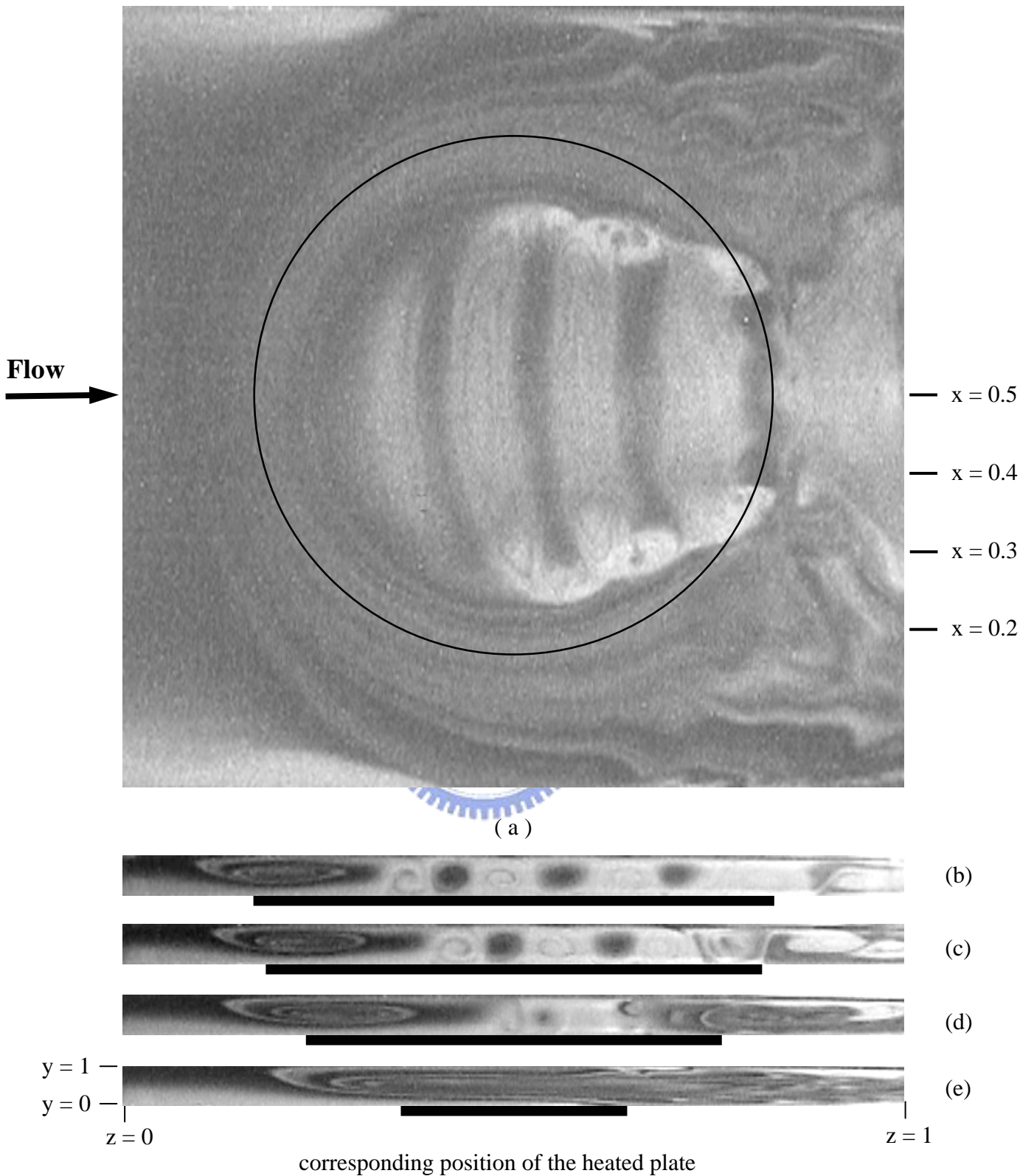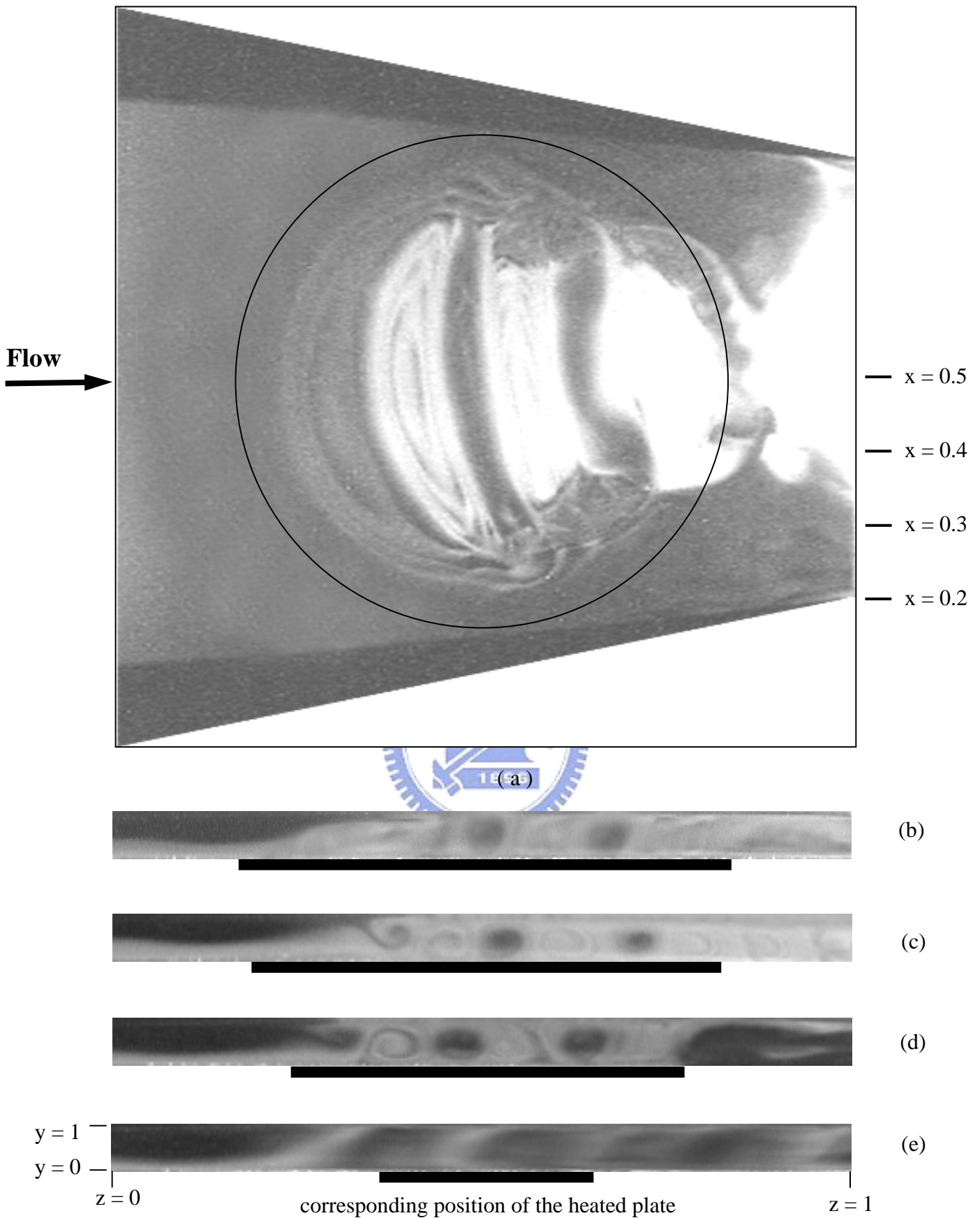
Fig. 3.6 Top view flow photo taken at the plane y = 1/2 (a) and side view flow photos taken at the planes: x = 0.5 (b), 0.4 (c), 0.3 (d), 0.2 (e) at statistical state for Re = 5.1 and Ra = 11,600 in convergent duct (=11°). (The dark bars right below the side view photos signify the location of the heated circular disk)

47

(a)

(b)

(c)

Onset

(d)

(e)

Flow

(f)

(g)

(h)

(i)

(j)

(k)

Fig 3.7   Side view flow photos taken at the middle vertical plane (x = 0.5) of the rectangular duct at Ra=11,600 for (a) Re=50, (b) Re=40, (c) Re=30, (d) Re=25, (e) Re=20, (f) Re=17.5, (g) Re=15 (h) Re=12.5, (i) Re=10, (j) Re=7.5, and (k) Re=5.

(a)

(b)

(c)

(d)

Onset
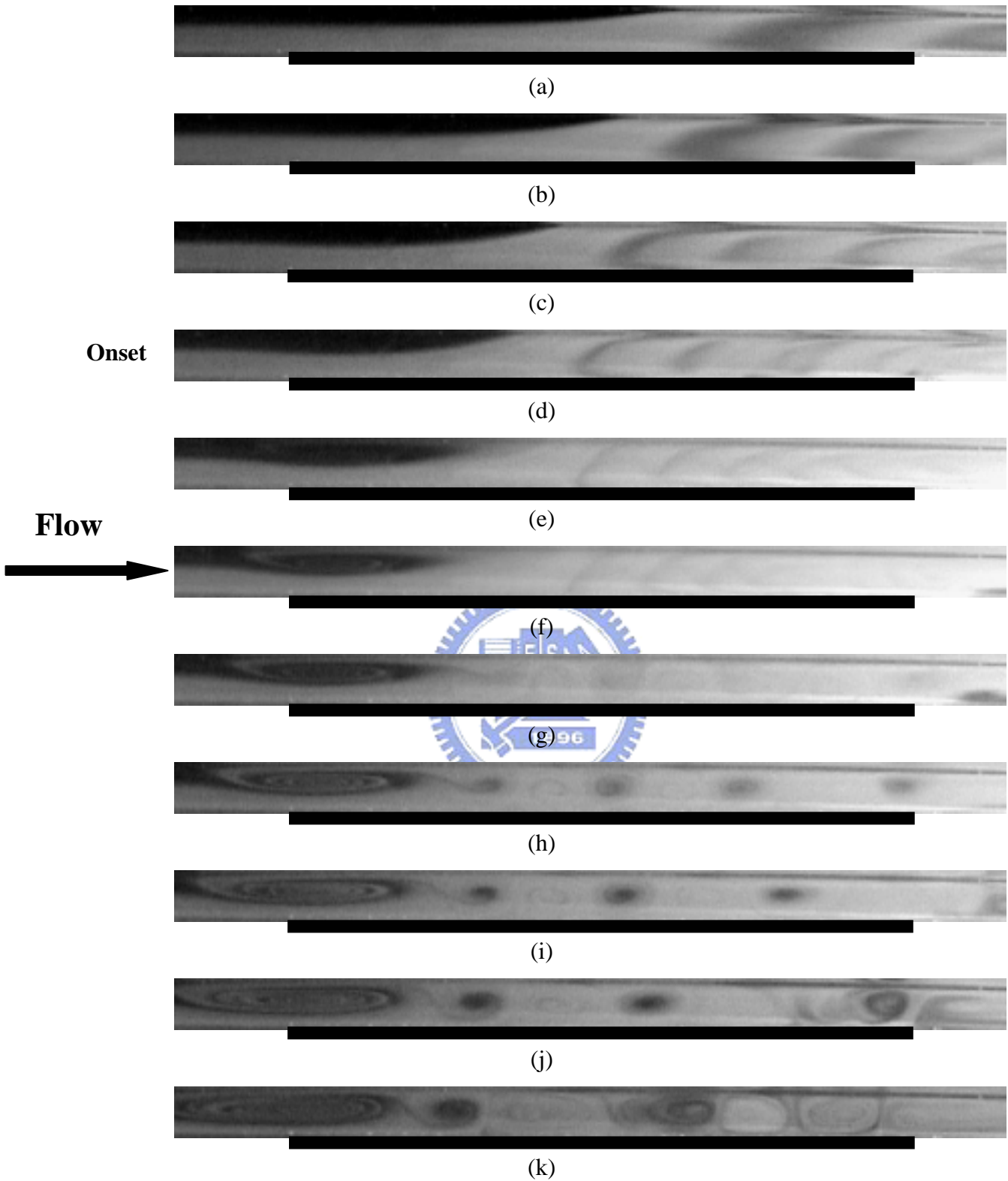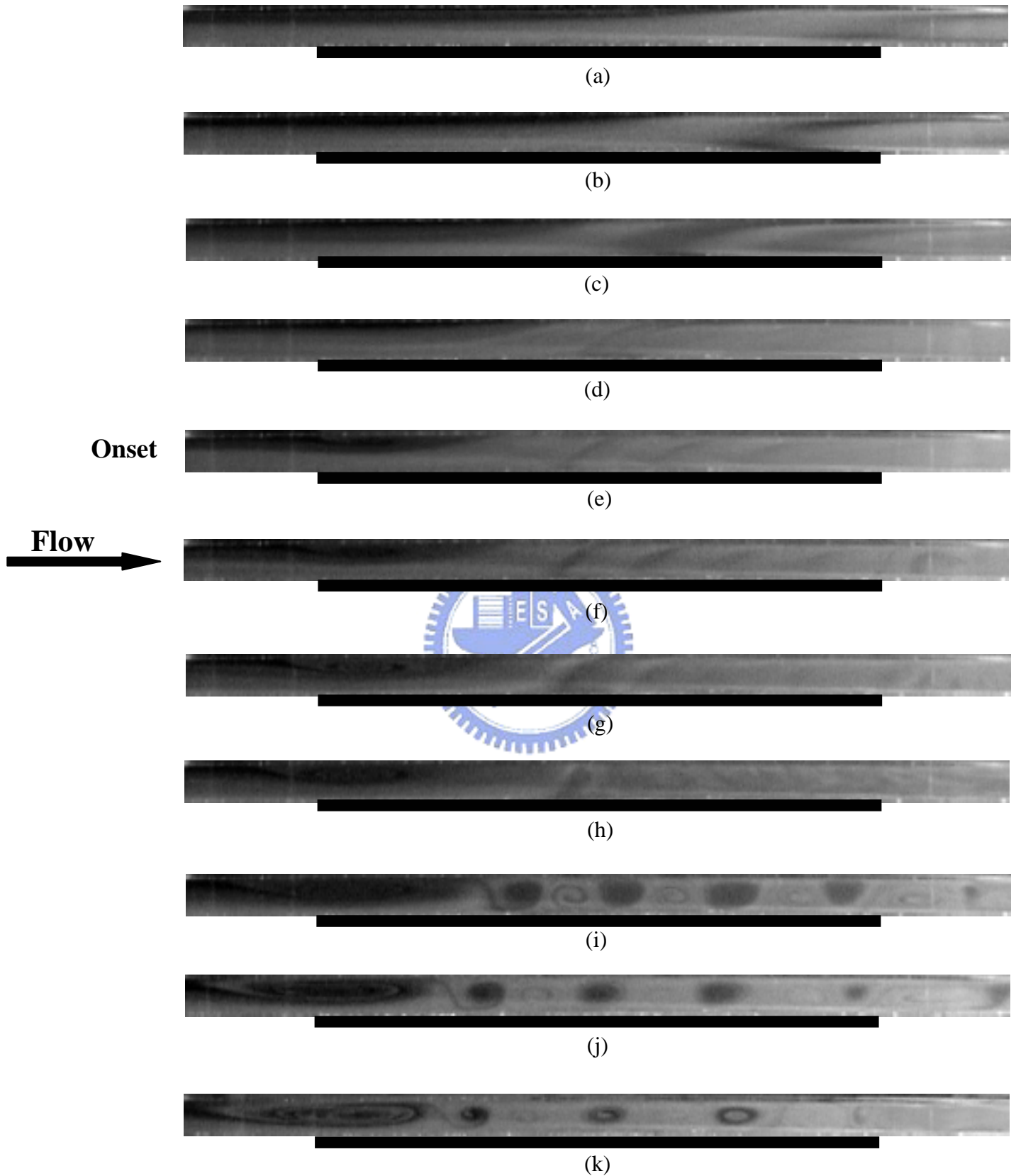
(e)

Flow →

(f)

(g)

(h)

(i)

(j)

(k)

Fig 3.8 Side view flow photos taken at the middle vertical plane (x = 0.5) of the sidewall inclined duct (=11°) at Ra=11,600 for (a) Re=50, (b) Re=40, (c) Re=30, (d) Re=25, (e) Re=18.4, (f) Re=17.5, (g) Re=15 (h) Re=12.5, (i) Re=10, (j) Re=7.5, and (k) Re=5.

49

= 0°

Flow   = 11°

(a) Re = 10

= 0°

Flow   = 11°

(b) Re = 7.5

= 0°

Flow   = 11°

Corresponding position of the heated plate

(c) Re = 5
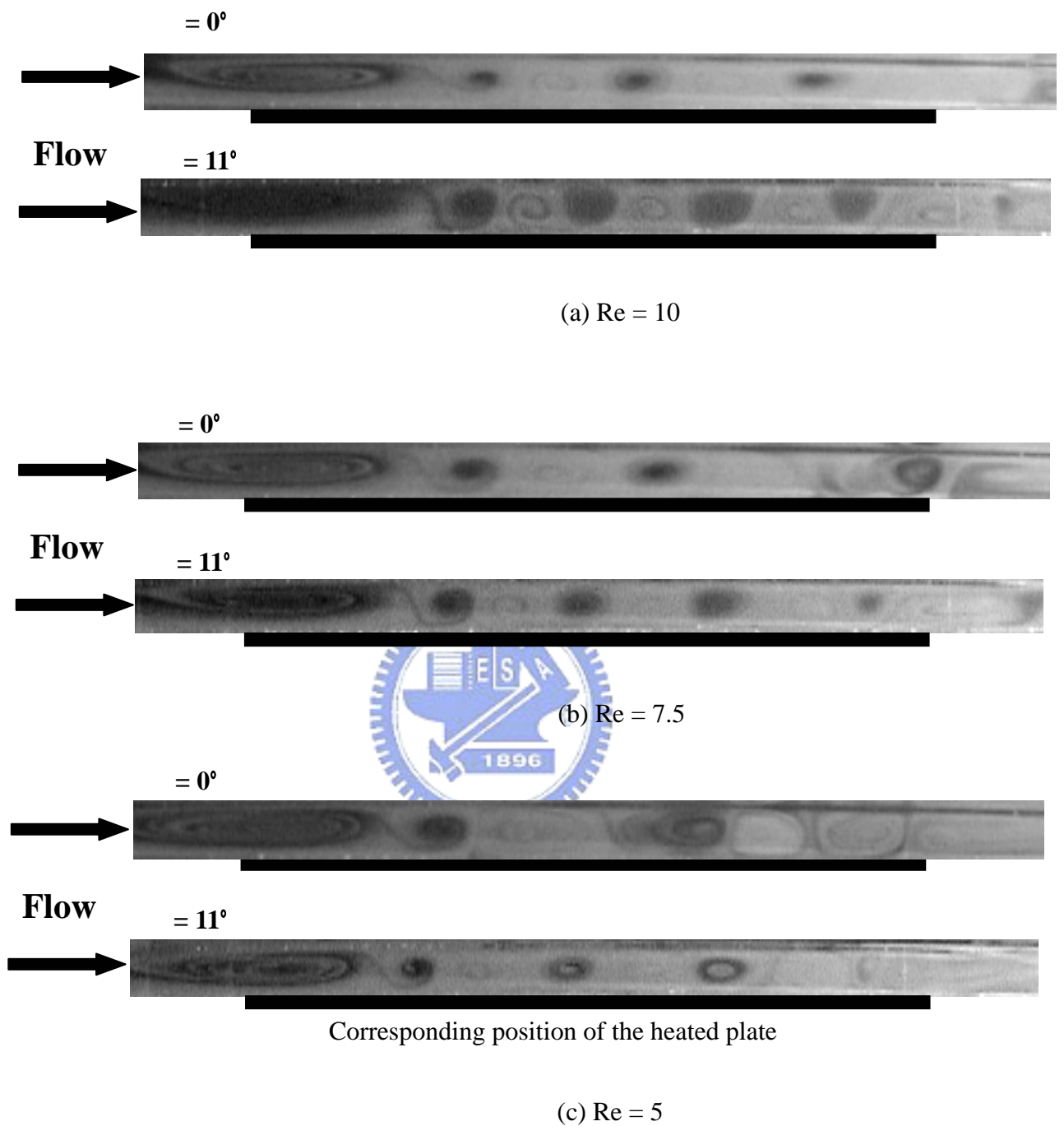
Fig 3.9   Side view flow photos taken at the vertical central plane x = 0.5 at steady or statistical state in the duct with   = 0°and 11° for Ra= 11,600 at Re = 10 (a), 7.5 (b), and 5(c). (The dark bars right below the side view photos signify the location of the heated circular disk)
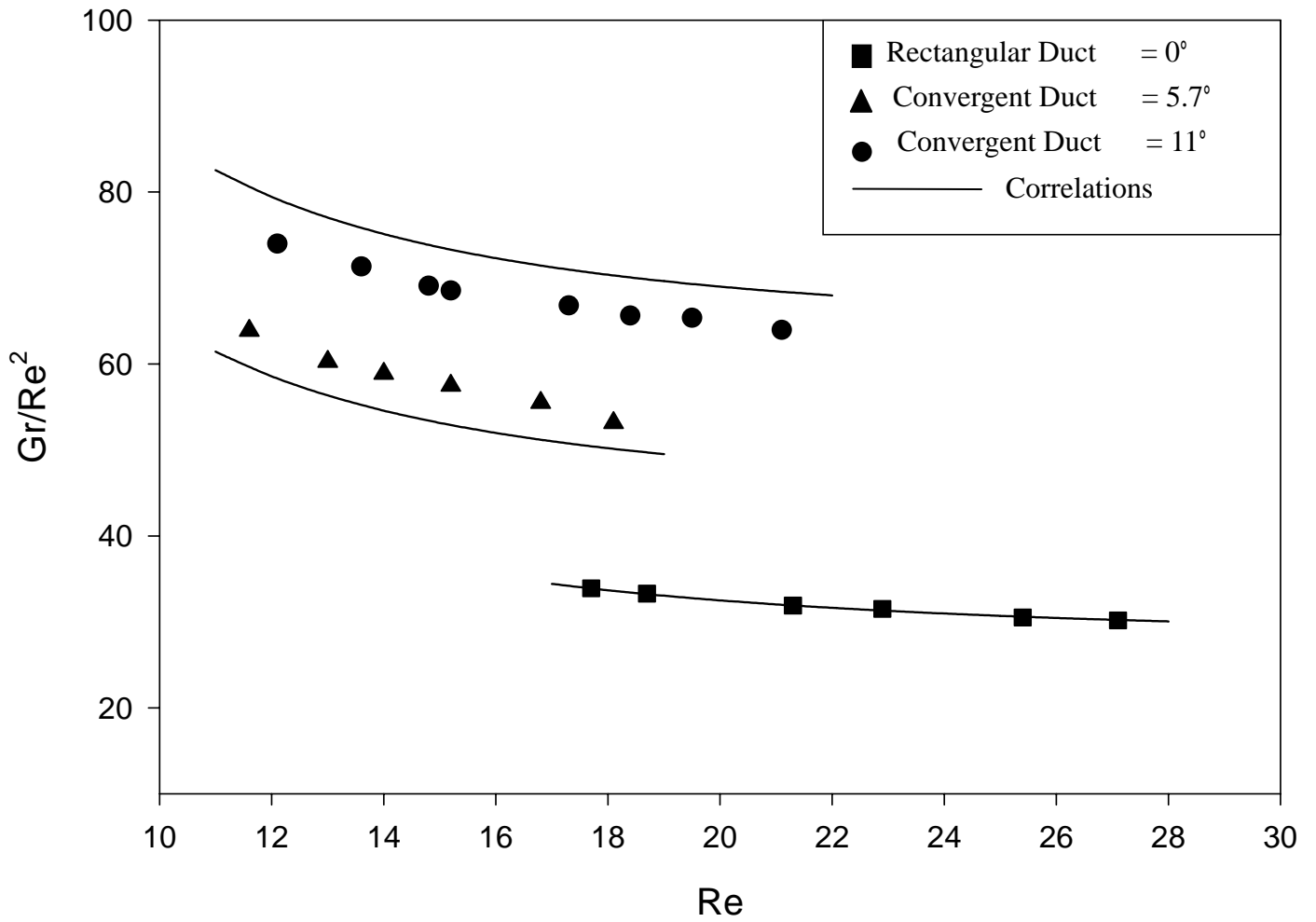
Fig 3.10　Critical conditions for the onset of return flow in the duct with　=0°, 5.5°and 11°.

(a) x=0.5

(b) x=0.4

(c) x=0.2
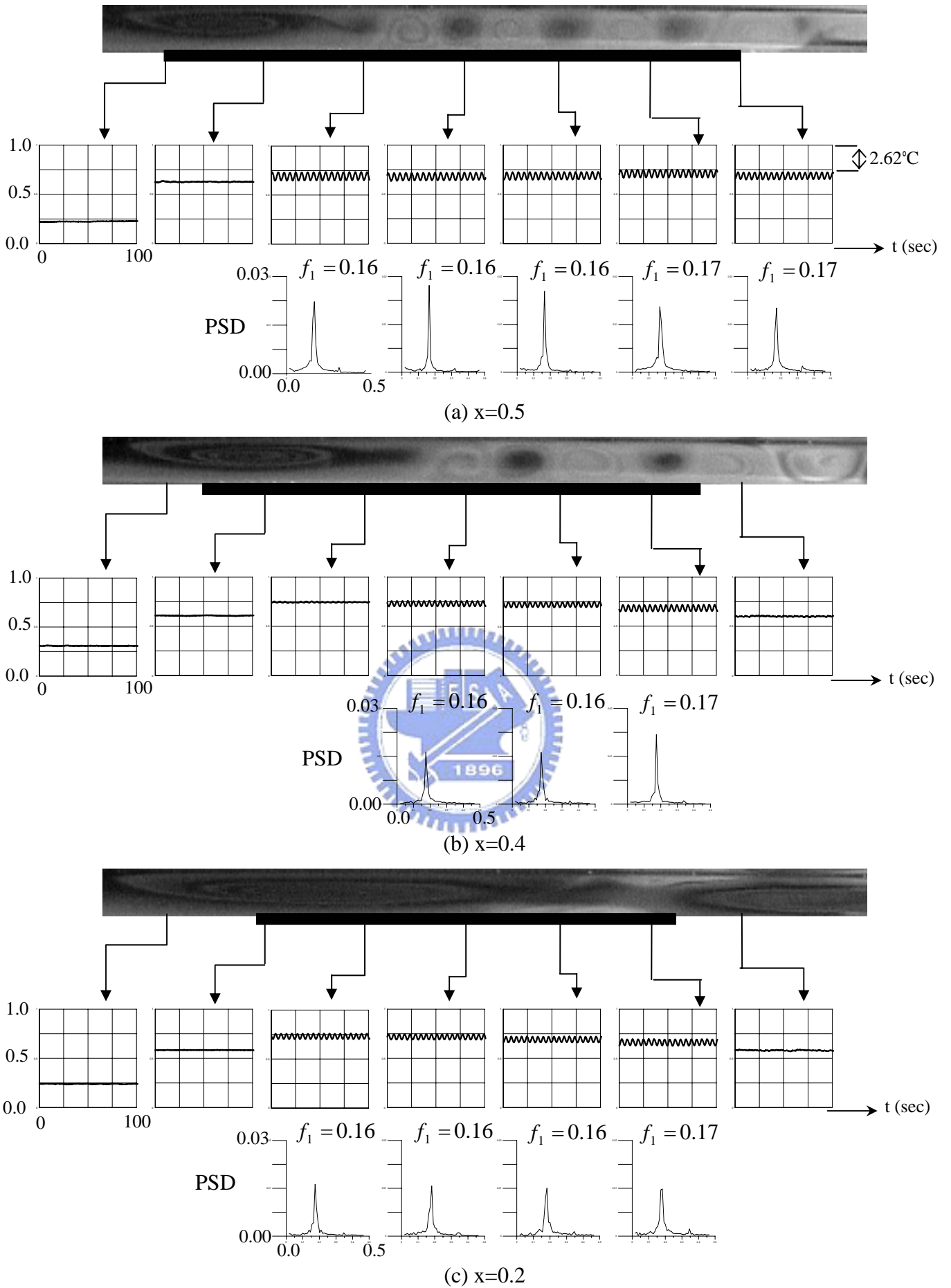
Fig. 3.11   Side view flow photos of vortex flow in rectangular duct at certain time instants in the statistical state and time records of air temperature at selected locations on the plane y=1/2 at x=0.5 (a), 0.4 (b) and 0.2 (c) for Re=10.1 and Ra=11,600. (The dark bars right below the side view photos signify the location of the heated circular disk)

52

(a) x=0.5

(b) x=0.4

(c) x=0.2

Fig. 3.12   Side view flow photos of vortex flow in the convergent duct (= 11°) at certain time instants at the statistical state and time records of air temperature at selected locations on the plane y=1/2 at x=0.5 (a), 0.4 (b) and 0.2 (c) for Re=10.1 and Ra=11,600. (The dark bars right below the side view photos signify the location of the heated circular disk)
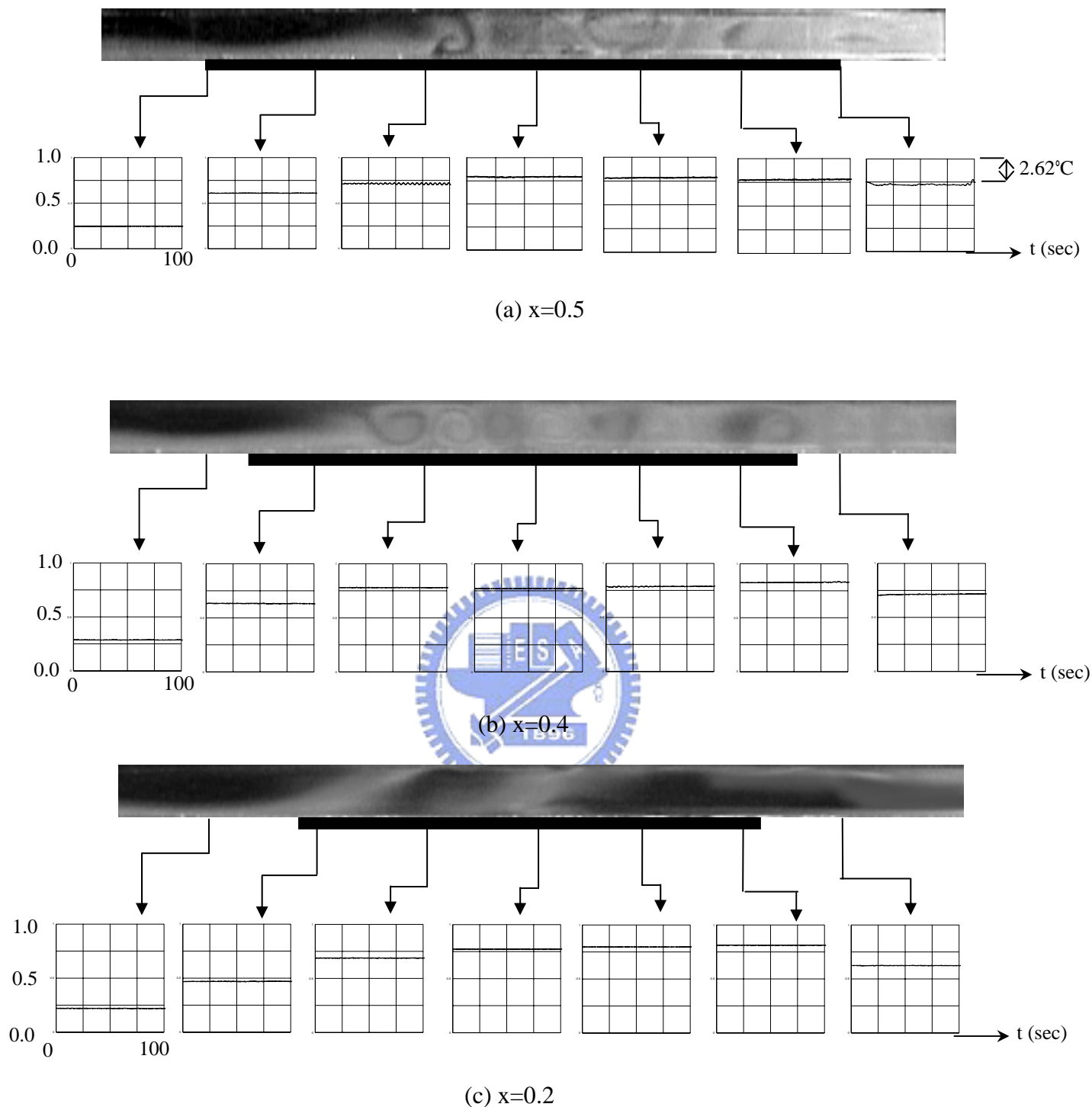
CHAPTER 4

EFFECTS OF DUCT INCLINATION ON BUOYANCY-DRIVEN SECONDARY FLOW

Results obtained in the second part of the present study are presented in this chapter to illustrate how the buoyancy driven vortex flow and return flow are affected by the slight inclination of the duct. Attention is focused on the effects of the slight duct inclination from horizontal on the longitudinal, transverse and mixed vortex flows. In this investigation the inclined angle of the duct measured from horizontal is varied from 0° to 2°, the Reynolds number of the flow ranges from 5 to 50, and the Rayleigh number varies from 7,200 to 21,000.
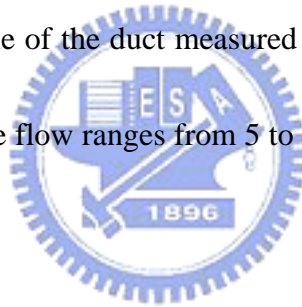
4.1 Vortex Flow Characteristics

To illustrate the influences of the duct inclination on the vortex flow, the long time top flow view photos taken at the middle horizontal plane y = 1/2 at steady or statistically stable state are shown in Figs. 4.1 and 4.2 for the horizontal duct (= 0°) and inclined duct (= 2°) at Ra =11,600 for various Reynolds numbers. The results indicate that at the low buoyancy-to-inertia ratios for high Reynolds numbers only some thermals are induced near the exit edge of the duct (Fig. 4.1(a) for Re=50 and Figs. 4.2(a) & (b) for Re 40). Note that at this low Gr/Re^2 the buoyancy driven thermals do not possess enough

54

momentum to rise to the top plate of the duct to form L-rolls. Apparently, it takes a

shorter axial distance for the thermals to be initiated for a higher Gr/Re^2. We further note

that only in the duct core the thermals are evenly spaced in the spanwise direction. The

thermals induced in the region near the duct sides are much weaker. They are slightly

unstable and irregular to a certain degree. As the Reynolds number is lower, the thermals

in the duct core evolve into L-rolls near the duct exit (Fig. 4.1(b) for Re=40 and Fig.

4.2(c) for Re= 30). For a further reduction of Re to 30 and 20 in the horizontal duct (Fig.

4.1) and for Re reduced to 25 and 15 in the inclined duct (Fig. 4.2), all the thermals

eventually evolve to L-rolls (Figs. 4.1(c)-(e) and Figs. 4.2(d)-(f)). Obviously, the onset

points of the L-rolls move upstream for a lower Re. At an even lower Re of 15 for = 0°

(Fig. 4.1) and lower Re of 10 & 5 for = 2° (Fig. 4.2), the buoyancy-to-inertia ratio is

very high and the vortex flow in the duct becomes somewhat irregular (Fig. 4.1(f) and

Figs. 4.2(g) & (h)). For a still lower Reynolds number with Re= 10 regular T-rolls

dominate in the horizontal duct (Fig. 4.1(g)). A close examination of the results in Fig.

4.1(g) discloses that the T-rolls are surrounded by an incomplete circular roll. The

circular roll is right above the edge of the heated circular plate and is open in the

downstream end of the duct. Besides, this circular roll becomes somewhat deformed in

the exit half of the duct. As the Reynolds number is further reduced to 5 the downstream

moving of the T-rolls is significantly blocked by the upward buoyancy from the heated
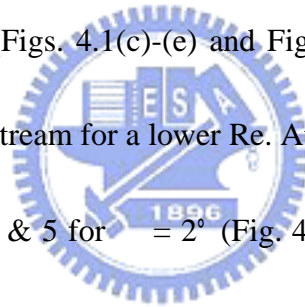
plate and the distortion of T-rolls is rather severe near the duct exit. A close inspection of

the corresponding flow photos in Figs. 4.1 and 4.2 reveals that a slight inclination of the

duct causes the delayed onset of the thermals, L-rolls and T-rolls. In the inclined duct

with   = 2°even when Re is lowered to 5 T-rolls do not appear at this high

buoyancy-to-inertia ratios. Additional comparison of the vortex flows in the two ducts is

shown in Figs. 4.3 and 4.4 for a higher Ra of 13,800. The results resemble those in Figs.

4.1 and 4.2 for a lower Ra. It is of interest to note from comparing the results in Figs.

4.3(f) and 4.4(f) that the unstable deformed L-rolls in the horizontal rectangular duct are

completely stabilized by the slight duct inclination to become relatively stable and

regular.

4.2 Return Flow Characteristics

To illustrate the return flow affected by the duct inclination, the side view flow photos

taken at the central vertical plane x = 0.5 at steady or statistically stable state for

Ra ≈ 11,600 at decreasing Re are presented in Figs. 3.7 and 4.5 respectively for   = 0°

and 2°. The detailed characteristics of the results given in Fig. 3.7 for the rectangular duct

have been examined in Chapter 3. Now for the duct inclined at   = 2°, the results in Fig.

4.5 clearly show that the return flow starts to appear at a lower Re of 12.3 (Fig. 4.5 (g)),

compared with Re = 25 in the horizontal duct at   = 0°. Thus, the relatively slight duct

inclination results in a substantial delay in the onset of the return flow. Besides, even for

the lower Re ($\leq$12.3) in the inclined duct the buoyancy induced return flow is much

weaker in intensity and smaller in size (Figs. 4.5 (g)-(h)) than that in the horizontal duct

(Figs. 3.7(i)-(k)). The weakening of the return flow by the duct inclination can be more

clearly demonstrated by comparing the sideview flow photos at the same Re and Ra for

the horizontal and inclined ducts. A close inspection of the results in Figs. 3.7 and 4.5

reveals that the reduction in the size of the return flow zone by the duct inclination is

more effective at a higher Re.

To further illustrate the effects of the inclined duct (= 1°) on the return flow, the

results for a lower Rayleigh number with Ra=7,500 are shown in Fig. 4.6. The return

flow is initiated at Re=9.5 (Fig. 4.6(g)) for the duct inclined at = 1°. At this lower Ra

the return flow is significant at the lower Reynolds numbers for 5.0 (Fig. 4.7 (k)) for the

horizontal duct (= 0°). Note that in the horizontal duct for the same Ra the return flow

is initiated at Re=17.5 (Fig. 4.7). At a slightly higher inclined angle of 2° the onset of the

return flow occurs at an even lower Re of 5.7, as evident from the flow photos shown in

Fig. 4.8. The suppression of the return flow by the duct inclination is also very significant

at this lower Rayleigh number. Then, the suppression of the return flow by the duct

inclination is illustrated by comparing the side view flow photos taken at the central

vertical plane shown in Figs. 4.9-4.11 for various at a higher Rayleigh number with
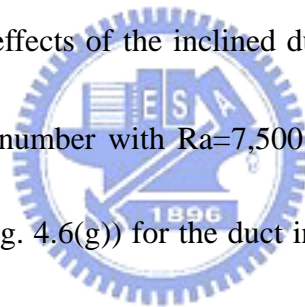
Ra=13,800.

This comparison discloses that when the duct inclination angle is increased from $\theta = 0°$ to $\theta = 2°$, the onset of the return flow is delayed from Re= 24.5 for $\theta = 0°$ to Re= 14.8 for $\theta = 1°$ and then to Re= 8.9 for $\theta = 2°$. Again Re= 14.8 to Re= 8.9 the return flow is significantly suppressed by the duct.

A close inspection of the results for Ra=7,500 and 13,800 reveals that the effects of the inclination duct on the return flow are more pronounced for the higher Rayleigh number.

Finally, it should be mentioned that the effects of the inclined duct on the buoyancy driven secondary flow in the duct are already illustrated by displaying the top view flow photos in Figs. 4.3   4.4 for Ra=13,800 at various Re in the inclined duct and the horizontal duct. The results clearly show the significant delayed onset of the longitudinal and transverse rolls by the duct inclination.

The stabilization of the longitudinal vortex flow by the duct inclination can be more clearly demonstrated by comparing the top view flow photos and time records of the air temperature at selected locations for the two ducts in Figs. 4.12 and 4.13. Note that at the inclined angle of 2° the unstable, somewhat irregular vortex flow prevailed in the horizontal duct becomes completely regular and steady in the inclined duct. The delayed onset of the L-rolls by the duct inclination is significant, as already seen in the preceding
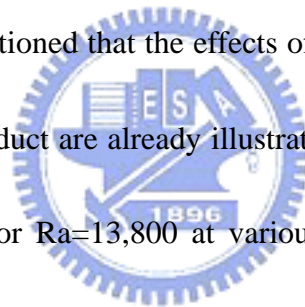
section.

4.3 Flow Regime Map

The results presented above can be summarized in the following. The longitudinal

vortex flow patterns observed in the present study for the inclined duct (= 2°) consist of

include the thermals, steady L-rolls, inertia and buoyancy driven unstable L-rolls and

irregular cells. A flow regime map is given in Fig. 4.14 to delineate the boundaries

separating various longitudinal vortex flow patterns in the inclined duct for = 2°. For

comparison, the flow regime map in the rectangular duct is also presented in Fig. 4.15.

This comparison indicate that at high Re and low Ra the thermals are suppressed by the

inclined duct and the flow becomes uni-directional. Similarly, the duct inclination can

cause the regular L-rolls to become thermals and deformed unstable L-rolls to become

regular L-rolls. It is also noted that the inertia driven unstable L-rolls and thermals

dominate over smaller ranges of Re and Ra in the inclined duct. Besides, the steady

L-rolls can exist at slightly higher buoyancy-to-inertia ratios in the inclined duct.

4.4 Critical Conditions for Onset of Return Flow

According to the data from the present experiment, the critical conditions for the

onset of the return flow in the horizontal duct (= 0°) and in the inclined duct (=1° & 2°)
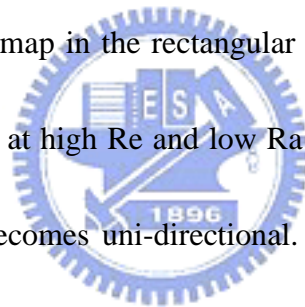
are plotted in Fig. 4.16. The results clearly show the significant increase in the critical

buoyancy-to-inertia ratio for the onset of the return flow by the duct inclination.

According to the present experimental data, the onset of the return flow driven by the

circular heated disk embedded in the convergent duct can be correlated as:

$$Gr/Re^2 = (a+b/Re^2)/\cos(0.02\phi) \qquad\qquad (4.1)$$

where

$$a=27.5(0.2\phi+1)^5 \qquad\qquad b=2000(0.44\phi+1)^{2.5}$$

The standard deviation of the above correlation is less than 10%.

The above equation is applicable for inclined duct at $\phi=0°$, 1°and 2°and for the Reynolds

and Rayleigh numbers at the duct inlet ranging respectively from 5.0 to 50.0 and

from 7,200 to 21,000.
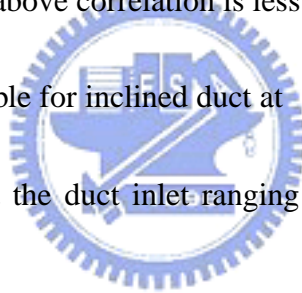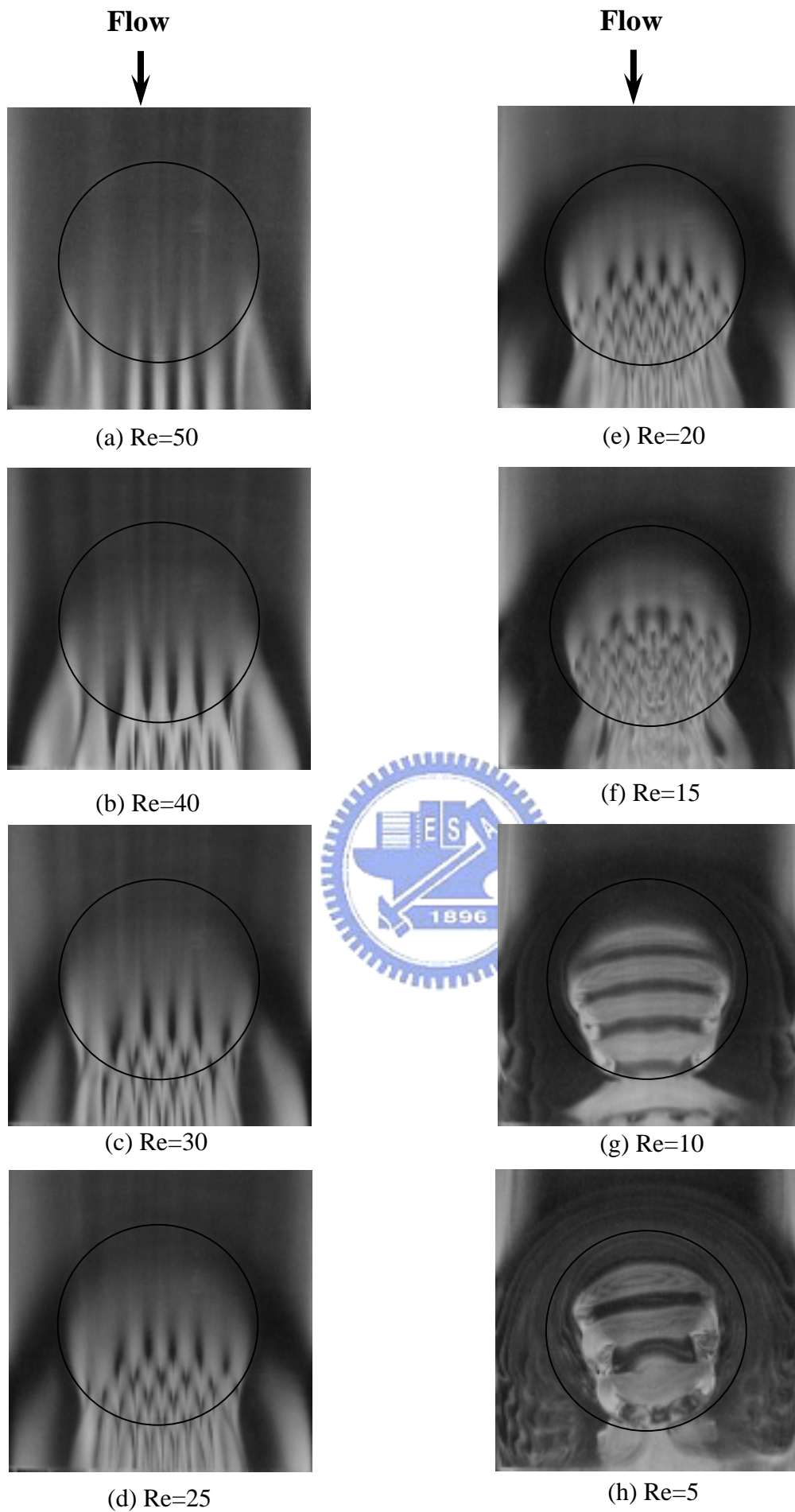
Fig 4.1 Top view flow photos taken at the middle horizontal plane y = 1/2 at steady or statistical state in the horizontal duct (= 0°) for Ra =11,600 at (a) Re = 50, (b) Re = 40, (c) Re = 30, (d) Re = 25, (e) Re = 20, (f) Re = 15, (g) Re = 10, and (h) Re = 5.
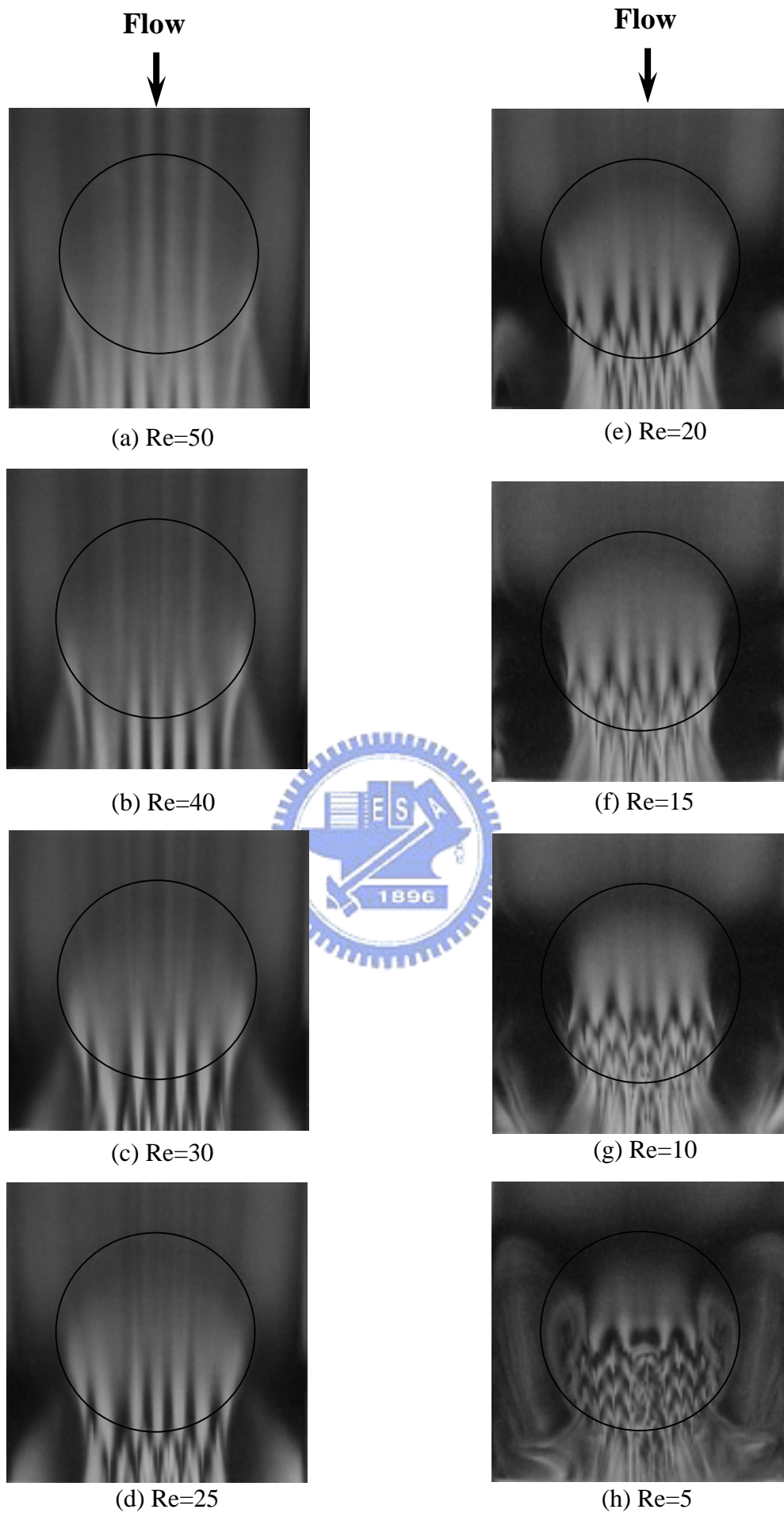
Fig. 4.2   Top view flow photos taken at the middle horizontal plane y = 1/2 at steady or statistical
state in the inclined duct (=2°) for Ra =11,600 at (a) Re = 50, (b) Re = 40, (c) Re = 30,
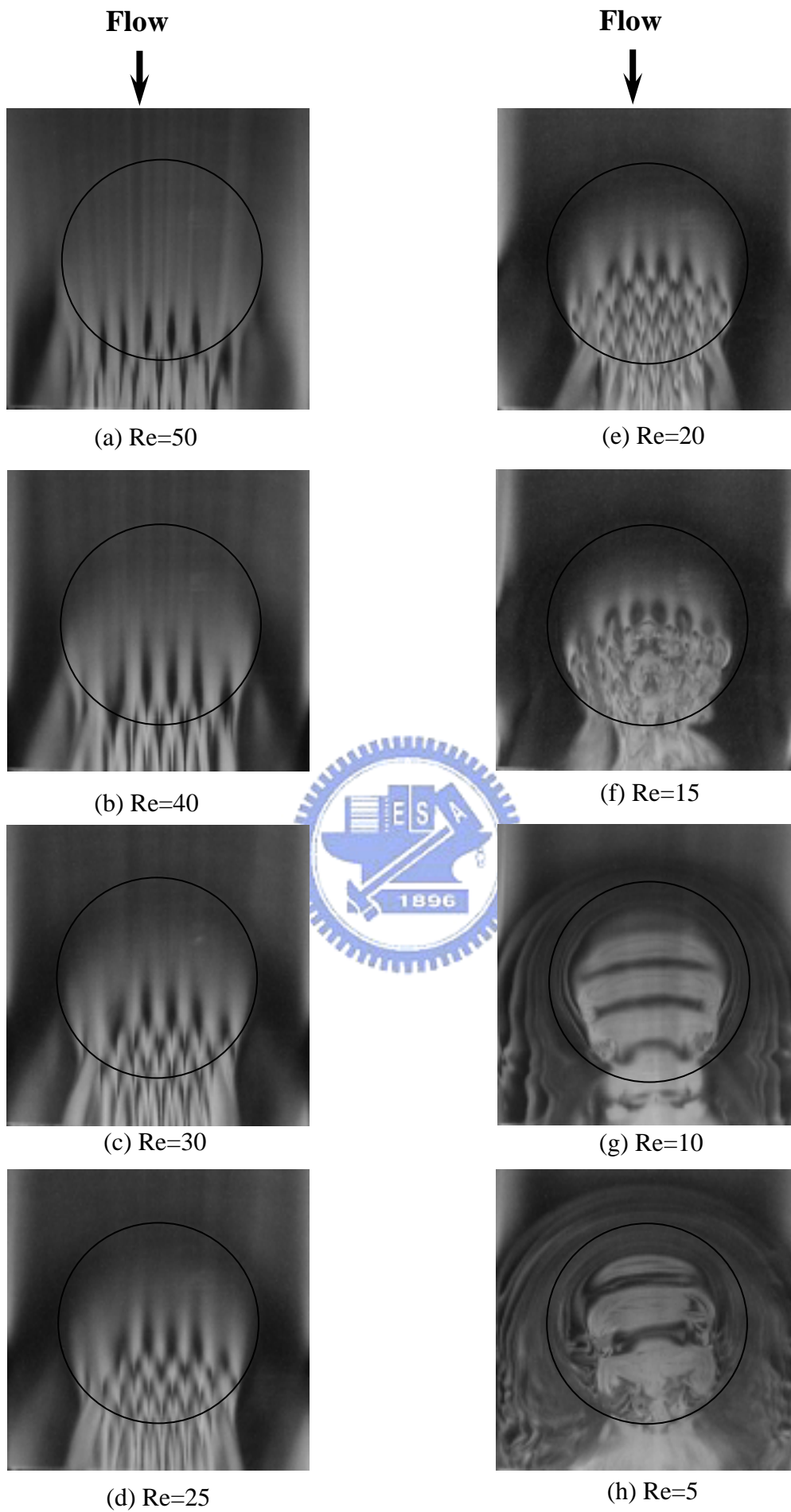(d) Re = 25, (e) Re = 20, (f) Re = 15, (g) Re = 10, and (h) Re = 5.

Fig. 4.3   Top view flow photos taken at the middle horizontal plane y = 1/2 at steady or statistical
state in the horizontal duct (= 0°) for Ra =13,800 at (a) Re = 50, (b) Re = 40, (c) Re =
30, (d) Re = 25, (e) Re = 20, (f) Re = 15, (g) Re = 10, and (h) Re = 5.

(a) Re=50

(e) Re=20
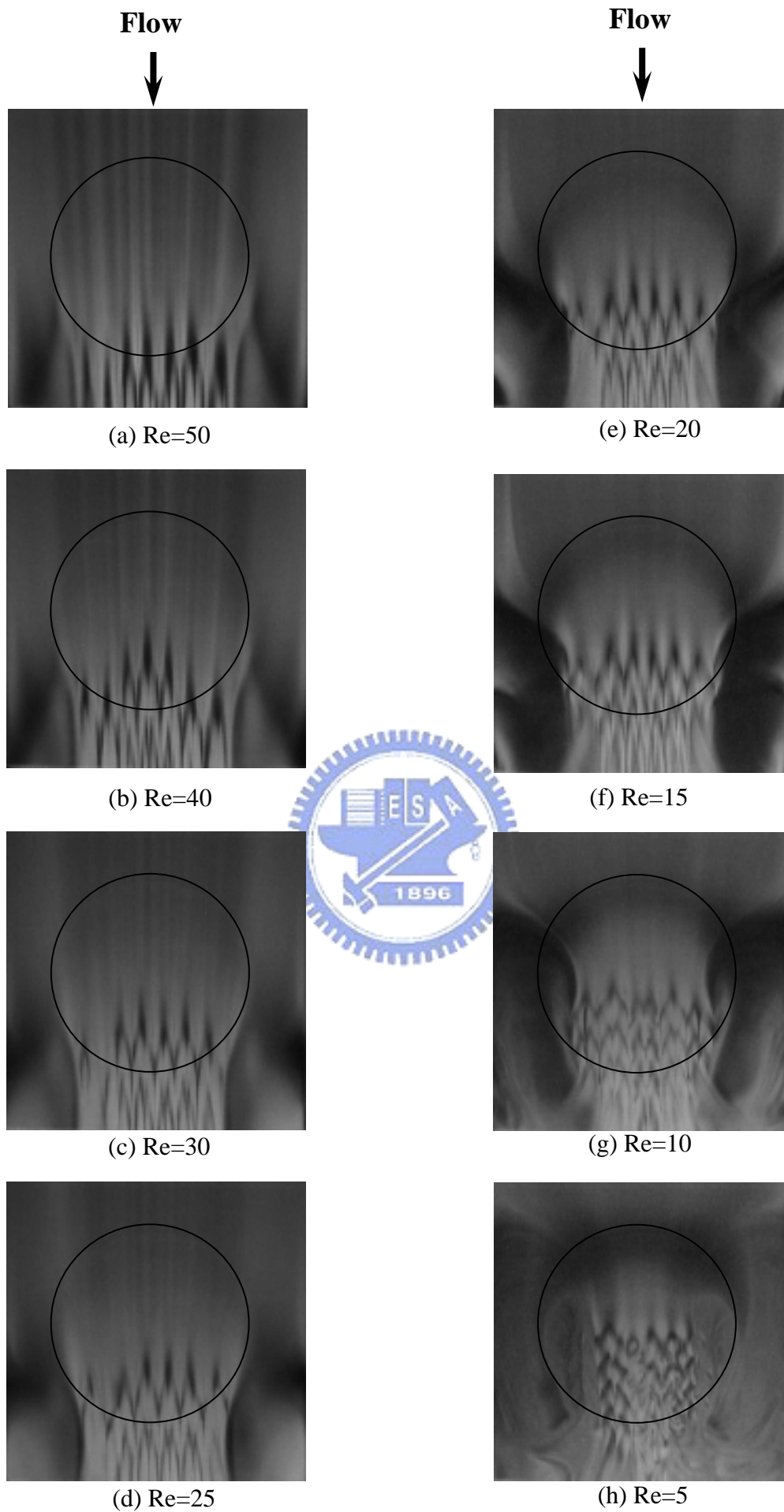
(b) Re=40

(f) Re=15

(c) Re=30

(g) Re=10

(d) Re=25

(h) Re=5

Fig. 4.4   Top view flow photos taken at the middle horizontal plane y = 1/2 at steady or statistical
state in the inclined duct (=2°) for Ra =13,800 at (a) Re = 50, (b) Re = 40, (c) Re = 30,
(d) Re = 25, (e) Re = 20, (f) Re = 15, (g) Re = 10, and (h) Re = 5.

64

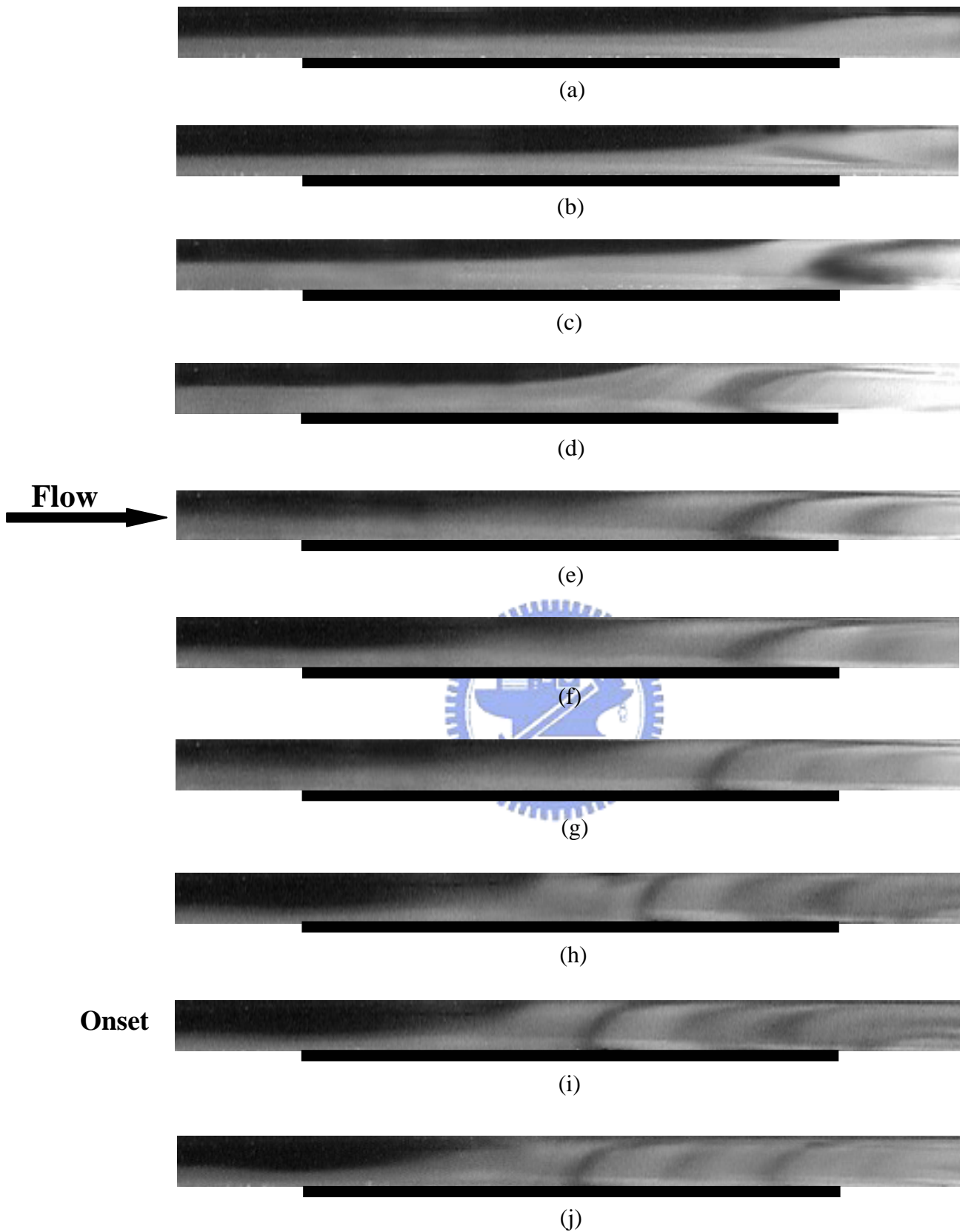Fig 4.5 Side view flow photos taken at the central vertical plane (x = 0.5) in the inclined duct (= 2°) at Ra=11,600 for (a) Re=50, (b) Re=40, (c) Re=30, (d) Re=25, (e) Re=20, (f) Re=17.5, (g) Re=15, (h) Re=12.5, (i) Re=7.8, and (j) Re=5.

Flow

Onset

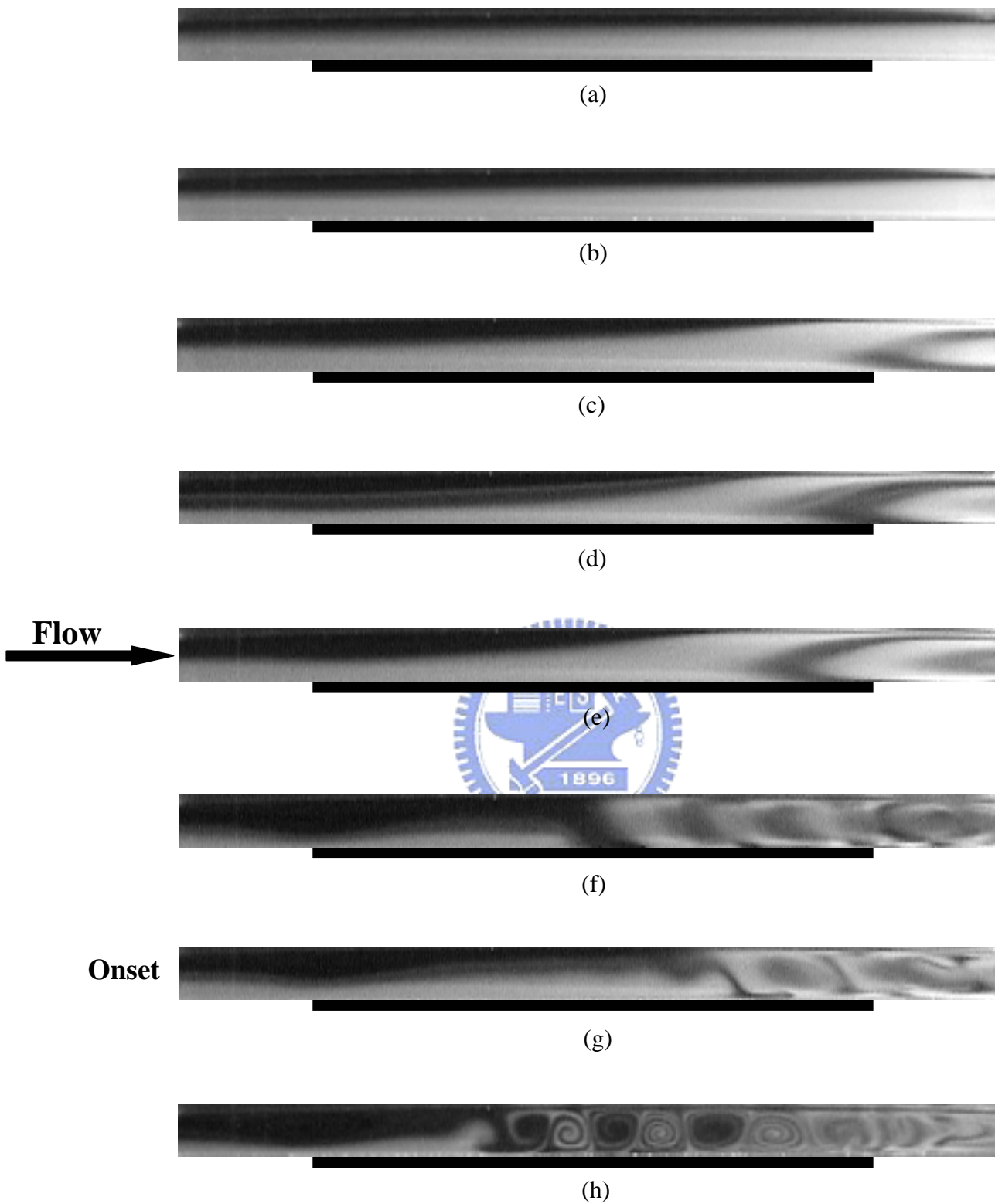Fig. 4.6   Side view flow photos taken at the central vertical plane (x = 0.5) in the inclined duct (= 1°) at Ra=7,500 for (a) Re=50, (b) Re=40, (c) Re=30, (d) Re=25, (e) Re=20, (f) Re=15, (g) Re=9.5, and (h) Re=5.
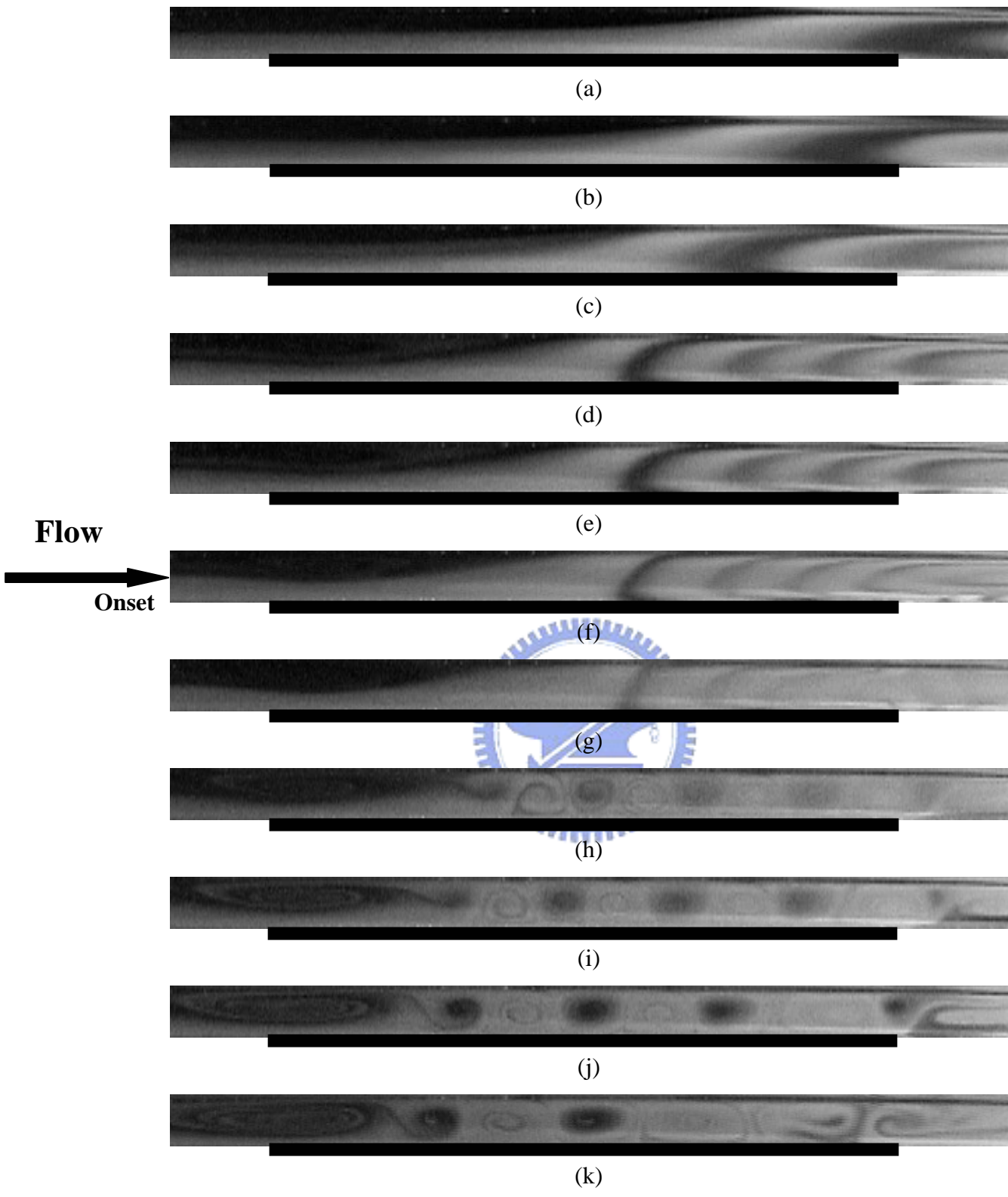
66

Flow →

Onset

Fig.4.7　Side view flow photos taken at the central vertical plane at steady or statistically stable state in the horizontal duct (= 0°) for Ra=7,500 at (a) Re=50.0, (b) Re=40.0, (c) Re=30.0, (d) Re=25, (e) Re=20.0, (f) Re=17.5, (g) Re=15.0 (h) Re=12.5, (i) Re=10.0, (j) Re=7.5, and (k) Re=5.0.

Fig. 4.8 Side view flow photos taken at the central vertical plane (x = 0.5) in the inclined duct (= 2°) at Ra=7,500 for (a) Re=50, (b) Re=40, (c) Re=30, (d) Re=25, (e) Re=20, (f) Re=15, (g) Re=10, and (h) Re=5.7.

Flow →

Onset

Fig.4.9   Side view flow photos taken at the central vertical plane (x = 0.5) for the horizontal duct (= 0°) at Ra=13,800 for (a) Re=50, (b) Re=40, (c) Re=30, (d) Re=25, (e) Re=24.5, (f) Re=15, (g) Re=12.3, and (h) Re=5.

69

Fig.4.10 Side view flow photos taken at the central vertical plane (x = 0.5) in the inclined duct
(= 1°) at Ra=13,800 for (a) Re=50, (b) Re=40, (c) Re=30, (d) Re=25, (e) Re=20,
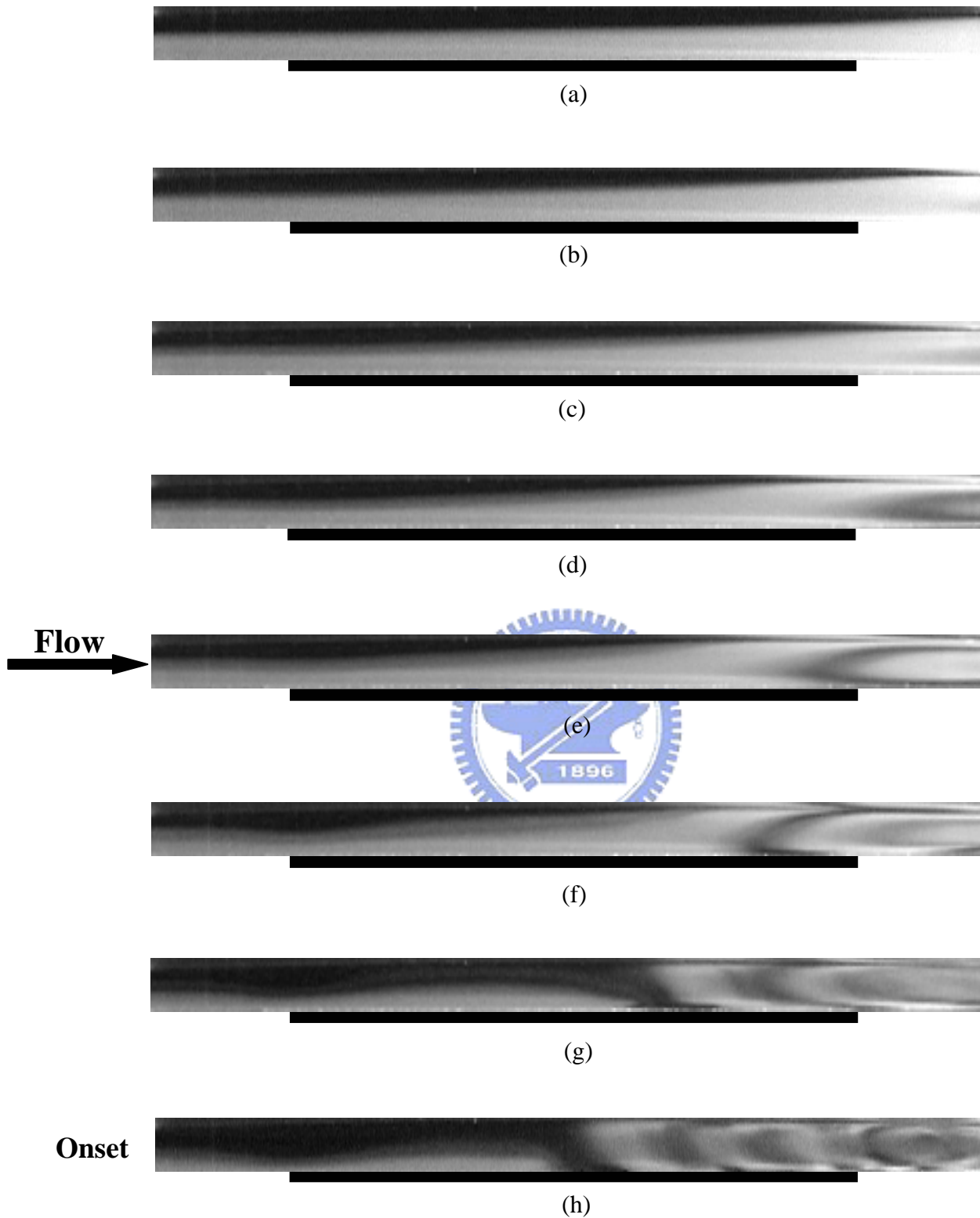(f) Re=15, (g) Re=14.8, and (h) Re=5.

Flow →

Onset
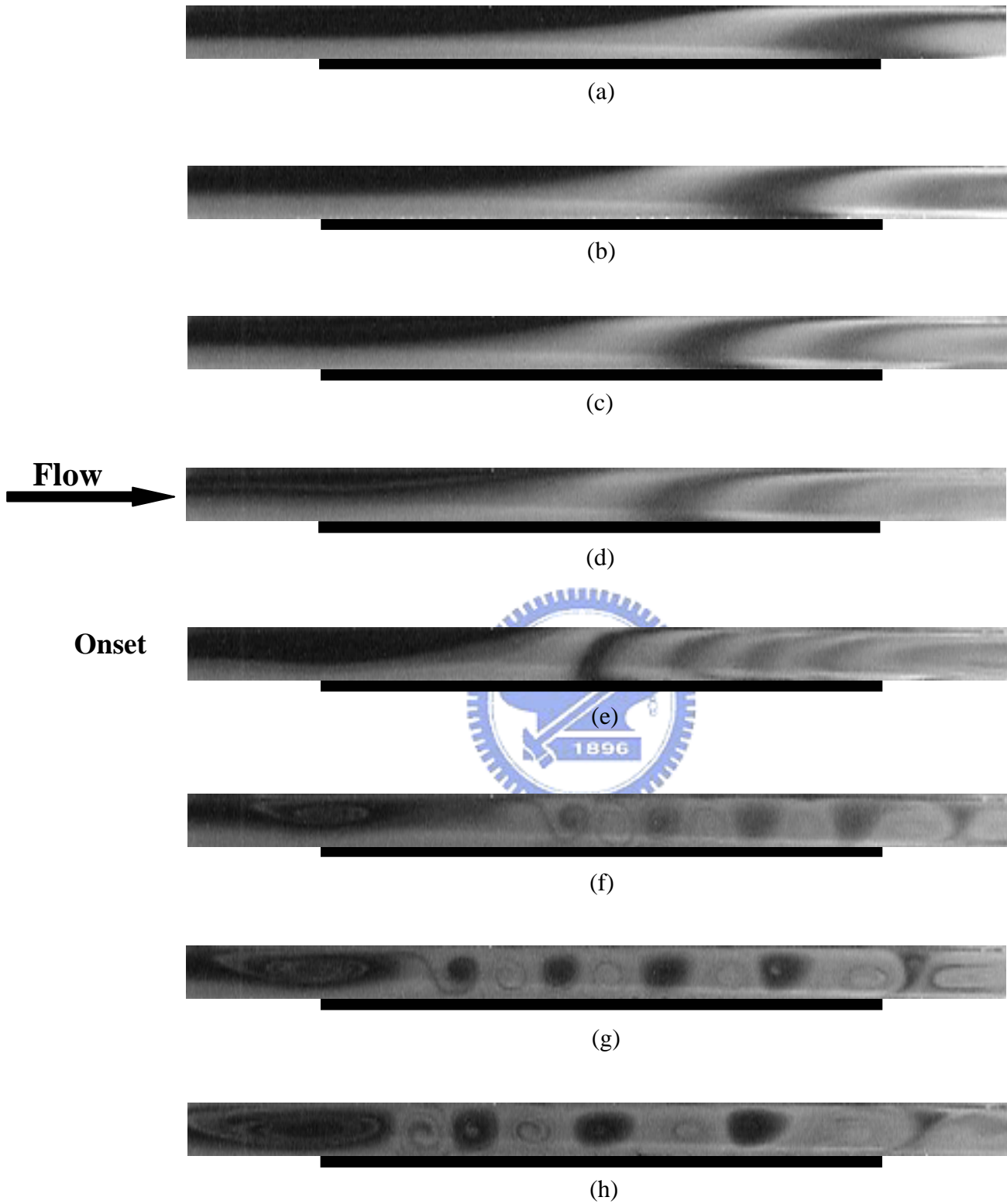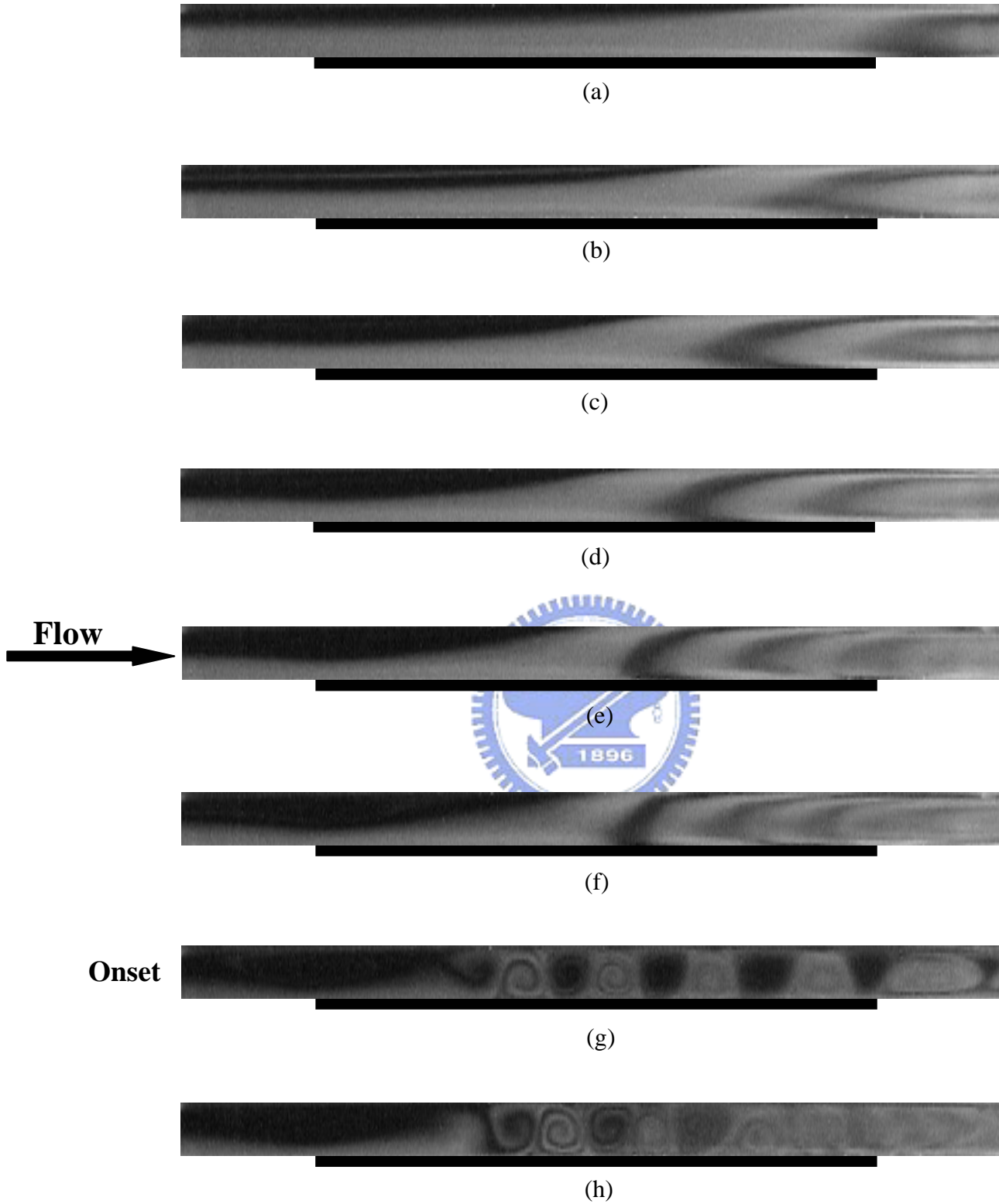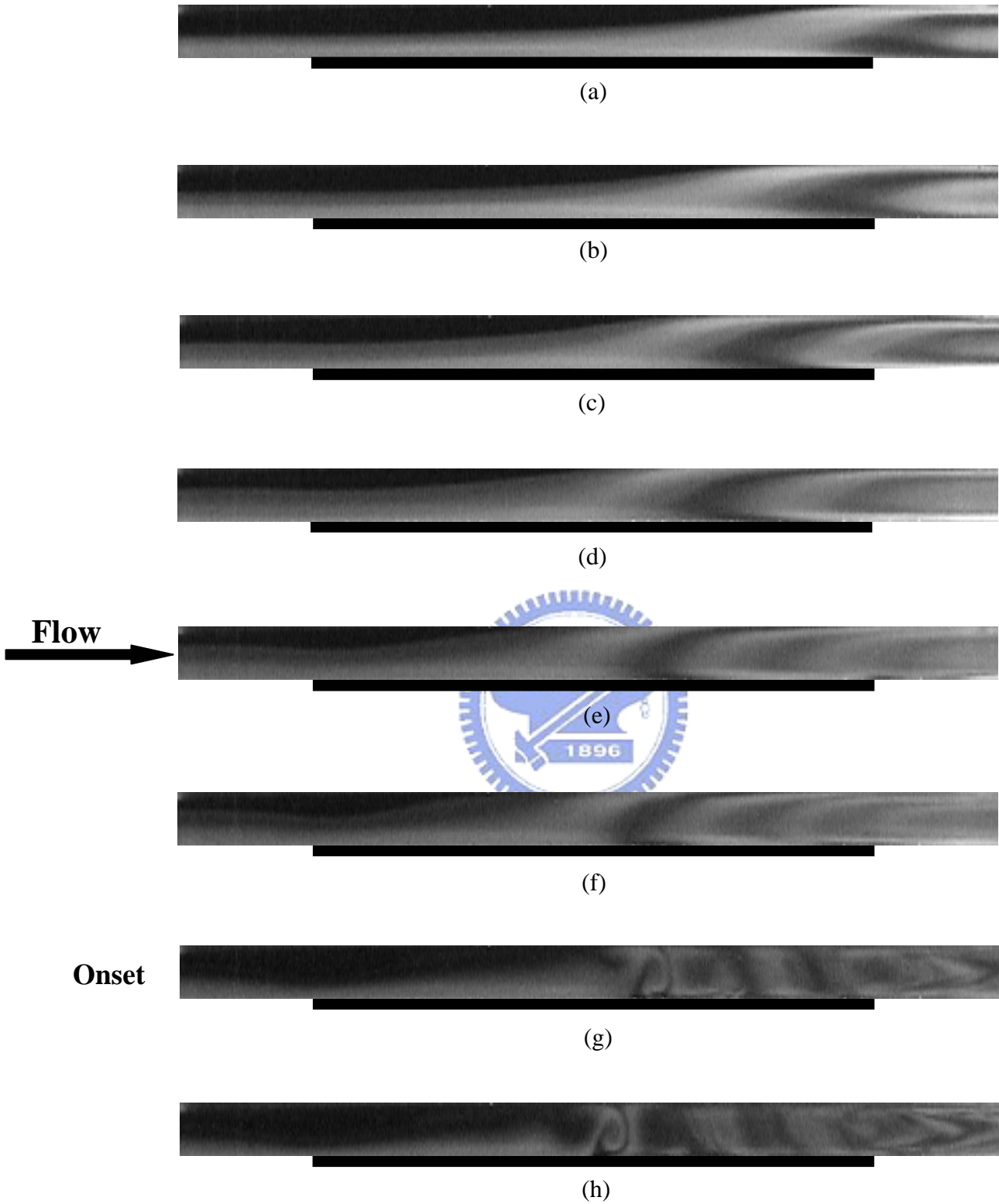
Fig.4.11   Side view flow photos taken at the central vertical plane (x = 0.5) in the inclined duct
(= 2˚) at Ra=13,800 for (a) Re=50, (b) Re=40, (c) Re=30, (d) Re=25, (e) Re=20,
(f) Re=15, (g) Re=8.9, and (h) Re=5.

71

z = 0.6 z = 0.8

Flow

x = 0.5

x = 0.4

x = 0.3

z = 0.5 z = 0.7 z = 0.9

(a)

0.9

1.05

0.7

x = 0.5

0.5

0.9

0.7

x = 0.4

0.5

0.9

0.7

x = 0.3

0.5

0

100

t   sec

z = 0.5   z = 0.6   z = 0.7   z = 0.8   z = 0.9

(b)
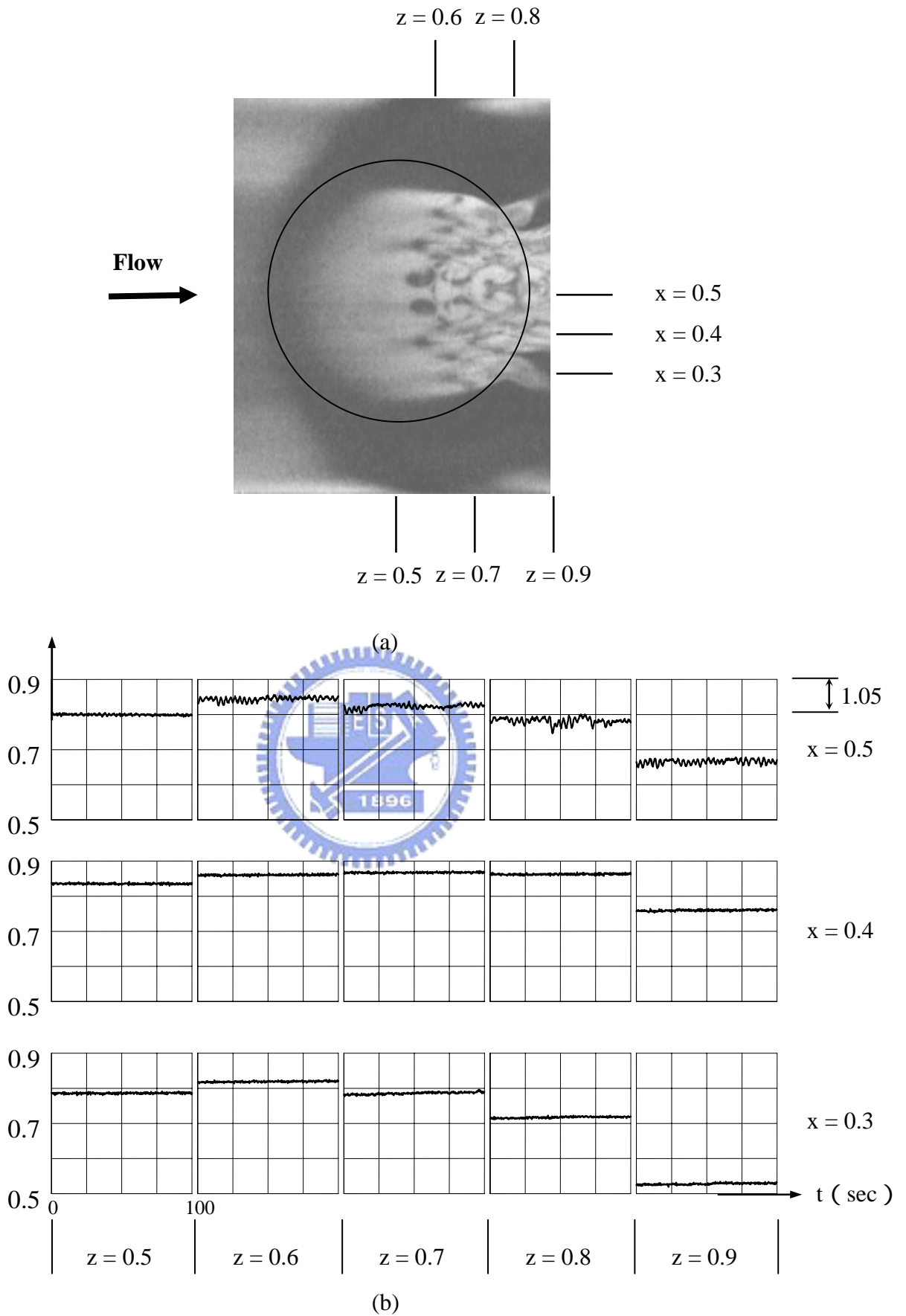
Fig. 4.12   Temporal structure of unsteady vortex flow in the horizontal duct (ϕ = 0°) illustrated by (a) top view photo taken at the middle plane y = 1/2 and (b) time records of air temperature at selected locations on the plane y = 1/2 at x = 0.5, 0.4 and 0.3 for Re = 15.1 and Ra = 10,500.

72

(a)

(b)
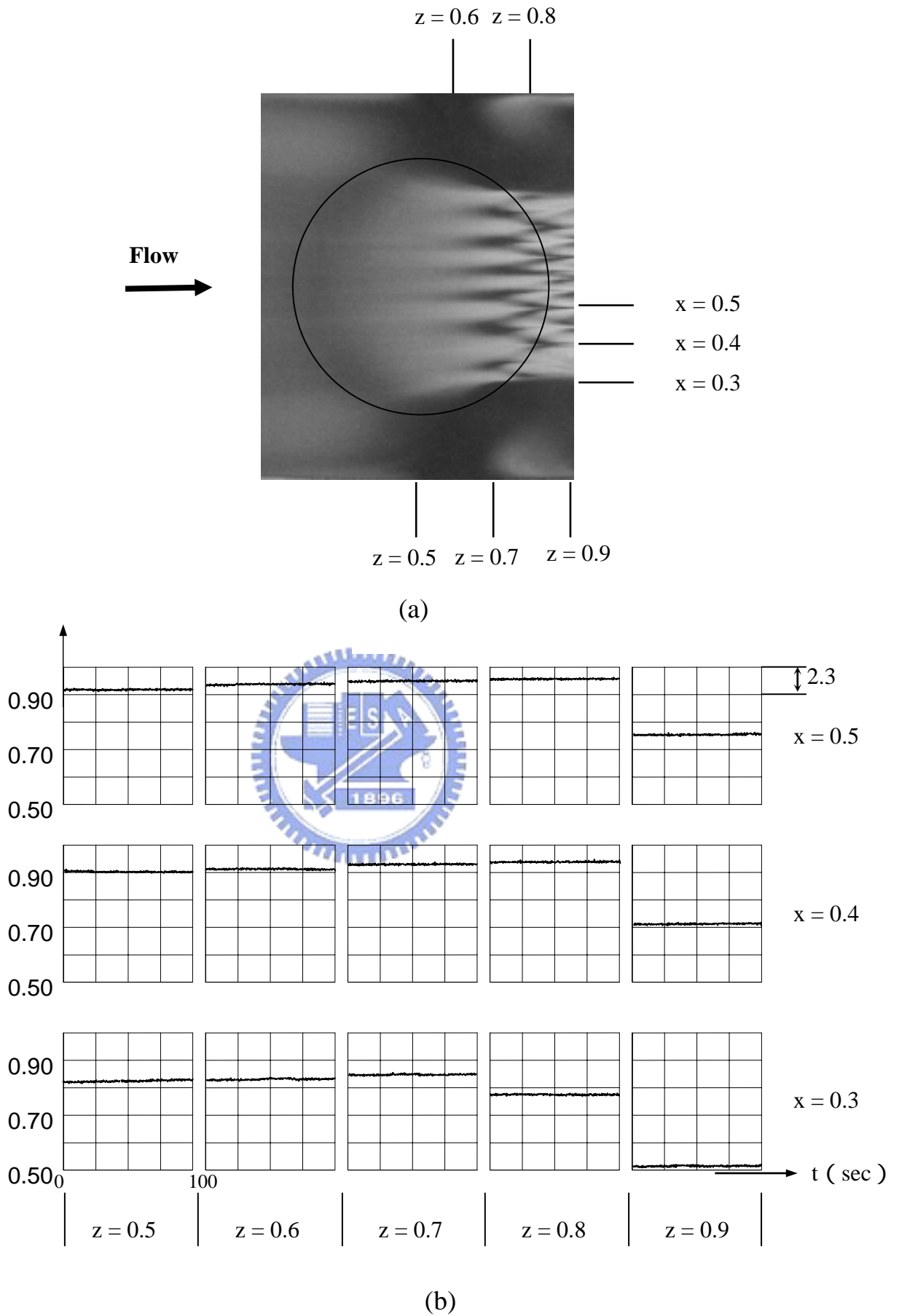
Fig. 4.13 Temporal structure of vortex flow in the duct inclination (= 2°) illustrated by (a) top view photo taken at the plane y = 1/2 and (b)time records of air temperature at selected locations on the plane y = 1/2 at x=0.5, 0.4 and 0.3 for Re = 15.3 and Ra = 10,500.

73
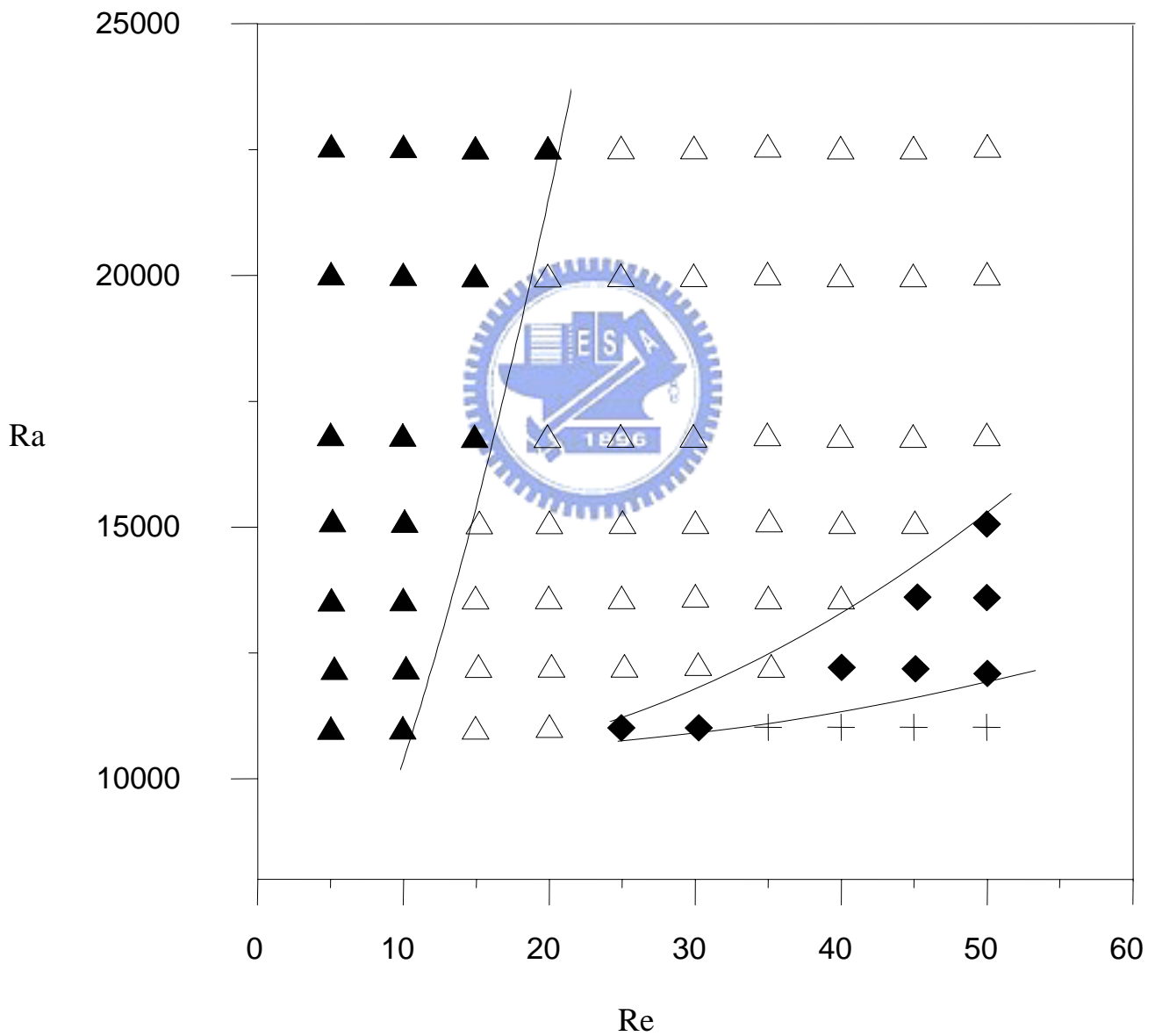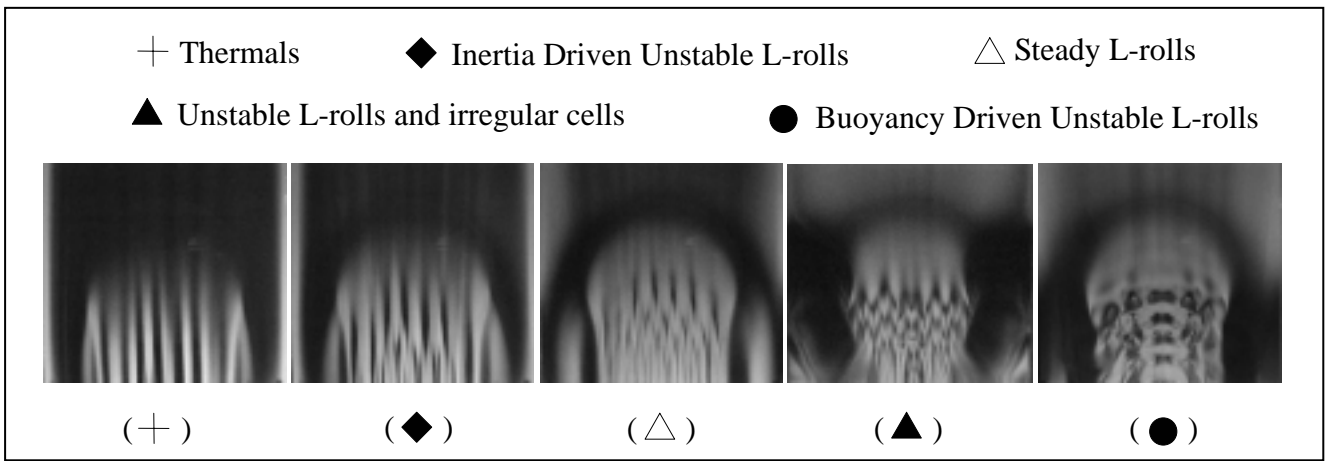
Fig.4.14   Flow regime maps delineating various longitudinal vortex flow patterns in the

inclined duct (= 2°).

Fig.4.15   Flow regime maps delineating various longitudinal vortex flow patterns in the

horizontal duct (= 0°).
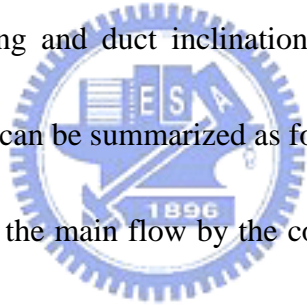
Fig 4.16   Critical conditions for the onset of return flow in the inclined duct with   =0°, 1°and 2°.

CHAPTER 5

CONCLUDING REMARKS

Experimental flow visualization and temperature measurement have been conducted here to explore the effects of the sidewall converging and the duct inclination on the buoyancy induced vortex flo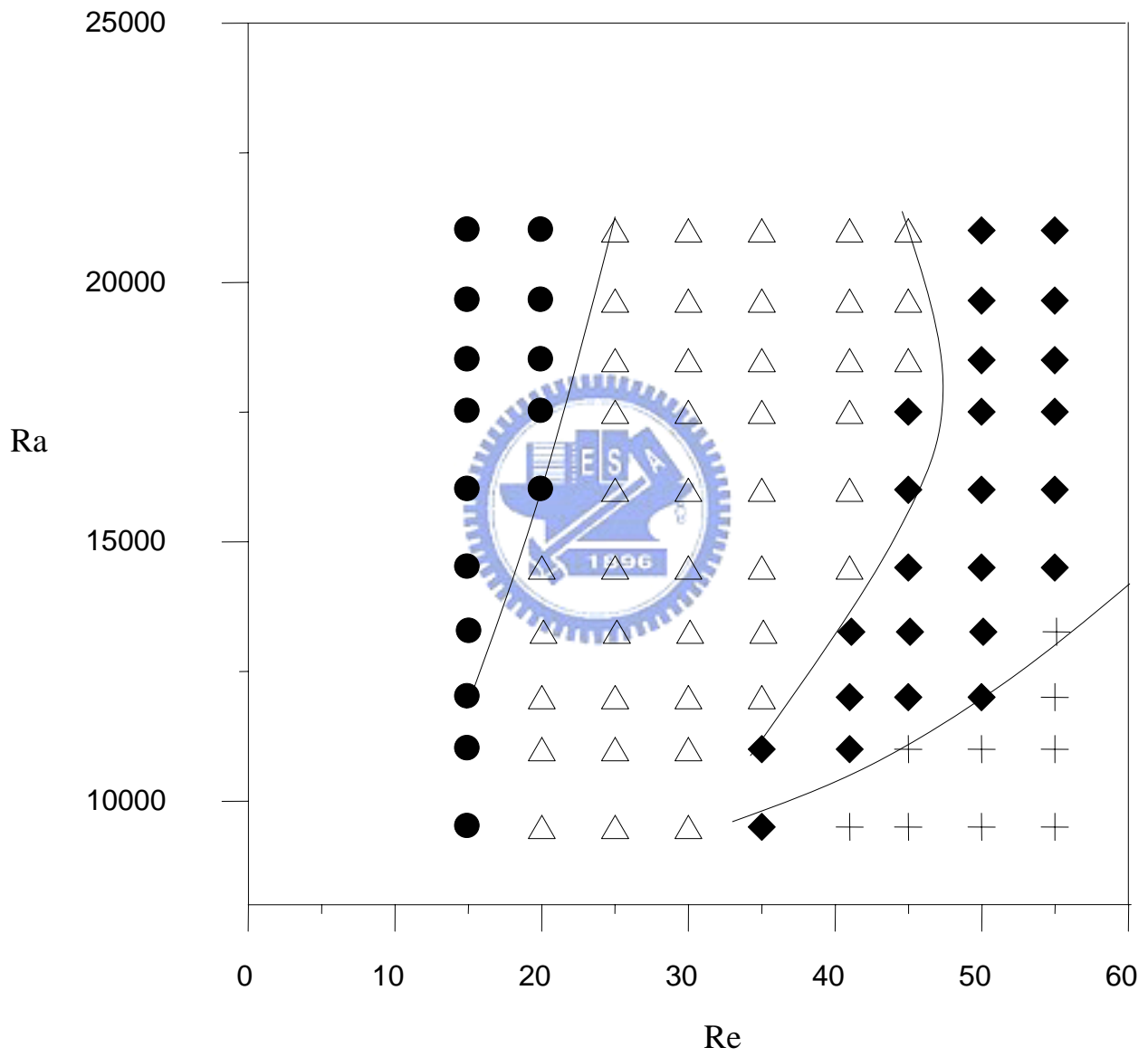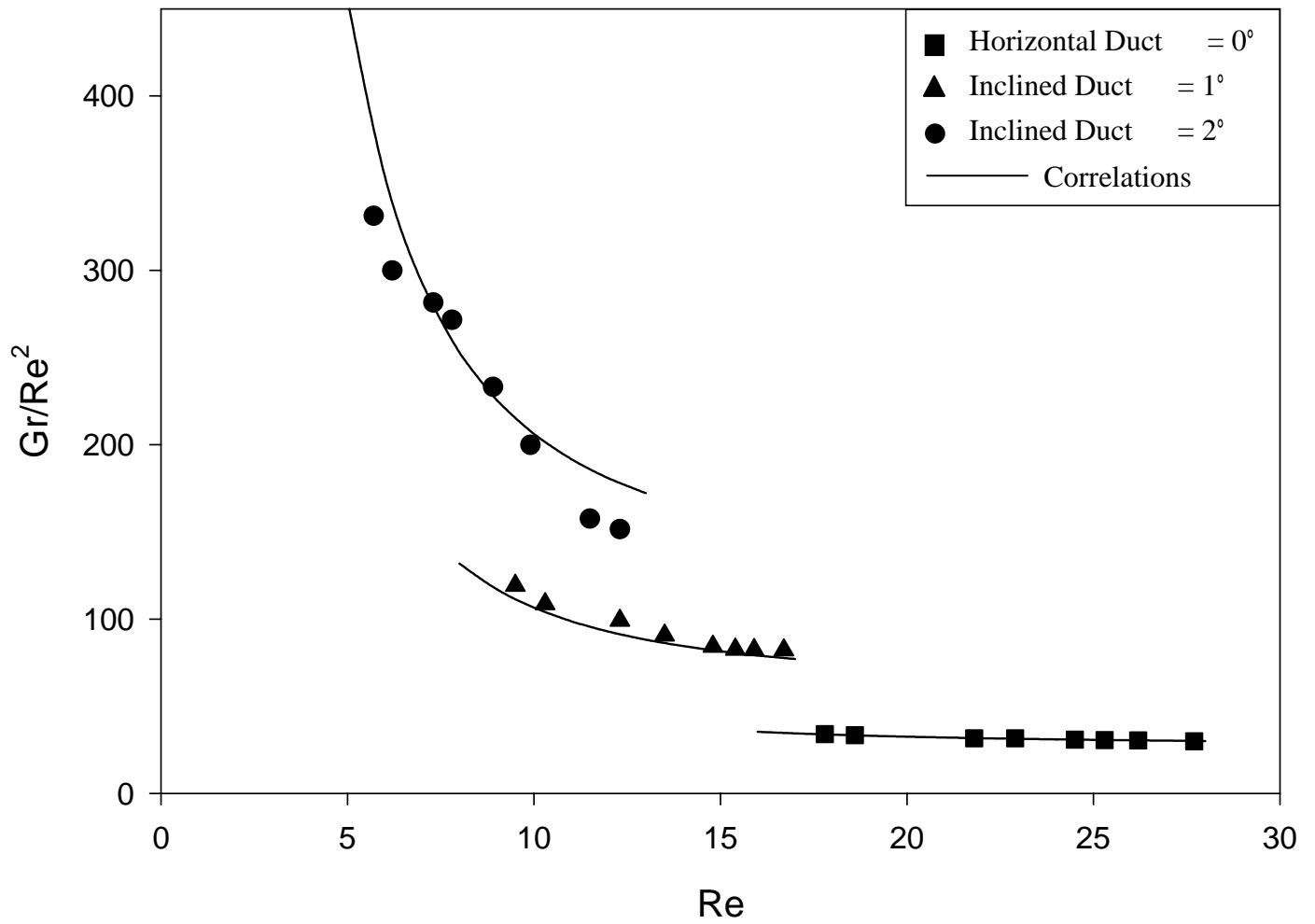w and return flow in mixed convection of air in a horizontal flat duct, modeling horizontal MOCVD processes. In the experiment the Reynolds number is varied from 5 to 50 and Rayleigh number from 7,200 to 21,000 for various degrees of sidewall converging and duct inclination. The major conclusions obtained from the results obtained here can be summarized as follows:

(1) Due to the acceleration of the main flow by the converging of the sidewalls, and the reduction of normal buoyancy component by the duct inclination, the buoyancy driven unstable L-rolls and T-rolls can be effectively stabilized. Besides, the onsets of longitudinal and transverse vortex rolls are delayed to a significant degree.

(2) The main flow acceleration in the convergent duct and the duct inclination noticeably delay the onset of the return flow and weakens it to some degree.

(3) Empirical equations have been proposed to correlate the onset conditions of the return flow.

(4) The sidewall converging and duct inclination also greatly suppress the temporal

oscillation of the flow. At a high converging angle of the sidewalls or a small inclined angle of the duct the buoyancy driven unstable flow oscillation can be completely suppressed.

(5) The reduction in the size of the return flow zone by the sidewall converging and the duct inclination are more effective at a higher Re.

(6) When the duct is inclined slightly, the onsets of thermals and longitudinal and transverse vortex rolls are significantly delayed.

During the course of this investigation, it is recognized that the elimination of the return flow is still very important in the MOCVD processes. Simple methods to delay and even eliminate the return flow need to be further developed and explored in the future.
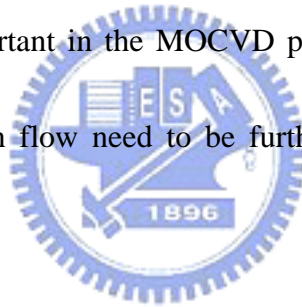
REFERENCES

[1] J.T. Lir, M.Y. Chang, T. F. Lin, Vortex Flow Patterns near Critical State for Onset of Convection in Air Flow through a Bottom Heated Horizontal Flat Duct, International Journal of Heat and Mass Transfer 44 (2001) 705-719.

[2] T.C. Cheng, J.T. Lir, T.F. Lin, Stationary Transverse Rolls and U-rolls in Limiting low Reynolds number Mixed Convective Air Flow near the Convective Threshold in a Horizontal Flat Duct, International Journal of Heat and Mass Transfer 45 (2002) 1211-1227

[3] E. P. Visser, C. R. Kleijn, C. A. M. Govers, C. J. Hoogendoorn, L. J. Giling, Return flows in horizontal MOCVD reactors studied with the use of TiO_2 particle injection and numerical calculations, Journal of Crystal Growth 94 (1989) 929-946.

[4] J.L. Tuh, Experimental Study on the Mixed Convective Air Flow Structure Driven by a Heated Circular Plate Embedded in the Bottom of a Horizontal Flat Duct, Ph.D. thesis, Nation Chiao Tung University, Hsinchu, Taiwan, 2003.

[5] H. Zhang, X.Y. Huang, H.S. Li, L.P. Chua, Flow Pattern and Heat Transfer Enhancement in low-Reynolds-Rayleigh-number Channel Flow, Applied Thermal Engineering 22 (2002) 1277-1288.

[6] Y. Kamotani, S. Ostrach, Effect of thermal instability on thermally developing channel flow, ASME Journal of Heat Transfer 98 (1976) 62-66.

[7] E. L. Koschmieder, S. G. Pallas, Heat transfer through a shallow, horizontal convecting fluid layer, International Journal of Heat and Mass Transfer 17 (1974) 991-1002.

[8] Y. Mori, Y. Uchida, Forced convective heat transfer between horizontal flat plates, International Journal of Heat and Mass Transfer 9 (1966) 803-817.

[9] J. M. Luijkx, J. K. Platten, J. C. Legros, On the existence of thermoconvective rolls, transverse to a superimposed mean Poiseuille flow, International Journal of Heat and Mass Transfer 24 (7) (1981) 1287-1291.

[10] J. L. Tuh, T. F. Lin, Visualization of Return Flow Structure in Mixed Convection of Gas over a Heated Circular Plate in a Horizontal Flat Duct, Journal of Crystal Growth 257 (2003) 199-211.

[11] W. k. Cho, D.H. Choi, Optimization of a Horizontal MOCVD Reactor for Uniform Epitaxial Layer Growth, International Journal of Heat and Mass Transfer 43 (2000) 1851-1858.

[12] M. Akiyama, G. J. Hwang, K. C. Cheng, Experiments on the onset of longitudinal vortices in laminar forced convection between horizontal plates, ASME Journal of Heat Transfer 93 (1971) 335-341.

[13] X. Nicolas, J.M. Luijkx, J.K. Platten, Linear Stability of Mixed Convection Flows in Horizontal Rectangular Channels of Finite Transversal Extension Heated from

Below, International Journal of Heat and Mass Transfer 43 (2000) 589-610.

[14] S. Ostrach, Y. Kamotani, Heat transfer augmentation in laminar fully developed channel flow by means of heating from below, ASME Journal of Heat Transfer 97 (1975) 220-225.

[15] Y. Kamotani, S. Ostrach, H. Miao, Convective heat transfer augmentation in thermal entrance regions by means of thermal instability, ASME Journal of Heat Transfer 101 (1979) 222-226.

[16] M.Y. Chang, C. H. Yu and T. F. Lin., Changes of Longitudinal Vortex Roll Structure in a Mixed Convective Air Flow through a Horizontal Plane Channel: an Experimental Study, International Journal of Heat and Mass Transfer 40 (1997) 347-363.

[17] K.C. Chiu, J. Ouazzani, F. Rosenberger, Mixed convection between horizontal plates-II. Fully developed flow, International Journal of Heat and Mass Transfer 30 (1987) 1655-1662.

[18] E. M. Sparrow and W. J. Minkowycz, Buoyancy effects on horizontal boundary-layer flow and heat transfer, International Journal of Heat and Mass Transfer 5 (1962) 505-511.

[19] X. Nicolas and A. Mojtabi, J. K. Platten, Two-dimensional numerical analysis of the Poiseuille-Benard flow in a rectangular channel heated from below, Physics of

Fluids 9 (2) February (1997)

[20] C.H. Yu, M.Y. Chang, T.F. Lin, Structure of moving transverse and mixed rolls in mixed convection of air in a horizontal plane channel, International Journal of Heat and Mass Transfer 40 (2) (1997) 333-346.

[21] C.H. Yu, M.Y. Cheng, T.F. Lin, Unsteady vortex roll structures in a mixed convective air flow through a horizontal plane channel: a numerical study, International Journal of Heat and Mass Transfer 40 (3) (1997) 505-518.

[22] M.L. Hitchman, K.F. Jensen, Chemical Vapor Deposition Principle and Applications, Academic Press, San Diego, 1993, Chapter 6.

[23] Y. Mori, Buoyancy effects in forced laminar convection flow over a horizontal flat plate, ASME Journal of Heat Transfer (1961) 479-482.

[24] F. C. Eversteyn, P. J. W. Severin, C. H. J. v. d. Brekel, H. L. Peek, A stagnant layer model for the epitaxial growth of silicon form silane in a horizontal reactor, Journal of the Electrochemical Society 117 (1970) 925-931.

[25] L. J. Giling, Gas flow patterns in horizontal epitaxial reactor cells observed by interference holography, Journal of the Electrochemical Society 129 (1982) 634-644.

[26] D. I. Fotiadis, M. Boekholt, K. F. Jensen, W. Richter, Flow and heat transfer in CVD reactors comparison of Raman temperature measurements and finite element model predictions, Journal of Crystal Growth 100 (1990) 577-599.
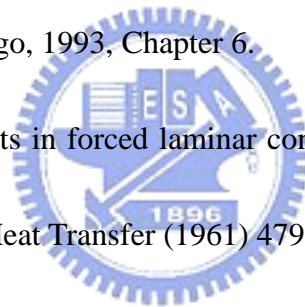
[27] J. Ouazzani, K. C. Chiu, F. Rosenberger, On the 2D modeling of horizontal CVD reactors and its limitations, Journal of Crystal Growth 91 (1988) 497-508.

[28] J. Ouazzani, F. Rosenberger, Three-dimensional modeling of horizontal chemical vapor deposition- . MOCVD at atmospheric pressure, Journal of Crystal Growth 100 (1990) 545-576.

[29] E. O. Einset, K. F. Jensen, C. R. Kleijn, On the origin of return flows in horizontal chemical vapor deposition reactors, Journal of Crystal Growth 132 (1993) 483-490.

[30] N. K. Ingle, T. J. Mountziaris, The onset of transverse recirculations during flow of gases in horizontal ducts with differentially heated lower walls, Journal of Fluid Mechanics 277 (1994) 249-269.

[31] D. B. Ingham, P. Watson, P. J. Heggs, Recirculating laminar mixed convection in a horizontal parallel plate duct, International Journal of Heat and Fluid Flow 16 (3) (1995) 202-210.

[32] D. B. Ingham, P. Watson, P. J. Heggs, Upstream migration of heat during combined convection in a horizontal parallel plate duct, International Journal of Heat and Mass Transfer 39 (2) (1996) 437-440.

[33] T. M. Makhviladze, A. V. Martjushenko, Several aspects of the return flows formation in horizontal CVD reactors, International Journal of Heat and Mass Transfer 41 (16) (1998) 2529-2536.
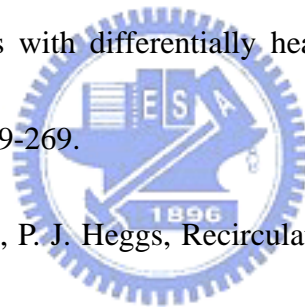
[34] K. W. Park, H. Y. Pak, Characteristics of three-dimensional flow, heat, and mass transfer in a chemical vapor deposition reactor, Numerical Heat Transfer 37 (2000) 407-423.

[35] T.S. Chen, A. Moutsoglou, B.F. Armaly, Thermal instability of Mixed convection flow over inclined surfaces, Numerical Heat Transfer 5 (1982) 343-352.

[36] C. Gau, C.W. Liu, T.M. Huang, Win Aung, Secondary flow and enhancement of heat transfer in horizontal parallel-plate and convergent channels heating from below, International Journal of Heat and Mass Transfer 42 (1999) 2629-2647.

[37] W.S. Tseng, W.L. Lin, C.P. Yin, C.L. Lin, T.F. Lin, Stabilization of buoyancy-driven unstable vortex flow in mixed convection of air in a rectangular duct by tapering its top plate, ASME Journal of Heat Transfer 122 (2000) 58-65.

[38] S.H. Sun, Buoyancy Driven Vortex Flow Structures in Mixed Convective Air Flow through a Horizontal Bottom Heated Convergent Flat Duct, M.S. thesis, National Chiao Tung University, Hsinchu, Taiwan, 2002.

[39] J.Y. Wang, Stabilization of Mixed Convective Air Flow Driven by a Heated Circular Plate Embedded in the Bottom of Horizontal Rectangular Duct by Inclining its Bottom Plate, M.S. thesis, National Chiao Tung University, Hsinchu, Taiwan, 2003.

[40] R.Y. Bai, Elimination of Return Flow in Mixed Convection of Gas over a Heated Circular Plate in a Horizontal Flat Duct by Inserting Curved Blocks Ahead of the

Plate, M.S. thesis, National Chiao Tung University, Hsinchu, Taiwan, 2004.

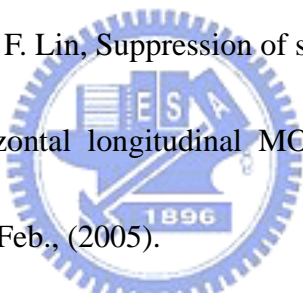[41] R.K. Shah, A.L. London, Laminar Flow Forced Convection in Ducts, Academic Press, New York, 1987, pp. 196-198.

[42] S.J. Kline, F.A. McClintock, Describing uncertainties in single-sample experiments, Mechanical Engineering 75 (1953) 3-12.

[43] M.L. Hitchman, K.F. Jensen, Chemical Vapor Deposition Principle and Applications, Academic Press, San Diego, 1993, Chapter 2.

[44] J. L. Tuh, T. F. Lin, Structure of Mixed Convective Longitudinal Vortex Air Flow Driven by a Heated Circular Plate Embedded in the Bottom of a Horizontal Flat Duct, International Journal of Heat and Mass Transfer 46 (2003) 1341-1357.
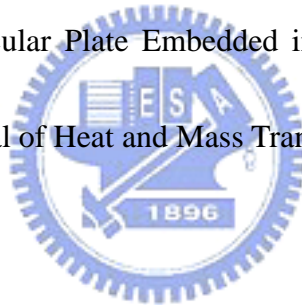
LIST OF PUBLICATOIN

1. <u>W. S. Kuo</u>, C. Y. Wang, J. L. Tuh, and T. F. Lin, Delayed onset of return flow by substrate inclination in model horizontal longitudinal MOCVD processes, Journal of Crystal Growth 274 (2005) 265-280.

2. <u>W. S. Kuo</u>, Y. M. Lie, Y. Y. Hsieh, and T. F. Lin, Condensation heat transfer and pressure drop of refrigerant R-410A flow in a vertical plate heat exchanger, International Journal of Heat and Mass Transfer, 48 (2005), 5205-5220.

3. <u>W. S. Kuo</u>, J. L. Tuh, and T. F. Lin, Suppression of secondary flow through sidewall converging in model horizontal longitudinal MOCVD processes, Submitted to Journal of Crystal Growth, Feb., (2005).

4. <u>W. S. Kuo</u>, S. W. Chen, D. S. Shu , J. T. Lir, and T. F. Lin, Buoyancy driven vortex flow and its stability in mixed convection of air through a blocked horizontal flat duct heated from below, Submitted to International Journal of Heat and Mass Transfer, Jul., (2005).